NASA
Technical
Paper
2769

1987

Effects of the Installation and Operation of Jet-Exhaust Yaw Vanes on the Longitudinal and Lateral-Directional Characteristics of the F-14 Airplane

David E. Reubush
and Bobby L. Berrier

Langley Research Center
Hampton, Virginia

National Aeronautics
and Space Administration

Scientific and Technical
Information Division

Summary

An investigation was conducted in the Langley 16-Foot Transonic Tunnel to determine the effects of the installation and operation of jet-exhaust yaw vanes on the longitudinal and lateral-directional characteristics of the F-14 airplane. The model was tested at Mach numbers from 0.70 to 1.25 at angles of attack from 0° to 4.3°. Compressed air was used to simulate nozzle exhaust flow from jet off up to a nozzle pressure ratio of 8. The results of the investigation show that the yaw vanes can augment the rudders to provide directional control, but further investigation will be necessary to optimize the deflection schedule associated with the various nozzle power settings. Installation of the yaw vanes also resulted in a drag penalty that will have to be considered in determining the overall benefits of the yaw vanes.

Introduction

Most of today's high-performance fighter airplanes are limited in high-angle-of-attack maneuvering capability by the fact that the lateral-directional stability and control characteristics of the configurations deteriorate as a result of the complex separated flow field that exists at high angles of attack on the lee side of the body. Modifications would be desirable to enable the airplane to maneuver even though this flow condition exists. One method proposed to give configurations high-angle-of-attack maneuvering capability is to utilize the propulsion system and vector the exhaust for powered control. For future configurations, the use of vectoring nonaxisymmetric nozzles could provide the desired maneuvering capability. However, for existing configurations, this solution is not possible and other methods have to be developed. One of the proposed solutions for augmenting high-angle-of-attack directional control for an existing airplane, the F-14, is to mount yaw vanes on the airplane afterbody that can be rotated into the exhaust flow, thus vectoring the exhaust and producing the desired yawing moment. This concept has been previously investigated (refs. 1 and 2) and has shown promise. The present investigation (which is part of an ongoing NASA-Navy-Grumman cooperative program involving the F-14, as described in refs. 3 through 6) was initiated to determine the effectiveness of the yaw vane concept on the F-14 at high subsonic and transonic speeds and to determine any drag penalties that might be associated with the installation.

The yaw vane concept was investigated on a 1/12-scale propulsion model of the F-14 in the Langley 16-Foot Transonic Tunnel at Mach numbers from 0.70 to 1.25. The angle of attack was set at either 0° or 4.3° at subsonic speeds and at either 0° or 2° at a Mach number of 1.25. Tests were conducted only at these low angles of attack because of model limitations. However, even though increasing the angle of attack would result in increased drag, this procedure would have only a very minor effect on the directional control contributions of the yaw vanes. Nozzle pressure ratio was varied from 1 (jet off) to about 8, depending on Mach number. Three nozzle configurations were investigated with the yaw vanes installed: nozzles representative of the cruise and maximum afterburning power settings for the General Electric F110-GE-400 engine (which will be installed on the future F-14D version of the airplane) and nozzles representative of the cruise power setting for the Pratt and Whitney TF30-P-414 engine (which is installed on the current F-14A version of the airplane). Configurations were tested with the yaw vanes off and at deflections of 0°, −10°, and −20°.

Symbols and Abbreviations

All longitudinal force and moment coefficients are referenced to the stability-axis system, and the lateral-directional coefficients are referenced to the body-axis system. Model reference geometric data are based on the geometry of a configuration having a wing leading-edge sweep of 20°. The moment reference center is at fuselage station 92.933 cm and waterline 31.749 cm. All reference dimensions are given in meters; model dimensions are shown in centimeters.

b	wing span, 1.6289 m
$C_{D,a}$	afterbody drag coefficient, Afterbody drag/qS
$C_{D,n}$	nozzle drag coefficient obtained from integration of nozzle pressures and calculated skin friction, Drag of two nozzles/qS
$C_{D,t}$	total afterbody-nozzle drag coefficient, (Afterbody drag + Nozzle drag)/qS
$C_{L,a}$	afterbody lift coefficient, Afterbody lift/qS
$C_{L,n}$	nozzle lift coefficient obtained from integration of nozzle pressures, Lift of two nozzles/qS
$C_{L,t}$	total afterbody-nozzle lift coefficient, (Afterbody lift + Nozzle lift)/qS
$C_{l,a}$	afterbody rolling-moment coefficient, Afterbody rolling moment/qSb

$C_{m,a}$	afterbody pitching-moment coefficient, Afterbody pitching moment/$qS\bar{c}$
$C_{m,n}$	nozzle pitching-moment coefficient, Pitching moment of two nozzles/$qS\bar{c}$
$C_{m,t}$	total afterbody-nozzle pitching-moment coefficient, (Afterbody pitching moment + Nozzle pitching moment)/$qS\bar{c}$
C_n	yawing-moment coefficient, Yawing moment/qSb
$C_{n,a}$	afterbody yawing-moment coefficient, Afterbody yawing moment/qSb
C_Y	side-force coefficient, Side force/qS
$C_{Y,a}$	afterbody side-force coefficient, Afterbody side force/qS
$\bar{c}$	mean aerodynamic chord of wing, 0.24896 m
M	free-stream Mach number
$p_{t,j}$	jet total pressure, Pa
p_∞	free-stream static pressure, Pa
q	free-stream dynamic pressure, Pa
S	wing reference area, 0.3645 m^2
α	angle of attack, deg
Δ	increment in force or moment coefficient
δ_h	horizontal-tail deflection angle, positive leading edge up, deg
δ_r	rudder deflection, positive trailing edge left, deg
δ_v	right yaw vane deflection, positive when vane deflected away from jet, deg
Λ	wing leading-edge sweep angle, deg

Abbreviations:

A/B	afterburning
BL	buttock line
Dia	diameter
FS	fuselage station
NPR	nozzle pressure ratio, $p_{t,j}/p_\infty$
WL	waterline

Apparatus and Procedure

Wind Tunnel

This investigation was conducted in the Langley 16-Foot Transonic Tunnel, which is a single-return, continuous-flow, air-exchange-cooled, atmospheric wind tunnel. The test section is a regular octagon in cross section with slots at the corners of the octagon. The tunnel speed is continuously variable for a Mach number range from essentially 0 to 1.30. Further description of the Langley 16-Foot Transonic Tunnel can be found in references 7 and 8.

Model

Photographs of the model mounted in the Langley 16-Foot Transonic Tunnel both with and without yaw vanes installed are shown in figure 1. A sketch showing the principal dimensions of the model is shown in figure 2(a). The model was supported in the 16-Foot Tunnel by a thin sweptback strut attached to the bottom of the fuselage just aft of the nose, as shown in figure 2(b). The strut blended into a sting that had a constant cross section beginning at the intersection with the strut trailing edge and extending downstream to a station well aft of the model. Additional model details and dimensions are presented in figure 3. For this investigation the model was tested with the wings swept to 68° with the glove vanes extended. The inlets, located on each side of the fuselage, maintained true geometric lines but were closed to flow passage a short distance inside the inlet lip.

The model consisted of three parts: the forebody and wings, the aft fuselage and empennage (hereinafter referred to as "the afterbody"), and the engine exhaust nozzles. The forebody and wings were rigidly attached to the support system and were not metric. The afterbody, which was the metric portion of the model and started at the model metric break (station 1.1261 m, FS 112.607), included the horizontal and vertical tails, ventral fins, aft fuselage, interfairing between the engines, and yaw vanes. There was another metric break between the afterbody and the nonmetric exhaust nozzles at FS 141.499. The metric breaks are indicated in the sketches of figure 2 and can be seen in the photographs of figure 1. A flexible Teflon[1] strip, inserted into slots machined into the metric and nonmetric portions of the model, was used as a seal at the upstream metric-break station to prevent flow through the gap between the afterbody and the forebody.

[1] Teflon: Registered trademark of E. I. du Pont de Nemours & Co., Inc.

The yaw vanes were installed on the inboard side of both the left and right engine nacelles. The yaw vane installed on the left nacelle was always set at 0° deflection, whereas the vane on the right nacelle could be set at deflections of 0°, −10°, and −20°. (See fig. 3(g).) Three different pairs of exhaust nozzles representing the cruise and afterburning power settings for the F110-GE-400 engines (F110) and the cruise power setting for the TF30-P-414 engines (TF30) were tested (fig. 4). The nozzle exhaust flow was simulated by the use of a high-pressure air system.

Instrumentation

A total of 46 external static-pressure orifices were located on each pair of exhaust nozzles, and the local pressure coefficients were measured and integrated to obtain nozzle force characteristics. The orifices were distributed, based on past experience, in a manner to ensure that anticipated variations in pressure coefficients would be measured. The areas assigned to each orifice for the force and moment integrations were determined through the use of a CAD-CAM system. In addition, internal static-pressure orifices were located in the afterbody cavity and at the seal station in the gaps between the forebody and afterbody and the afterbody and nozzles. The jet total pressures and temperature were measured in each tail pipe by use of total-pressure probes and a thermocouple. Forces and moments on the metric portion (afterbody) of the model were obtained by the use of a six-component strain-gauge balance.

Tests

Data were obtained at Mach numbers of 0.70, 0.80, and 0.90 for angles of attack of 0° and 4.3° and at a Mach number of 1.25 for angles of attack of 0° and 2°. It would have been desirable to test at higher angles of attack but model load limitations precluded this. The average Reynolds number per meter varied from about 11.2×10^6 at $M = 0.70$ to 12.6×10^6 at $M = 1.25$. The jet total-pressure ratio was varied from 1 (jet off) to about 5 at subsonic speeds and to about 8 at $M = 1.25$. Transition was fixed on the model by means of 0.32-cm-wide strips of No. 120 carborundum grains. The transition strips were located on the ventral fins and on the horizontal- and vertical-tail surfaces at a distance of 0.508 cm measured normal to the leading edge. The transition strips on the wing were located as shown in figure 5, which shows the wing at $\Lambda = 22°$. However, the transition pattern was the same for these tests at $\Lambda = 68°$. A 0.32-cm-wide ring of transition-strip grit was also located 1.35 cm aft of the nose of the fuselage.

Data Reduction

Model data recorded on magnetic tape were used to compute standard force, moment, and pressure coefficients. All longitudinal force and moment data in this paper are referenced to the stability axes, and all lateral-directional force and moment data are referenced to the body axes. Both sets of axes pass through the moment reference center (fig. 2). The model angle of attack was corrected for support deflection due to loads and for tunnel upflow. No correction was made for strut interference since data from references 9 and 10 indicate that the effect is small for a similar type of support system. The afterbody axial force was obtained from the recorded data for the strain-gauge-balance axial force corrected for pressure-area terms, which consisted of internal-cavity and seal-cavity forces. The forces were corrected to a condition of free-stream static pressure in the cavity. The forces and moments on the exhaust nozzles were obtained from pressure-measurement integrations by assigning an incremental projected area to each nozzle pressure orifice and summing the incremental forces. The skin friction on the nozzles was calculated by using the Frankl and Voishel method (ref. 11) for compressible, turbulent flow on a flat plate, and this value was added to the nozzle pressure axial force before the nozzle lift and drag were computed.

Accuracy

The strain-gauge balance and all pressure transducers utilized in this investigation were calibrated to an accuracy of ±0.5 percent of the full-scale readings. For the strain-gauge balance, this calibration results in the following accuracies: normal force, ±8.340 N; axial force, ±2.224 N; pitching moment, ±0.452 N-m; rolling moment, ±0.174 N-m; yawing moment, ±0.271 N-m; and side force, ±4.181 N. It is estimated that the accuracy is ±0.1° for angle of attack and ±0.003 for Mach number. Data were obtained at a rate of 50 samples per second for a period of 5 sec and were averaged to obtain the data presented.

Results and Discussion

Data for this model without yaw vanes installed have been previously reported in references 4 through 6. However, since the purpose of this paper is simply to report on the effects of yaw vane installation, no comparisons with the previous data will be made. It must also be pointed out that when this model was designed, there was no consideration made of the possibility of loadings on the afterbody in any but the

longitudinal components (lift, drag, and pitching moment). As a result, under some conditions when the yaw vane was deflected, fouling occurred between the afterbody and forebody at the forward metric break or between the afterbody and one nozzle. Fouling indicators were installed in the forebody-afterbody and afterbody-nozzle metric breaks to provide an indication of when fouling occurred. A thorough examination of the data has been made, and all fouled data have been deleted from the results presented. (The fouled data include some afterbody and total coefficients of drag, rolling moment, yawing moment, and side force. Afterbody and total coefficients of lift and pitching moment did not appear to be affected. Nozzle coefficients, since they resulted from pressure integrations, were not affected.)

Longitudinal Characteristics

The effects of installing the yaw vanes and of deflecting one vane on the longitudinal afterbody characteristics of the model with the F110 maximum afterburning nozzles installed are presented in figure 6. This configuration was the only one of the three nozzle configurations tested with the yaw vanes off since it was felt that the nozzle lift, drag, and pitching-moment increments resulting from the installation of the vanes at 0° deflection would be small. This assumption was confirmed and can be seen by examining figures 6(c), 6(f), 6(i), 6(l), 6(o), 6(r), 6(u), and 6(x). Installation of the yaw vanes did result in an increase in drag (afterbody drag and thus total drag also). At jet-off conditions (NPR = 1), the drag increment was very small at an angle of attack of 0° but was significant at 4.3° . For jet-on conditions, the drag increase was generally independent of nozzle pressure ratio, a condition indicating that the vanes were out of the nozzle exhaust at the 0° deflection position (as was desired) for these maximum afterburning nozzles (the worst case condition). However, the increase in drag from the installation of the yaw vanes was as much as 0.0018 for the jet-on conditions of this test. The benefits of increased lateral-directional control will have to be weighed against the drag increase which, it is anticipated, will increase significantly with increasing angle of attack.

Generally, there is also a relatively constant increment in drag (both afterbody and total) between the 0° deflection case and the 10° deflection case. This increment indicates that the vane is still not immersed in the jet flow for this condition, and thus the increase in drag is due to the increase in projected area facing into the flow. (That is, there is no jet turning, only external flow turning; if the vane were immersed in the jet flow, the drag should increase with nozzle pressure ratio.) The 20° deflection case does show an increase in drag (afterbody and total) with nozzle pressure ratio, an indication that the vane has finally reached the jet and is yielding some jet turning. This result of finding a "dead band," an area in which deflection of the vane yields no turning, is similar to that found in reference 2 where a dead band of about 10° was found in a full-scale static test of similar vanes mounted on an F-14 with TF30 engines. (See fig. 3(g) for a sketch of the nozzle-vane relationship.) Vane deflection has virtually no effect on either lift or pitching moment (afterbody or total), as would be expected since the flow turning is in the lateral direction.

Effects of vane deflection from 0° to 20° on the drag, lift, and pitching moment are shown in figure 7 for the F110 cruise nozzles. There are essentially no effects of vane deflection on nozzle drag, lift, or pitching moment; on afterbody lift and pitching moment; and, as a result, on total lift and pitching moment. The only effect shown is an increase in afterbody drag that is essentially constant with nozzle pressure ratio until the highest pressure ratios tested. This increase indicates that for this closed-down nozzle the vane was not deflected far enough (even for a 20° deflection) to reach the high pressure core of the jet. Thus, the vane turned only some external flow until the high pressure ratios were reached, and then the plume expanded enough to just reach the vane. In effect, this result means that the dead band for this nozzle configuration was almost 20°.

The effects of vane deflection from 0° to 20° on the longitudinal characteristics of the configuration with the TF30 cruise nozzles are shown in figure 8. The results for this nozzle (which is also closed down) are similar to those found for the F110 cruise nozzle. There are essentially no effects of vane deflection on nozzle drag, lift, or pitching moment (except for a slight decrease in nozzle drag for the $M = 1.25$ case) and no effects on afterbody and thus total lift and pitching moment. However, unlike the F110 cruise nozzle, the drag increment (both afterbody and total) between the 0° and 20° deflection cases is not constant with nozzle pressure ratio. This condition indicates that for this nozzle design the plume may have expanded enough to reach the vane for the 20° deflection case and perhaps have yielded some jet turning.

It is interesting to note that for this nozzle design the drag (afterbody and total) at the low nozzle pressure ratios is actually lower for the 20° deflection case than for the 0° deflection case. This result is believed to be due to the increased pressure created upstream of the deflected vane that cleared up an area of separation on the afterbody. (The TF30 cruise nozzles have such steep boattails that they are massively

separated at almost all conditions, which probably contributes to the afterbody separation characteristics. See nozzle pressure distributions in refs. 3 and 4.) It must also be noted that in order to help alleviate fouling, this configuration was tested with the horizontal tails set at $-2°$. Although, this means that the absolute values of afterbody lift, drag, etc., cannot be directly compared with those for the configurations with the F110 nozzles installed, the increments between the various yaw vane configurations should be comparable.

Drag increments for the installation of the yaw vanes on the F-14 with the F110 A/B nozzles are summarized in figure 9 where increments at a nozzle pressure ratio of 3 (which is a typical operating NPR) are shown for the Mach numbers and angles of attack investigated. The effects of installing the yaw vanes range from no drag increase at $M = 1.25$ with $\alpha = 0°$ to an increase in drag coefficient of 0.0018 at both $M = 0.70$ and 0.80 with $\alpha = 4.3°$. Note that the installation drag increments always increased with increasing angle of attack.

Drag increments for the deflection of the yaw vanes from 0° are summarized in figure 10 in which increments at a nozzle pressure ratio of 3 are shown for the various conditions investigated. Because of the large increase in drag, it is obvious that the vane is immersed in the jet for the 20° deflection condition for the F110 afterburning nozzles. However, it is not obvious that any of the other nozzle-vane deflection combinations have the vane immersed in more than just the periphery of the jet. This fact needs to be considered in the design of future yaw vane concepts that must operate with nozzles in other than afterburning power settings.

Lateral-Directional Characteristics

Afterbody lateral and directional characteristics for the model with F110 afterburning nozzles and yaw vanes installed are shown in figure 11. Installation of the yaw vanes at a deflection of 0° had essentially no effect on afterbody rolling moment, yawing moment, or side force. Deflection of the yaw vane at either 10° or 20° also had essentially no effect on afterbody rolling moment. These results are desirable and are as expected in that the vanes are arranged symmetrically around the airplane centerline, and thus their installation should not result in any nonsymmetrical forces in the lateral-directional planes. Deflecting the vane 10° did generate a positive yawing moment and a negative side force, both of which increased in magnitude slightly with increasing nozzle pressure ratio. Similarly, deflecting the vane 20° also resulted in a positive yawing moment and a negative side force, both of which increased at a rapid rate with an increase in nozzle pressure ratio. These results bear out the conclusions drawn from the drag data. That is, the 10° deflection case has the vane at the periphery of the jet with little jet turning, whereas the 20° deflection case has the vane immersed in the jet, thus yielding significant jet turning (i.e., a dead band of at least 10° for this configuration).

Afterbody lateral-directional characteristics for the model with the F110 and TF30 cruise nozzles installed and the yaw vanes deflected 0° and 20° are shown in figures 12 and 13, respectively. Again, these results bear out the conclusion reached from the drag data. That is, even with a deflection of 20°, the yaw vane does not reach the core of the jet to achieve significant jet turning. The yawing moment and side force produced by deflection of the yaw vane do not increase significantly with an increase in nozzle pressure ratio, an indication that the vane is at the periphery of the jet and most of the turning is being accomplished on the external flow (i.e., a dead band that is essentially 20°). As was the case for the F110 maximum afterburning nozzles, deflection of the yaw vane had essentially no effect on the afterbody rolling moment, as desired.

A summary of yawing-moment and side-force increments obtained at a nozzle pressure ratio of 3 are shown in figures 14 and 15. Also included in figures 14 and 15 is a dashed line indicating the yawing moment and side force, respectively, resulting from $\delta_r = -1°$ at $\alpha = 0°$ (ref. 12). The 20° vane deflection for the maximum afterburning nozzle configuration yields at least four times the yawing moment and side force as the 10° deflection, whereas at supersonic speeds the ratio is about 3 to 1. This result indicates that, as discussed previously, the vane is not significantly immersed in the jet flow at the 10° deflection for the maximum afterburning nozzles. Similarly, for both the F110 and the TF30 cruise nozzles with the 20° deflection, the data indicate that the vane is not immersed in the jet flow a significant amount for these two configurations. (That is, yawing moments and side forces are of the same order of magnitude as those for the F110 A/B nozzle configuration with the vane deflected 10°.)

The rudder-effectiveness line (the dashed line for $\delta_r = -1°$) is included in the figures to help understand how effective the yaw vanes are in relation to the rudders. (It must be noted that the rudder-effectiveness data were obtained at a Mach number of 0.15. Unpublished data indicate that the rudders were not quite as effective at the Mach numbers of this investigation. However, for the purposes of this discussion the rudder data presented can be considered approximately correct.) As can be seen, only

the 20° deflection case with the F110 maximum afterburning nozzles yields yawing-moment and side-force levels significantly above those available from a rudder deflection of −1°. Consequently, having the capability to deflect the vanes more than 20° would be desirable for this yaw vane geometry, especially if the vanes could be utilized for directional control with the nozzles in other than the maximum afterburning condition.

In evaluating the usefulness of the yaw vanes, particularly in maneuvering flight, it is important to consider the impact of the angle of attack on the rudder effectiveness. Figure 16 presents yawing-moment increments as a function of angle of attack for both the yaw vanes ($M = 0.70$, NPR = 3) and the rudder. Implicit in the figure is the assumption that the effectiveness of the yaw vane does not change with angle of attack. This assumption is felt to be reasonable. Indicated in figure 16 is the yawing moment as a function of angle of attack for $\delta_r = -1°$ and −9.5°. (The deflection of −9.5° is the maximum available for a dynamic pressure of 33.5 kPa because of structural considerations. This dynamic pressure is approximately that for $M = 0.70$ at sea level.)

For the case of a vane deflection of 20° with the maximum afterburning nozzles, the yaw vane provides a greater yawing moment than the rudders at angles of attack above about 27°. The crossover points for the other nozzle-vane configurations are somewhat higher in angle of attack. The actual values of the angles of attack for crossover are not really the important feature derived from this figure since, as mentioned previously, the rudder effectiveness for this Mach number is actually somewhat lower than that shown. The important part is that the yaw vanes, even without being optimized for jet turning for each nozzle configuration, provide an enhanced capability for directional control that can enable controlled maneuvering flight at higher angles of attack than is currently possible since the rudder effectiveness goes toward zero as angle of attack is increased. It is recommended that the vanes be further investigated utilizing expanded deflection and angle-of-attack ranges to provide an optimum deflection schedule with each nozzle configuration.

Conclusions

An investigation to determine the effects of the installation and operation of jet-exhaust yaw vanes on the longitudinal and lateral-directional characteristics of the F-14 airplane has been conducted in the Langley 16-Foot Transonic Tunnel. The results of this investigation indicate the following conclusions:

1. Jet-exhaust yaw vanes can be effective in augmenting the lateral-directional control available from conventional rudders, especially at high angles of attack where conventional aerodynamic controls become ineffective.

2. There is a "dead band" of deflection (an area in which deflection of the vane yields no turning) that produces little yawing moment or side force, and this dead band varies with nozzle power setting. Therefore, the deflection of the yaw vanes needs to be scheduled with nozzle power setting, and the range should be greater than the 20° of this investigation.

3. The drag penalty from the installation of the yaw vanes was as much as 0.0018 in drag coefficient for the conditions of this test, depending on Mach number and angle of attack. However, there was only a very slight effect on lift or pitching moment.

NASA Langley Research Center
Hampton, VA 23665
November 9, 1987

References

1. Lacey, David W.; and Murphy, Richard D.: *Jet Engine Thrust Turning by the Use of Small Externally Mounted Vanes.* DTNSRDC-82/080, U.S. Navy, Jan. 1983. (Available from DTIC as AD B070 970L.)
2. Lacey, David W.; and Murphy, Richard D.: *A Full-Scale Static Evaluation of the Yaw Vane Concept.* DTNSRDC/ASED-84/08, David W. Taylor Naval Ship Research and Development Center, Dec. 1984.
3. Mercer, Charles E.; and Reubush, David E.: *Sting and Jet Interference Effects on Longitudinal Aerodynamic Characteristics of a Twin-Jet, Variable-Wing-Sweep Fighter Model at Mach Numbers to 2.2.* NASA TM X-2825, 1973.
4. Reubush, David E.; and Mercer, Charles E.: *Exhaust-Nozzle Characteristics for a Twin-Jet Variable-Wing-Sweep Fighter Airplane Model at Mach Numbers to 2.2.* NASA TM X-2947, 1974.
5. Reubush, David E.; and Mercer, Charles E.: *Effects of Nozzle Interfairing Modifications on Longitudinal Aerodynamic Characteristics of a Twin-Jet, Variable-Wing-Sweep Fighter Model.* NASA TN D-7817, 1975.
6. Reubush, David E.; and Carlson, John R.: *Effects of Installation of F101 DFE Exhaust Nozzles on the Afterbody-Nozzle Characteristics of the F-14 Airplane.* NASA TM-83250, 1982.
7. Corson, Blake W., Jr.; Runckel, Jack F.; and Igoe, William B.: *Calibration of the Langley 16-Foot Transonic Tunnel With Test Section Air Removal.* NASA TR R-423, 1974.
8. Peddrew, Kathryn H., compiler: *A User's Guide to the Langley 16-Foot Transonic Tunnel.* NASA TM-83186, 1981.
9. Re, Richard J.; Wilmoth, Richard G.; and Runckel, Jack F.: *Investigation of Effects of Afterbody Closure and Jet Interference on the Drag of a Twin-Engine Tactical Fighter.* NASA TM X-1382, 1967.

10. Runckel, Jack F.; Lee, Edwin E., Jr.; and Simonson, Albert J.: *Sting and Jet Interference Effects on the Afterbody Drag of a Twin-Engine Variable-Sweep Fighter Model at Transonic Speeds.* NASA TM X-755, 1963.
11. Frankl, F.; and Voishel, V.: *Turbulent Friction in the Boundary Layer of a Flat Plate in a Two-Dimensional Compressible Flow at High Speeds.* NACA TM 1053, 1943.
12. Huffman, Jarrett K.; Fox, Charles H., Jr.; and Grafton, Sue B.: *Subsonic Longitudinal and Lateral Directional Static Stability Characteristics of a Variable Sweep Fighter Configuration Employing Various Control Surface Deflections at Angles of Attack of 0° to 50° and Large Sideslip Angles.* NASA TM-74050, 1977.

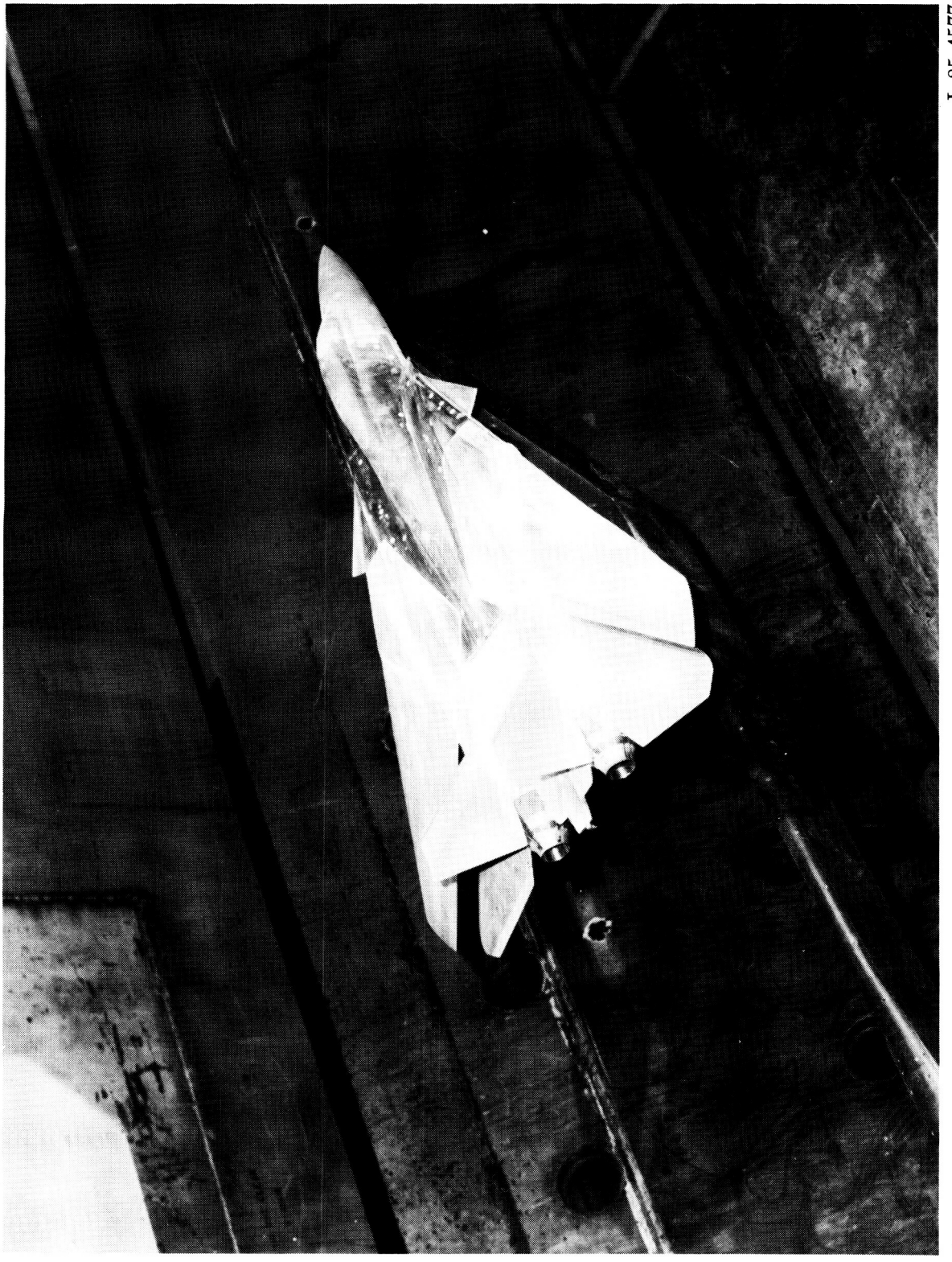

L-85-4577

(a) Model with TF30 cruise nozzles installed.

Figure 1. F-14 model mounted in the Langley 16-Foot Transonic Tunnel.

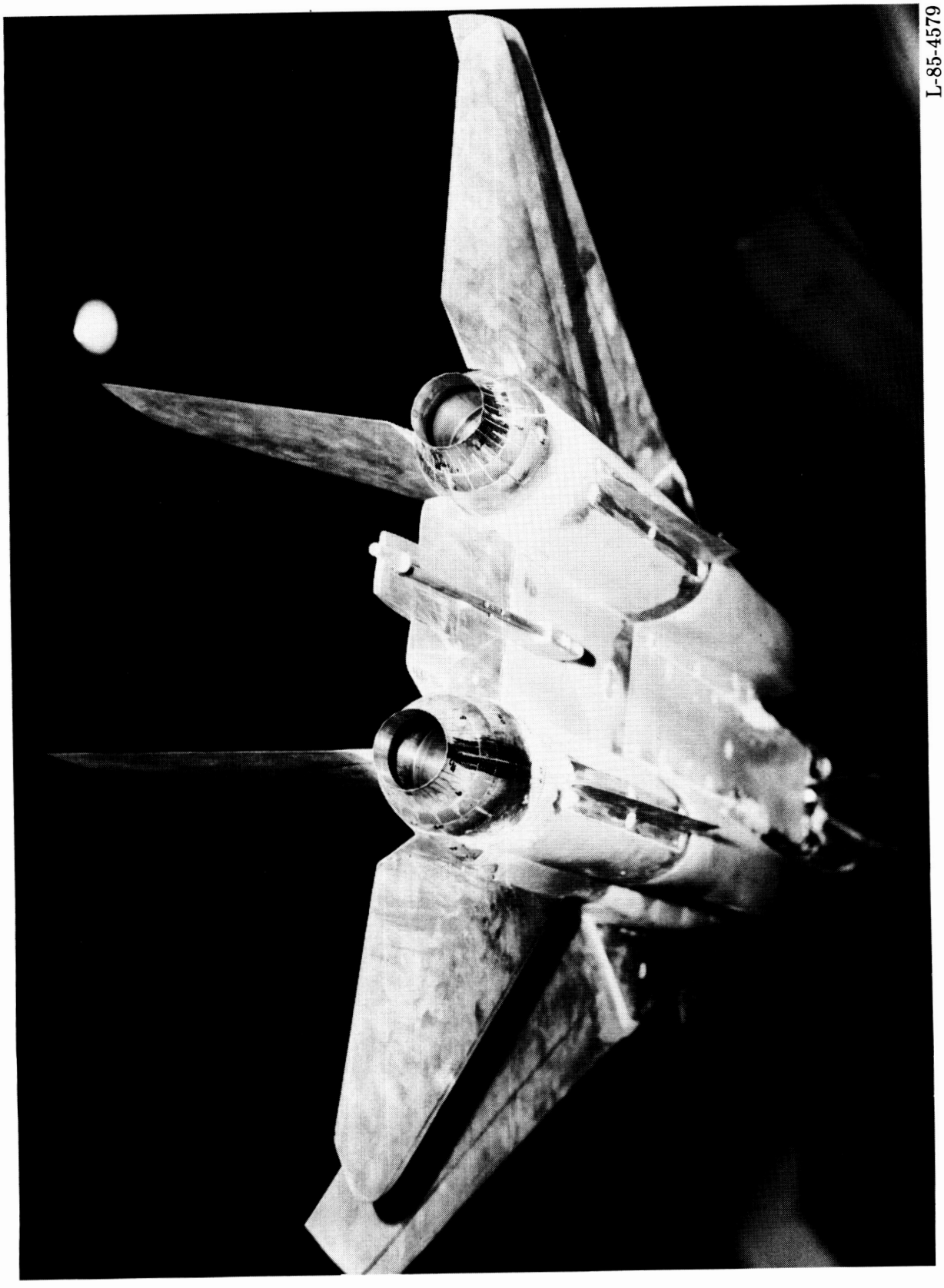

L-85-4579

(b) Lower rear view showing TF30 cruise nozzles.

Figure 1. Continued.

L-85-4242

(c) Lower rear view showing F110 cruise nozzles and yaw vanes. Right vane deflected 20°.

Figure 1. Continued.

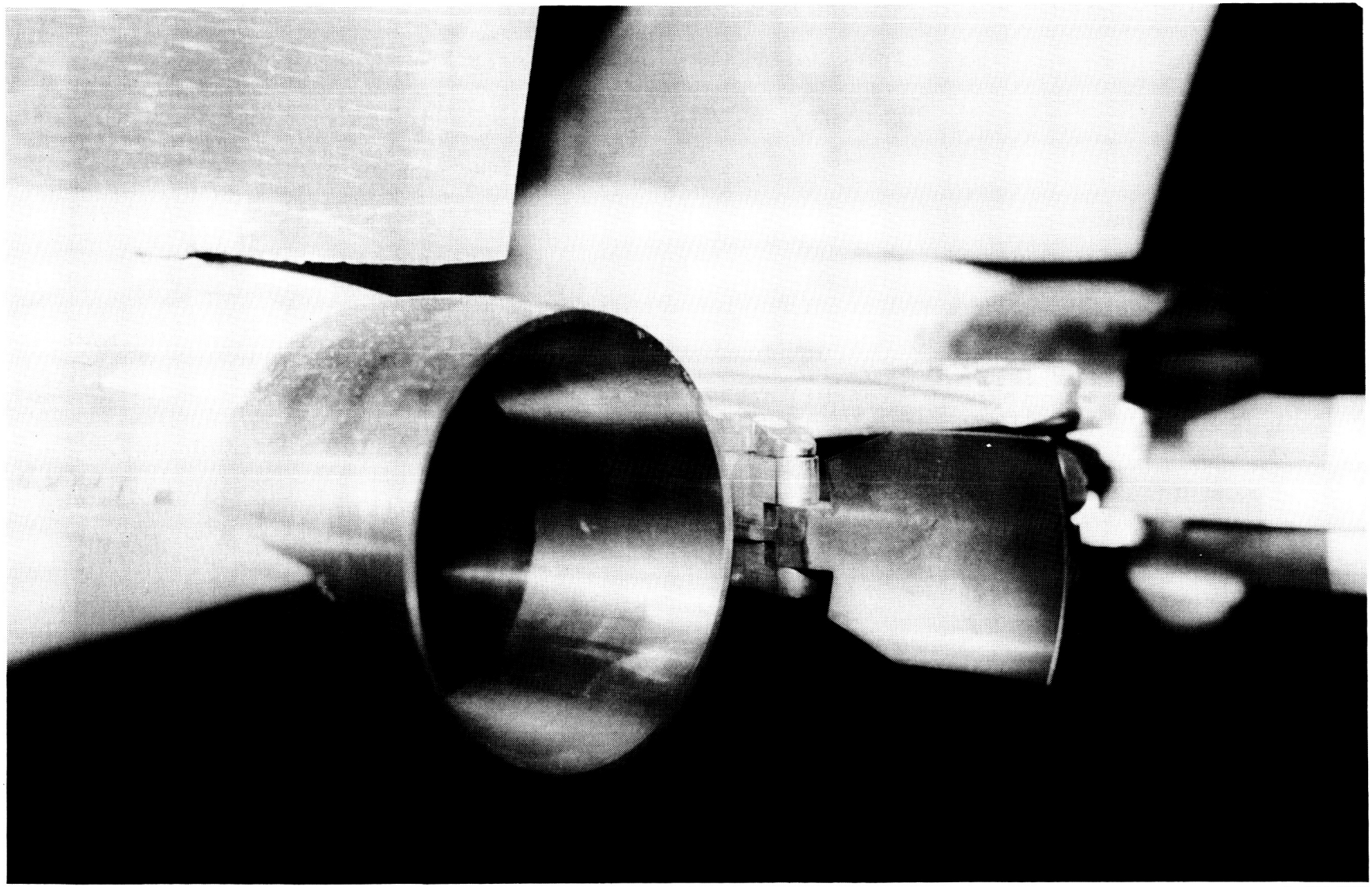

L-87-653

(d) Close-up of left F110 afterburning nozzle and undeflected yaw vane.

Figure 1. Continued.

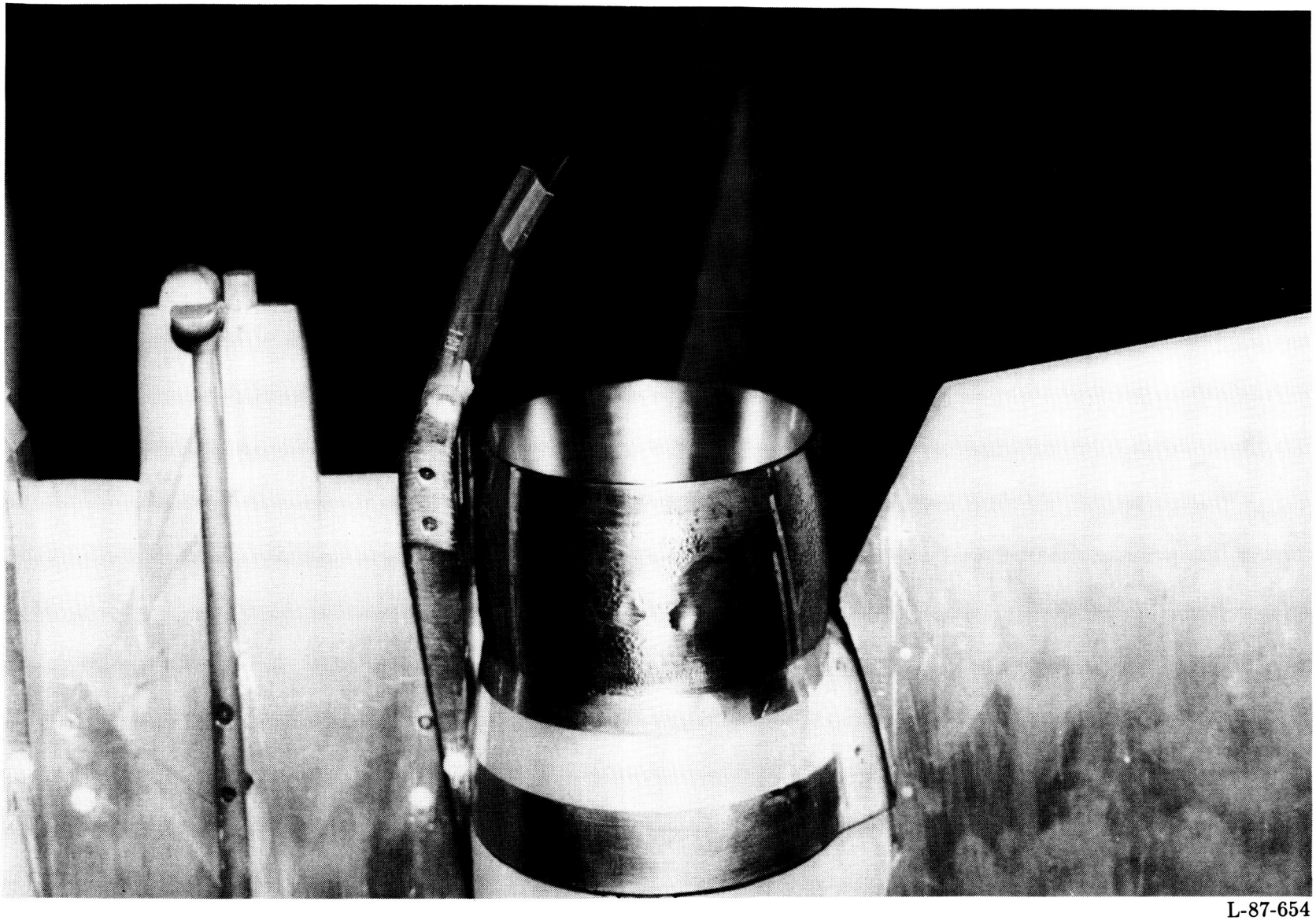

L-87-654

(e) Lower close-up of right F110 maximum afterburning nozzle and yaw vane deflected 20°.

Figure 1. Continued.

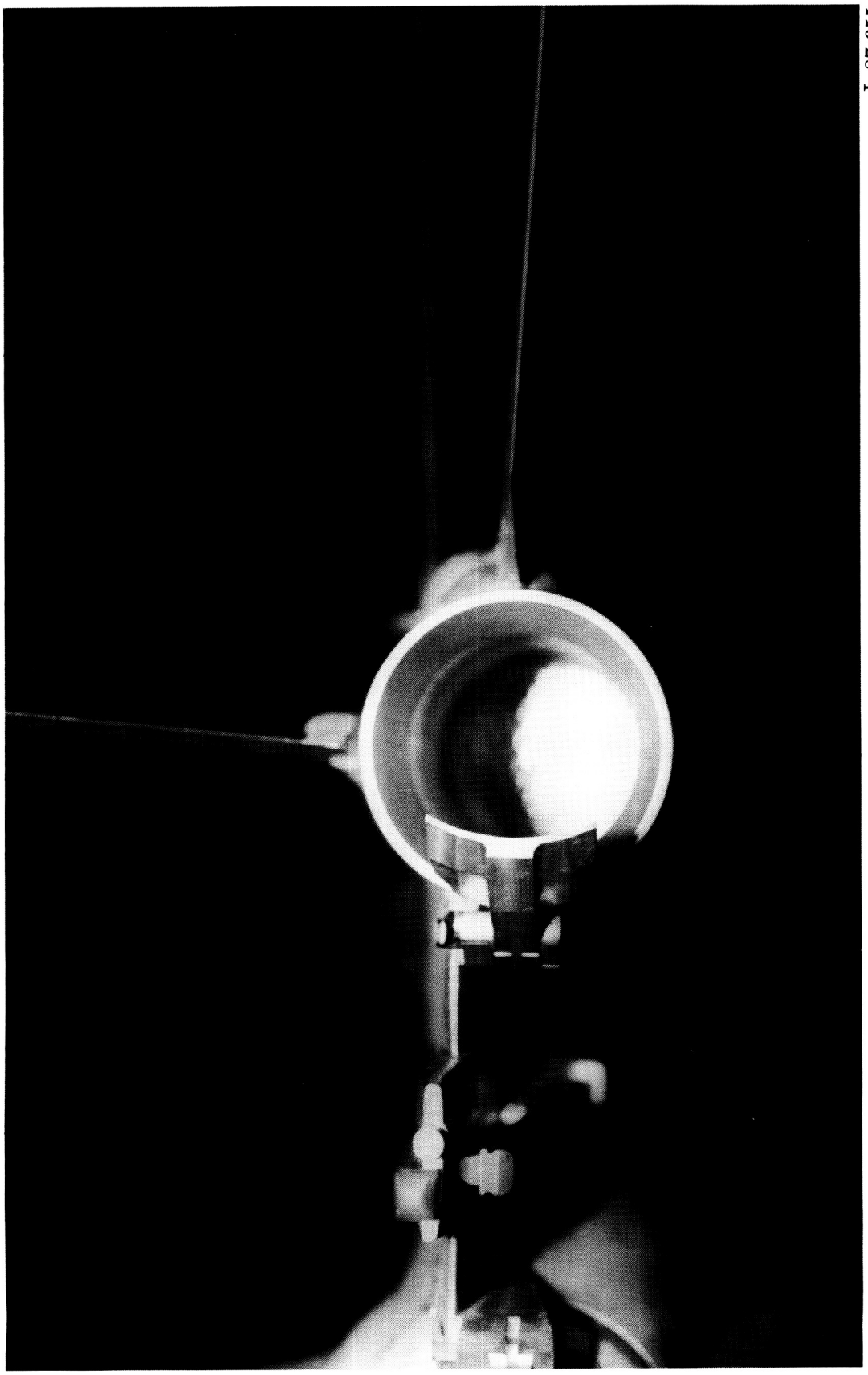

L-87-655

(f) Rear close-up of right F110 maximum afterburning nozzle and yaw vane deflected 20°.

Figure 1. Concluded.

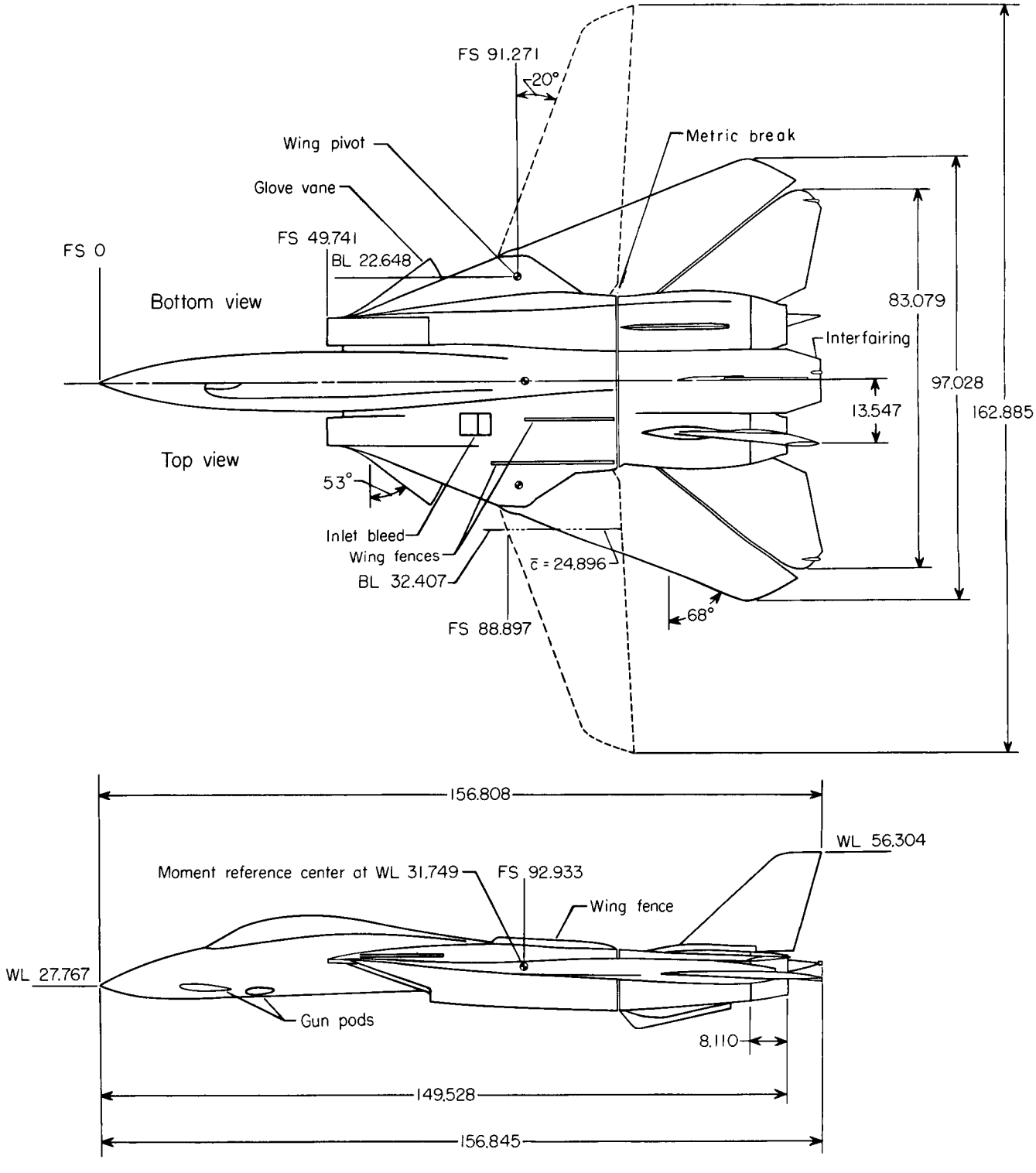

(a) Model.

Figure 2. Sketch of model and geometric details of model support. All dimensions are given in centimeters unless otherwise specified.

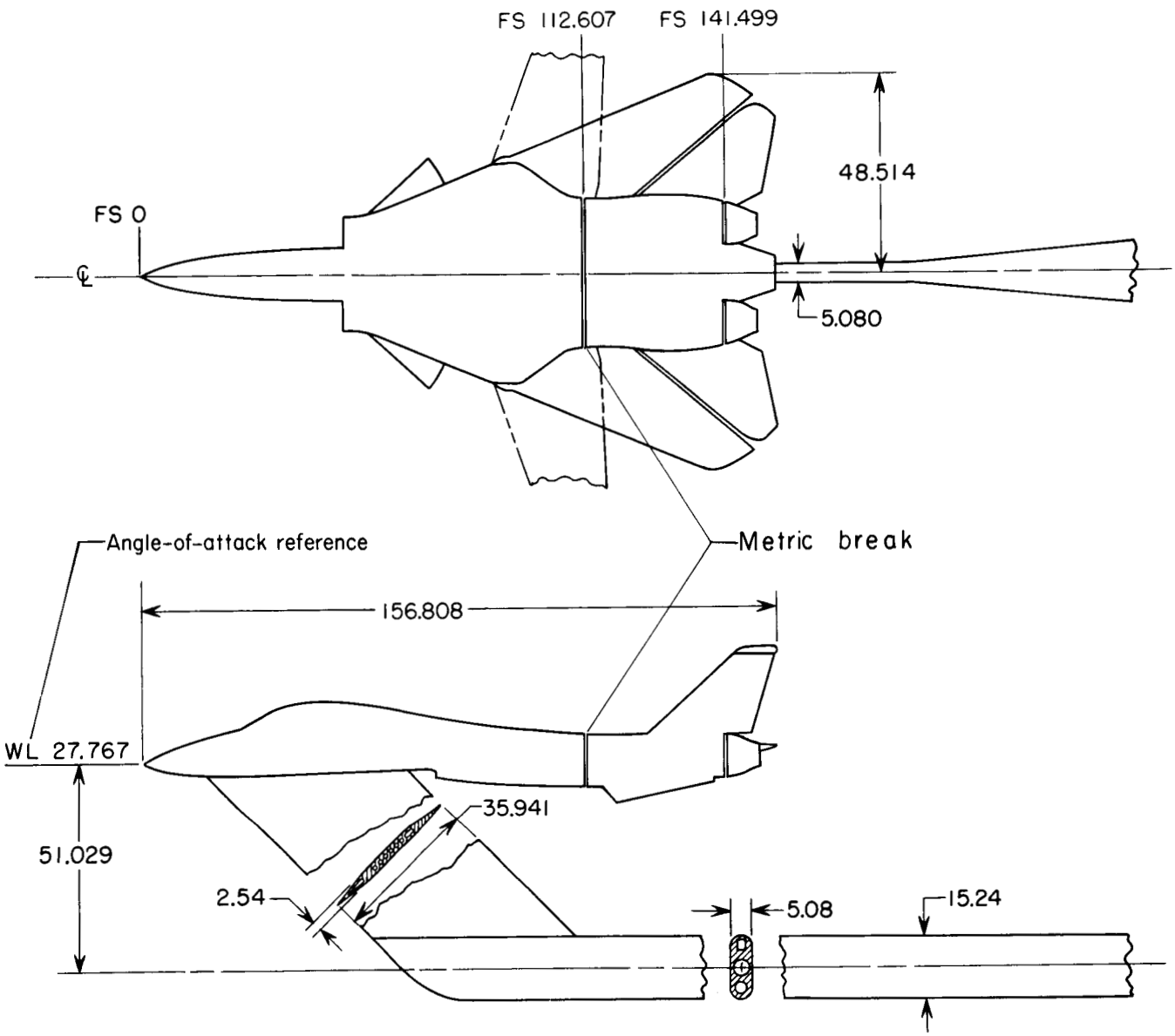

(b) Geometric details of model support.

Figure 2. Concluded.

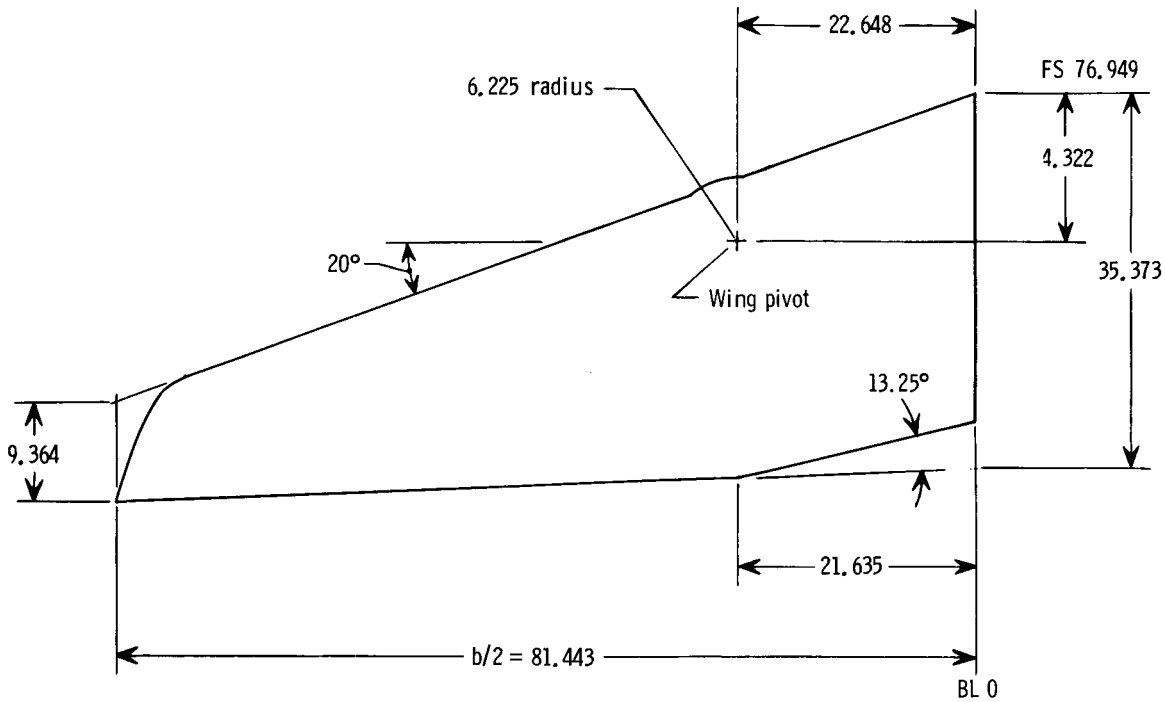

(a) Wing.

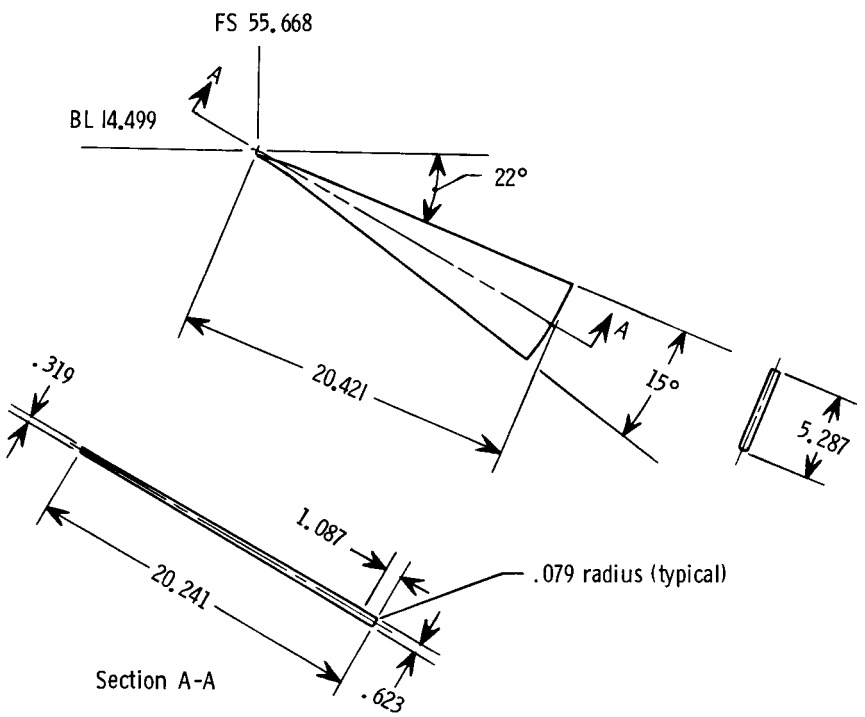

(b) Glove vane.

Figure 3. Additional details of model. All dimensions are given in centimeters unless otherwise specified.

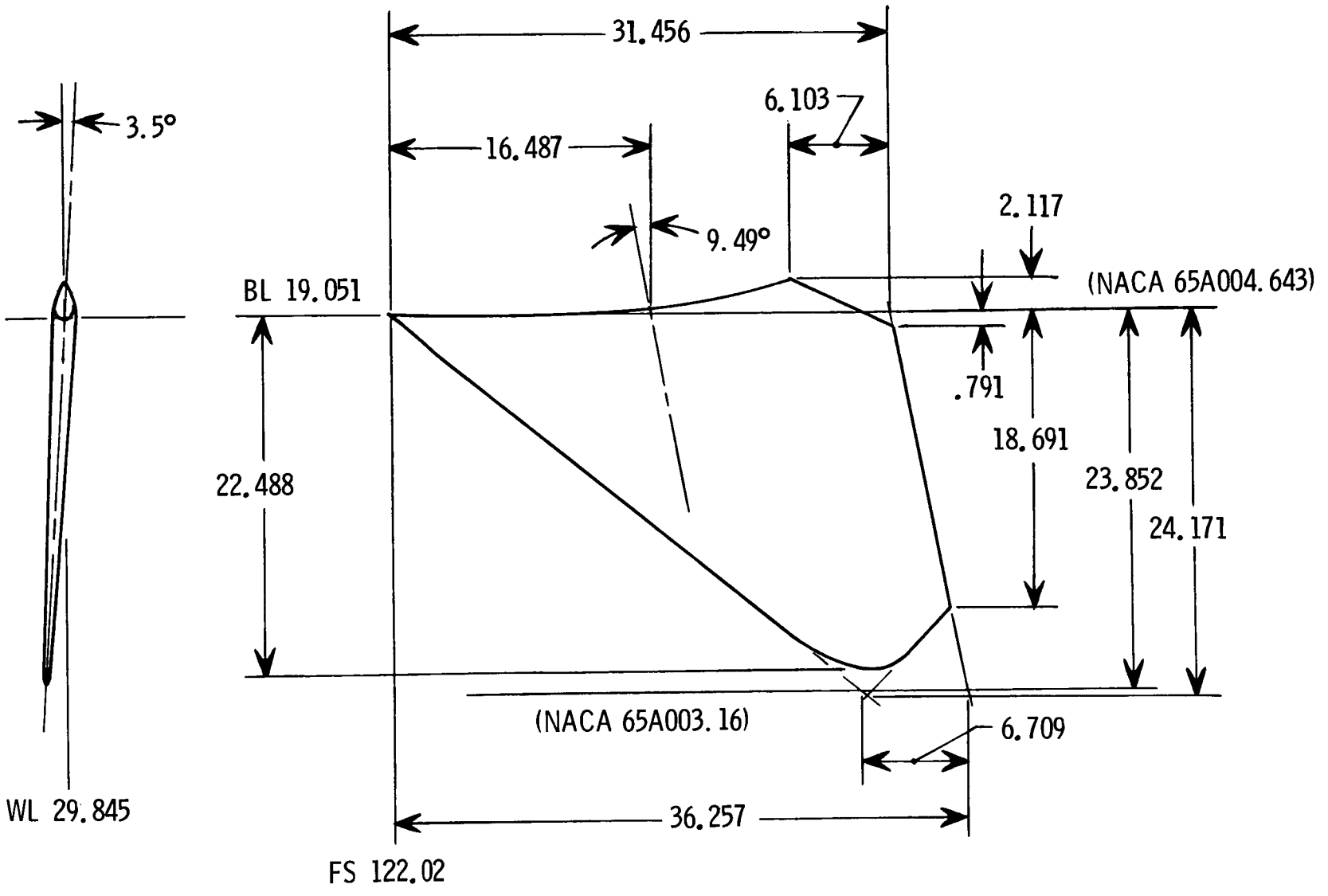

(c) Horizontal tail.

Figure 3. Continued.

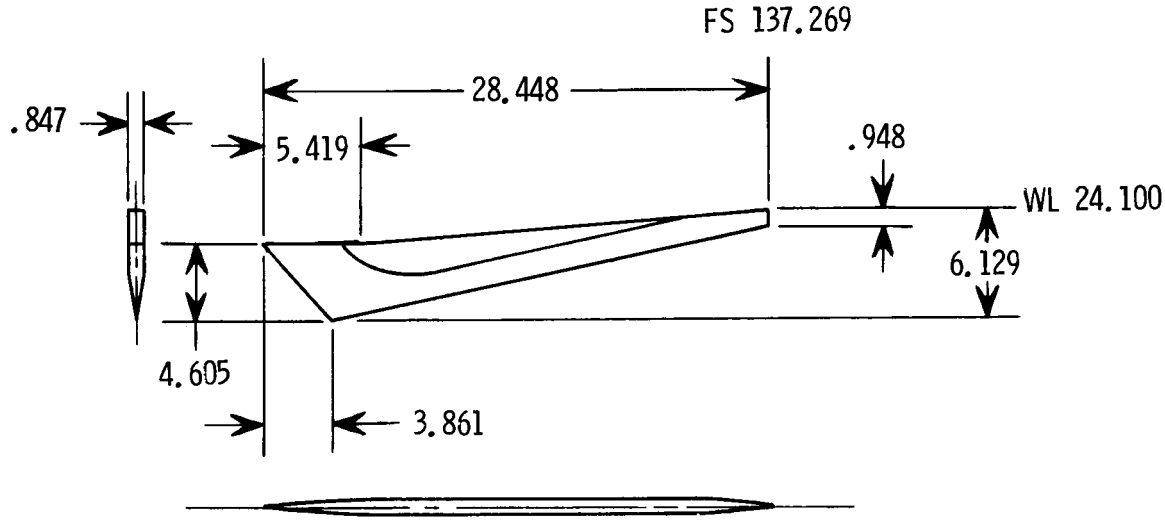

(d) Ventral fin.

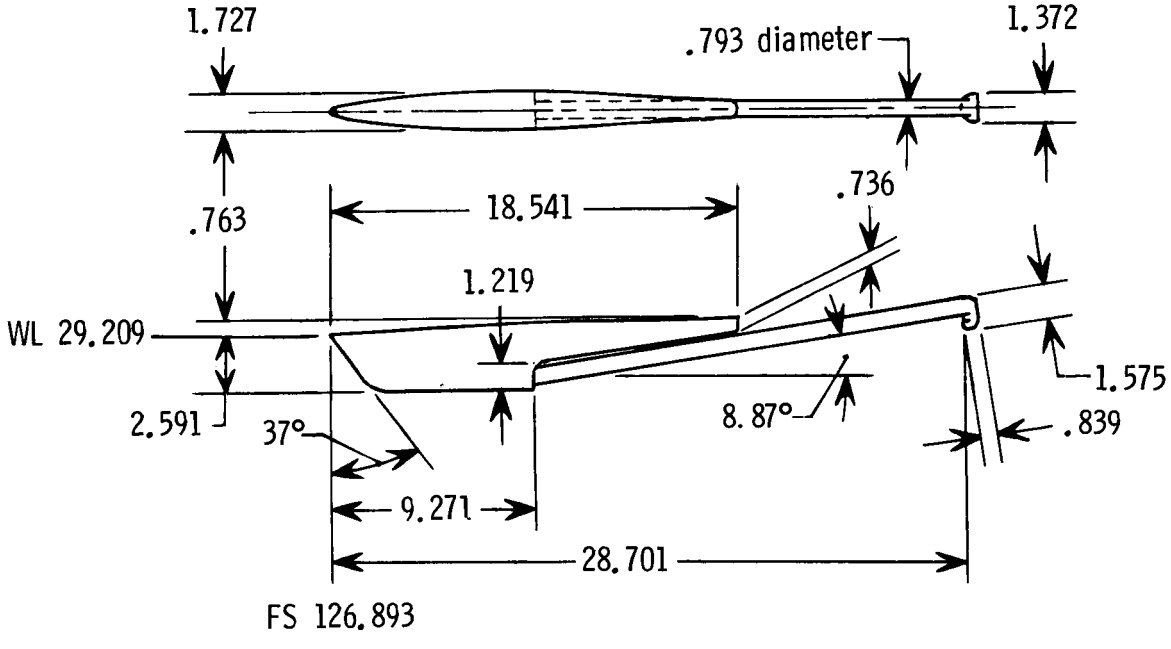

(e) Tail hook and fairing.

Figure 3. Continued.

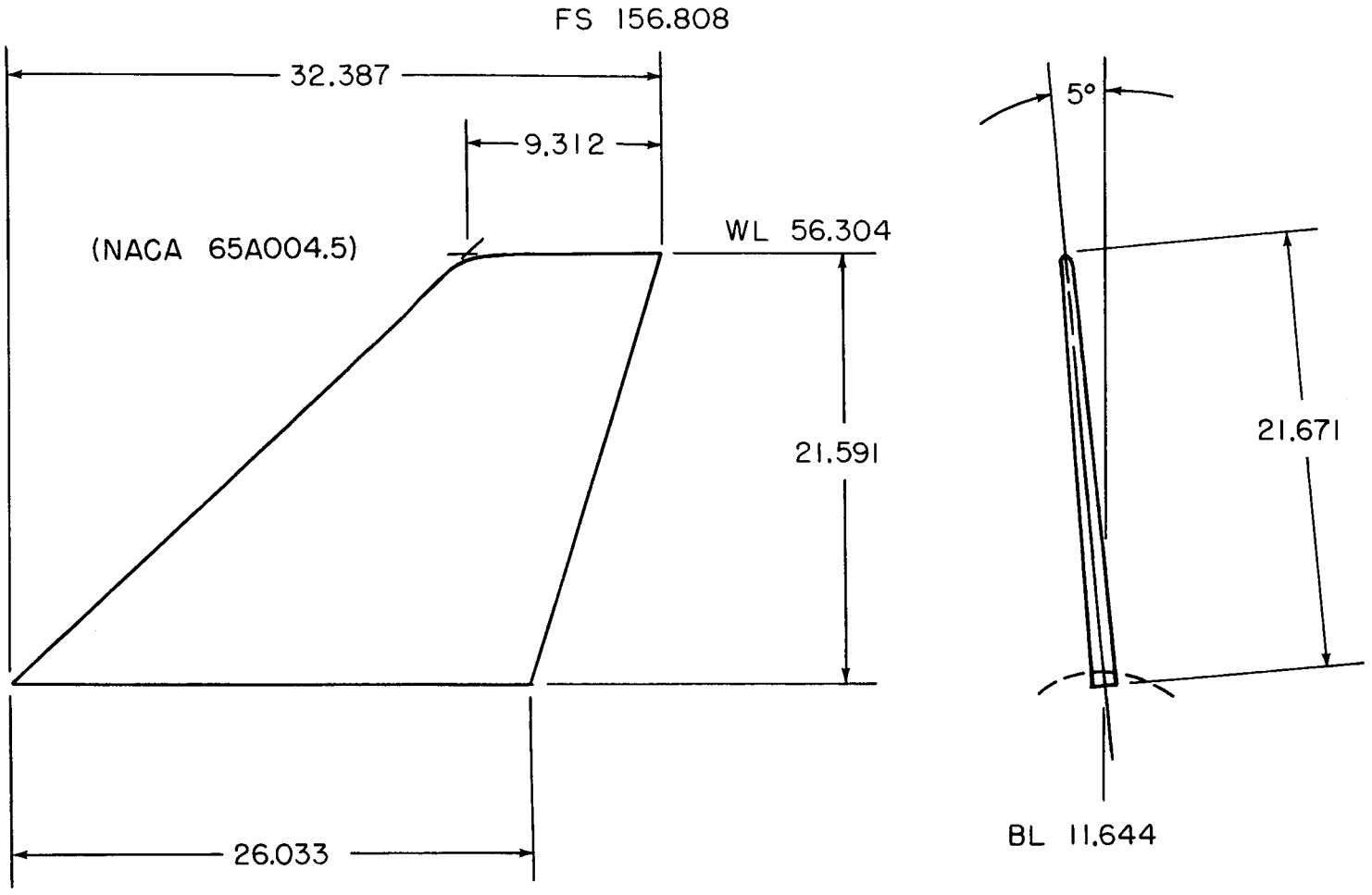

(f) Vertical tails (left tail shown).

Figure 3. Continued.

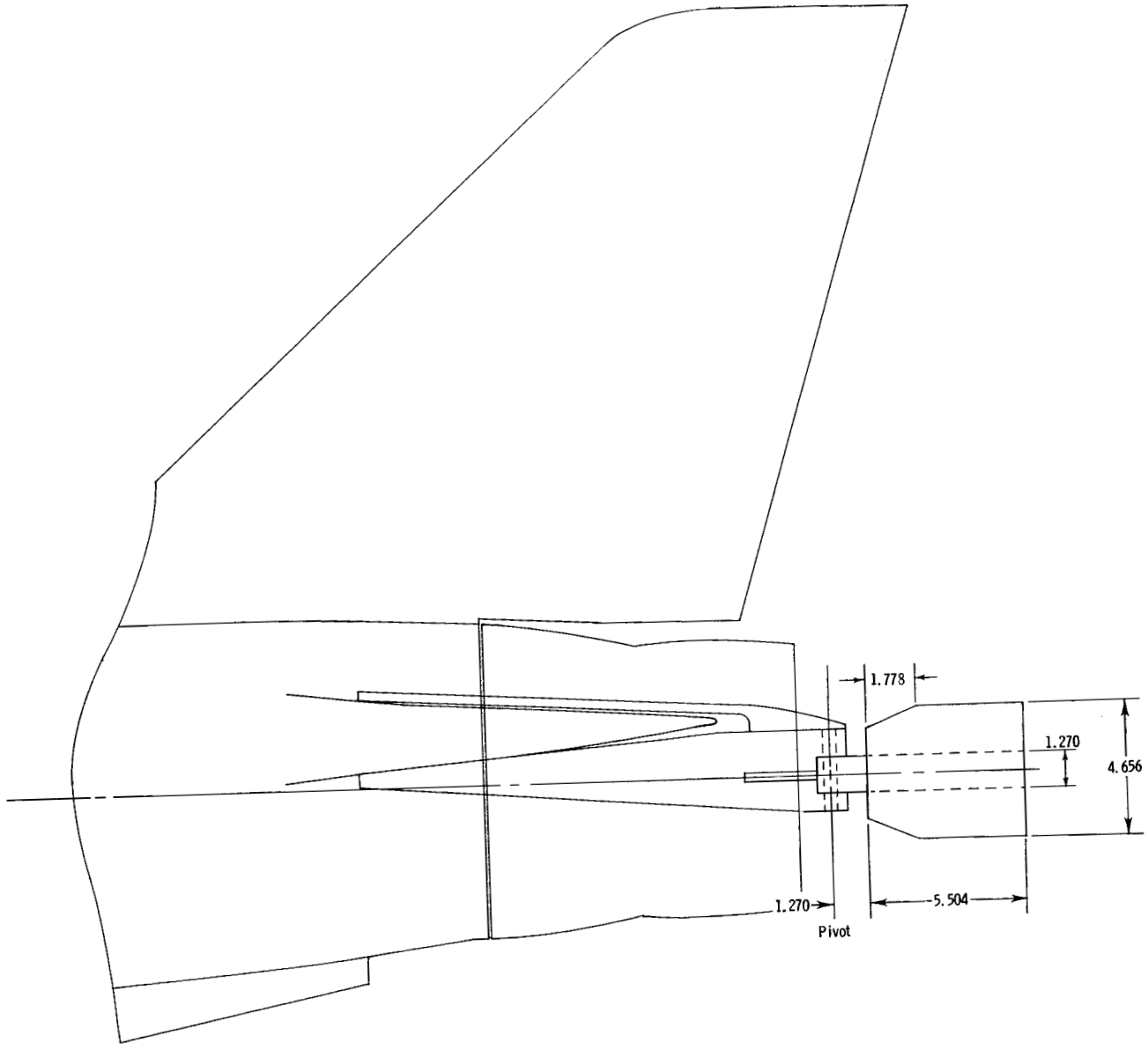

(g) Installation and details of yaw vane.

Figure 3. Continued.

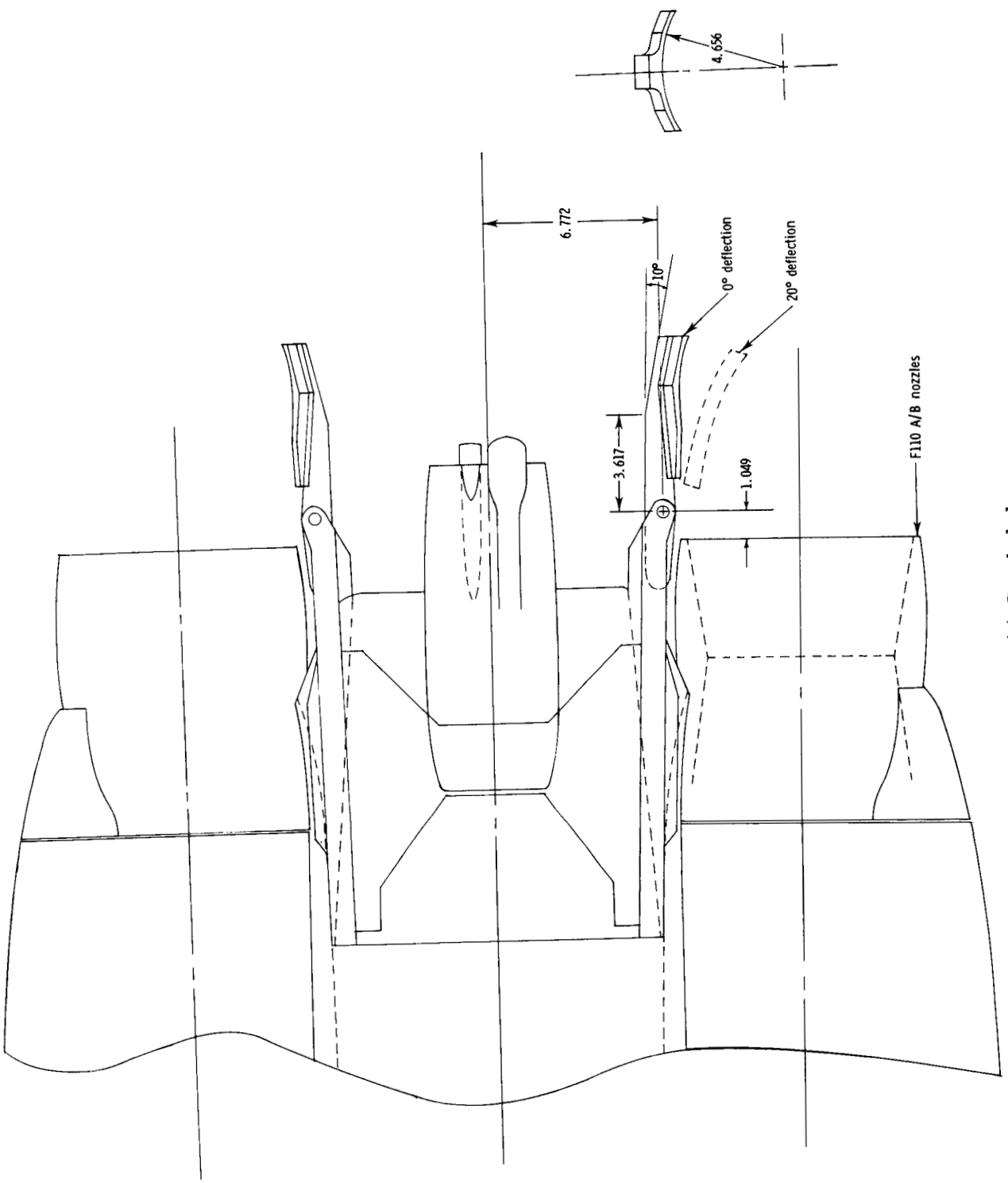

(g) Concluded.

Figure 3. Concluded.

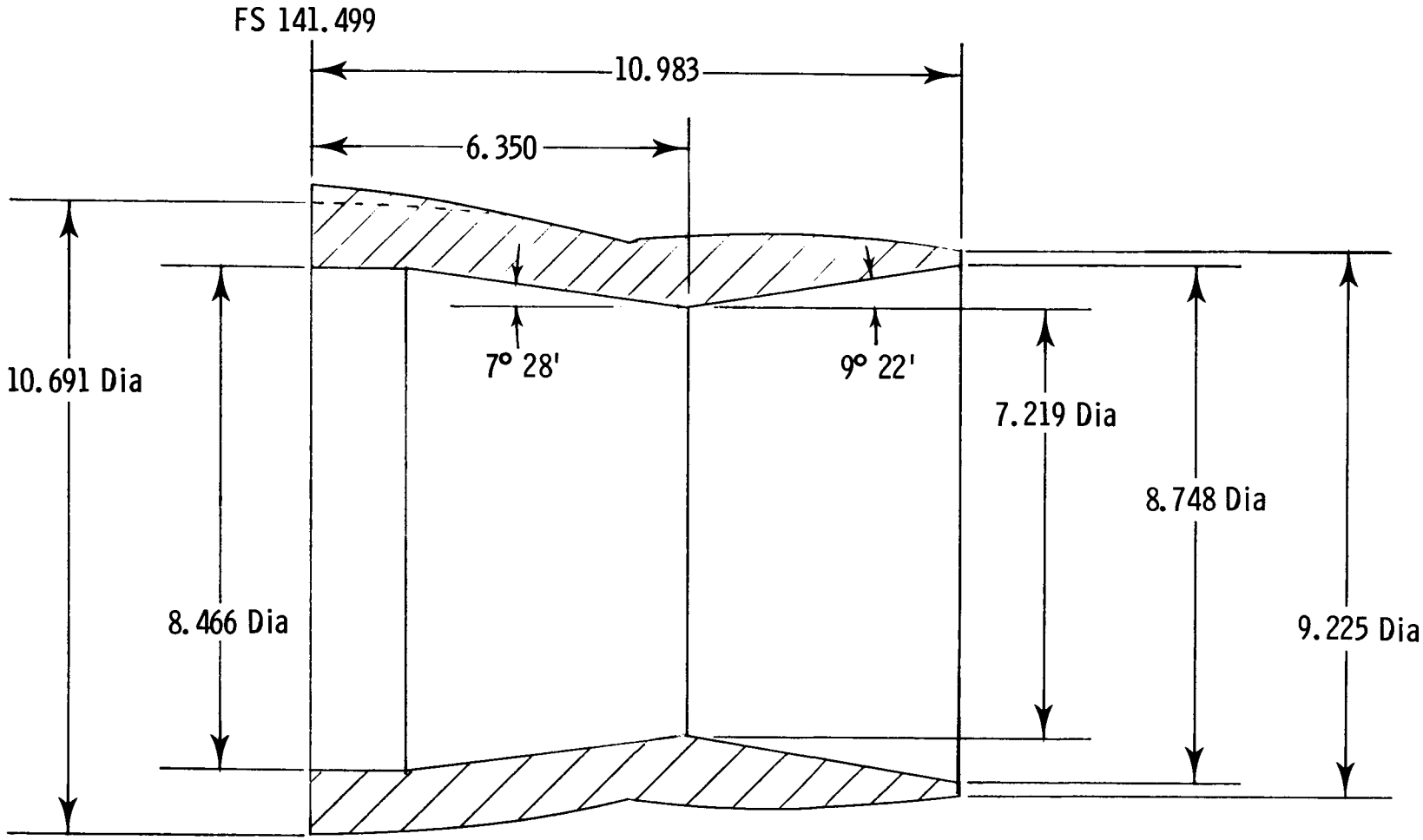

(a) F110 A/B nozzle.

Figure 4. Nozzle configurations. All dimensions are given in centimeters unless otherwise specified.

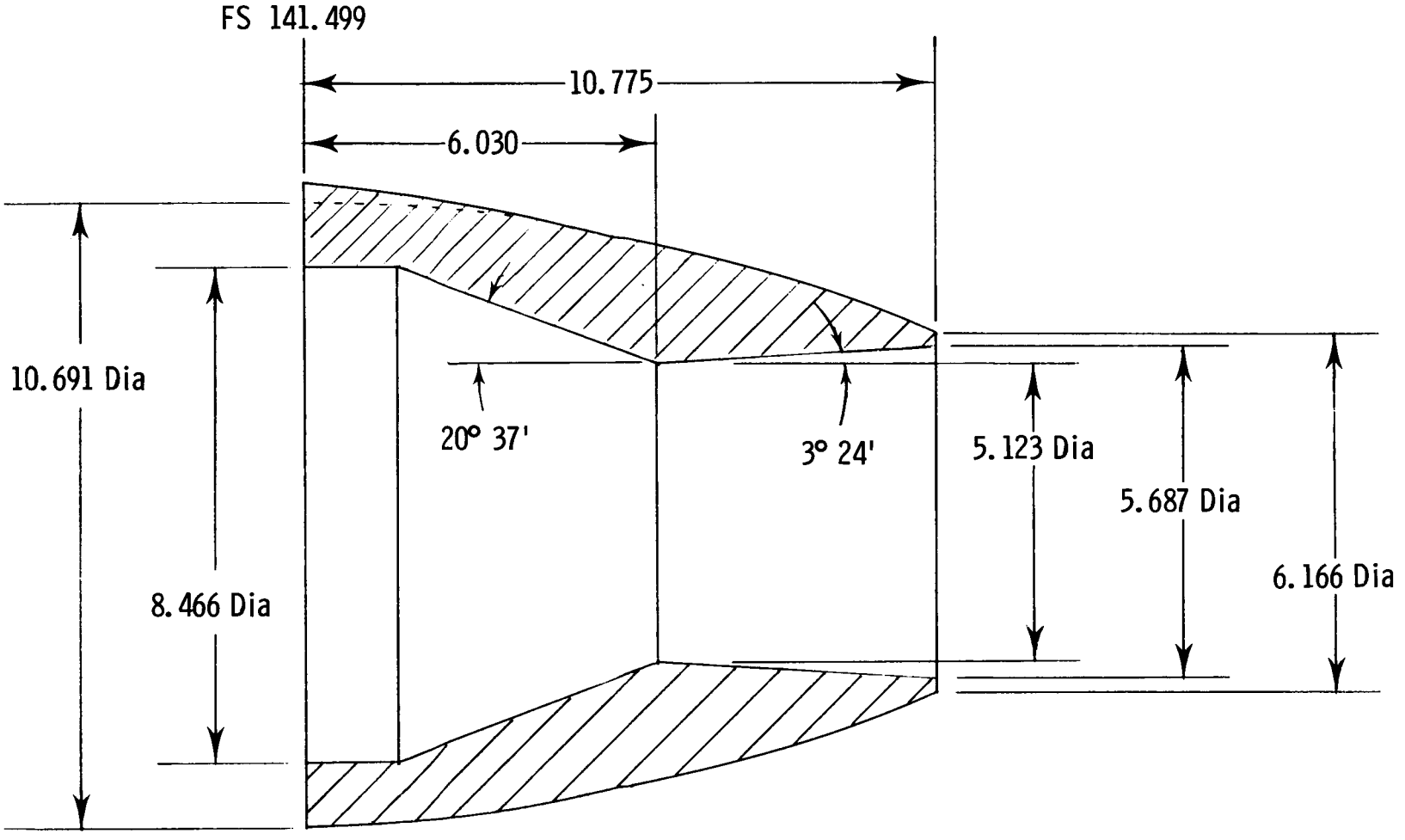

(b) F110 cruise nozzle.

Figure 4. Continued.

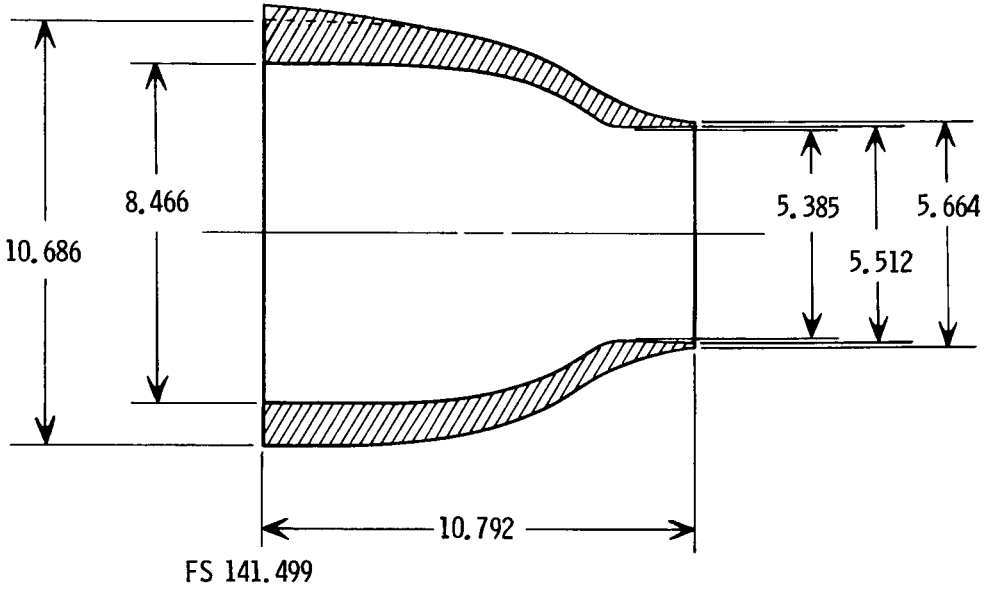

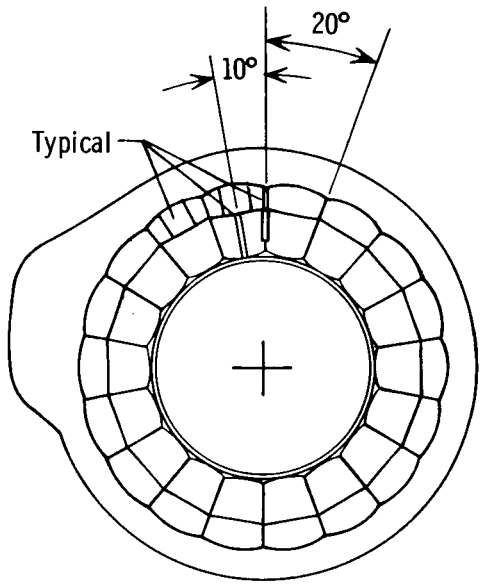

(c) TF30 cruise nozzle.

Figure 4. Concluded.

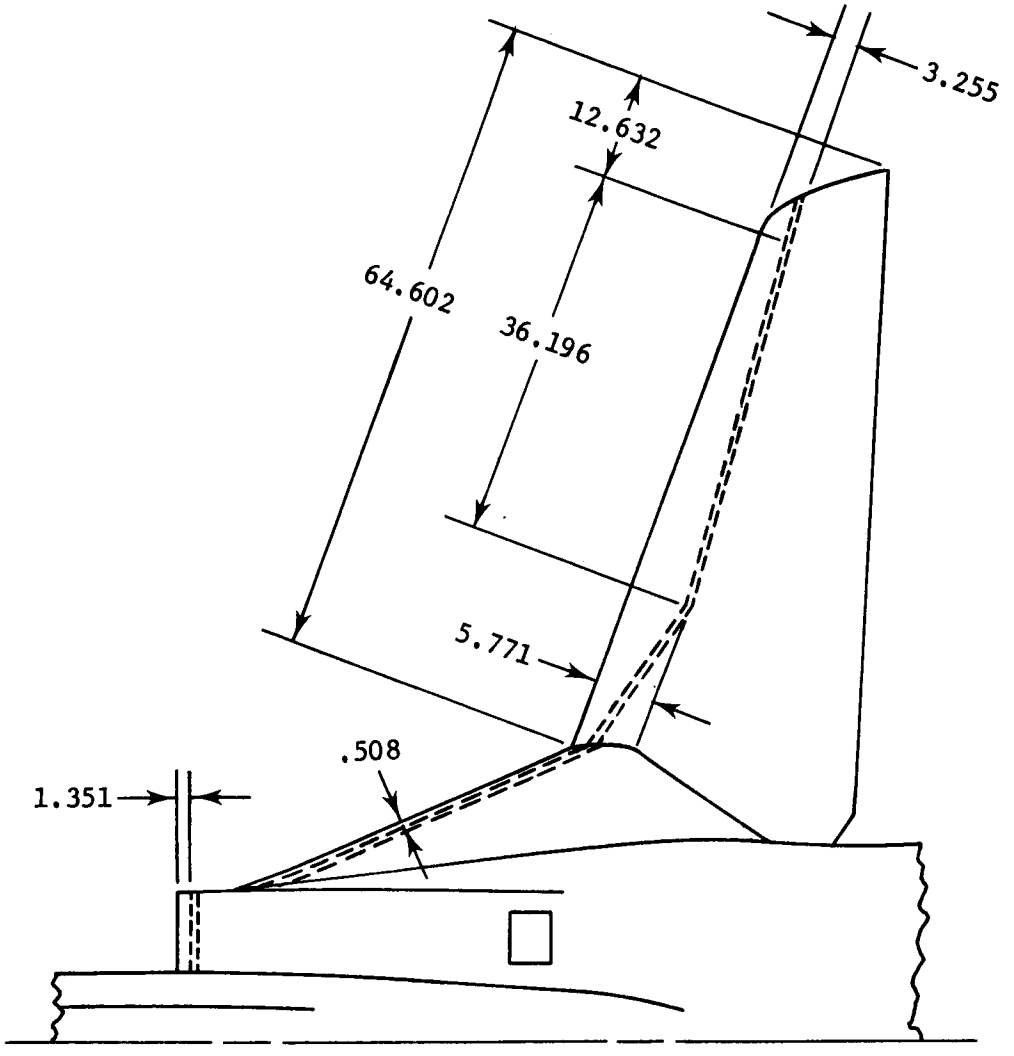

Figure 5. Sketch showing transition location on upper wing surface for configurations with $\Lambda = 22°$. All dimensions are given in centimeters.

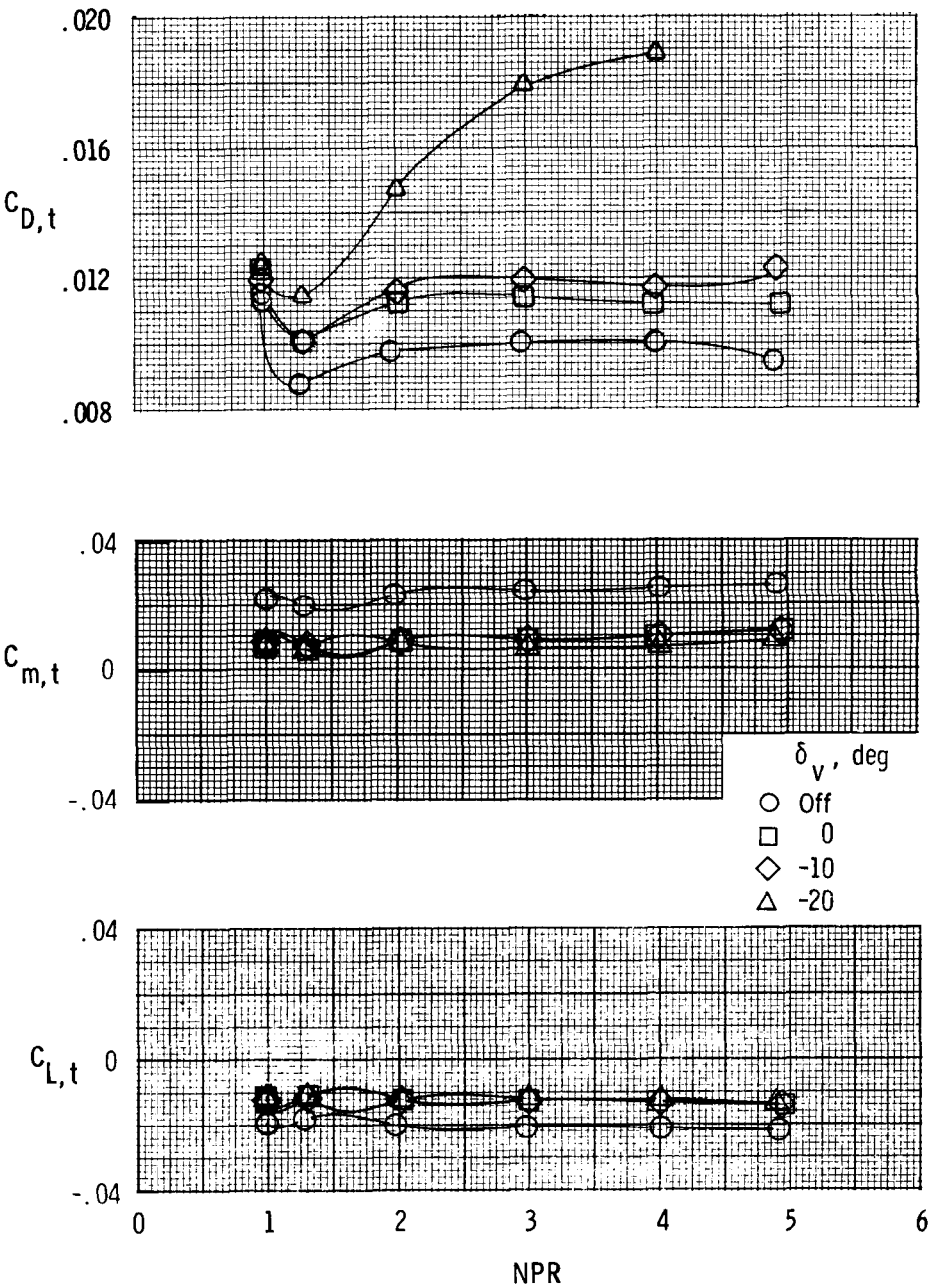

(a) Afterbody-nozzle characteristics with $M = 0.70$ and $\alpha = 0°$.

Figure 6. Afterbody and nozzle longitudinal characteristics for model with F110 A/B nozzles and yaw vanes installed. $\Lambda = 68°$; $\delta_h = 0°$.

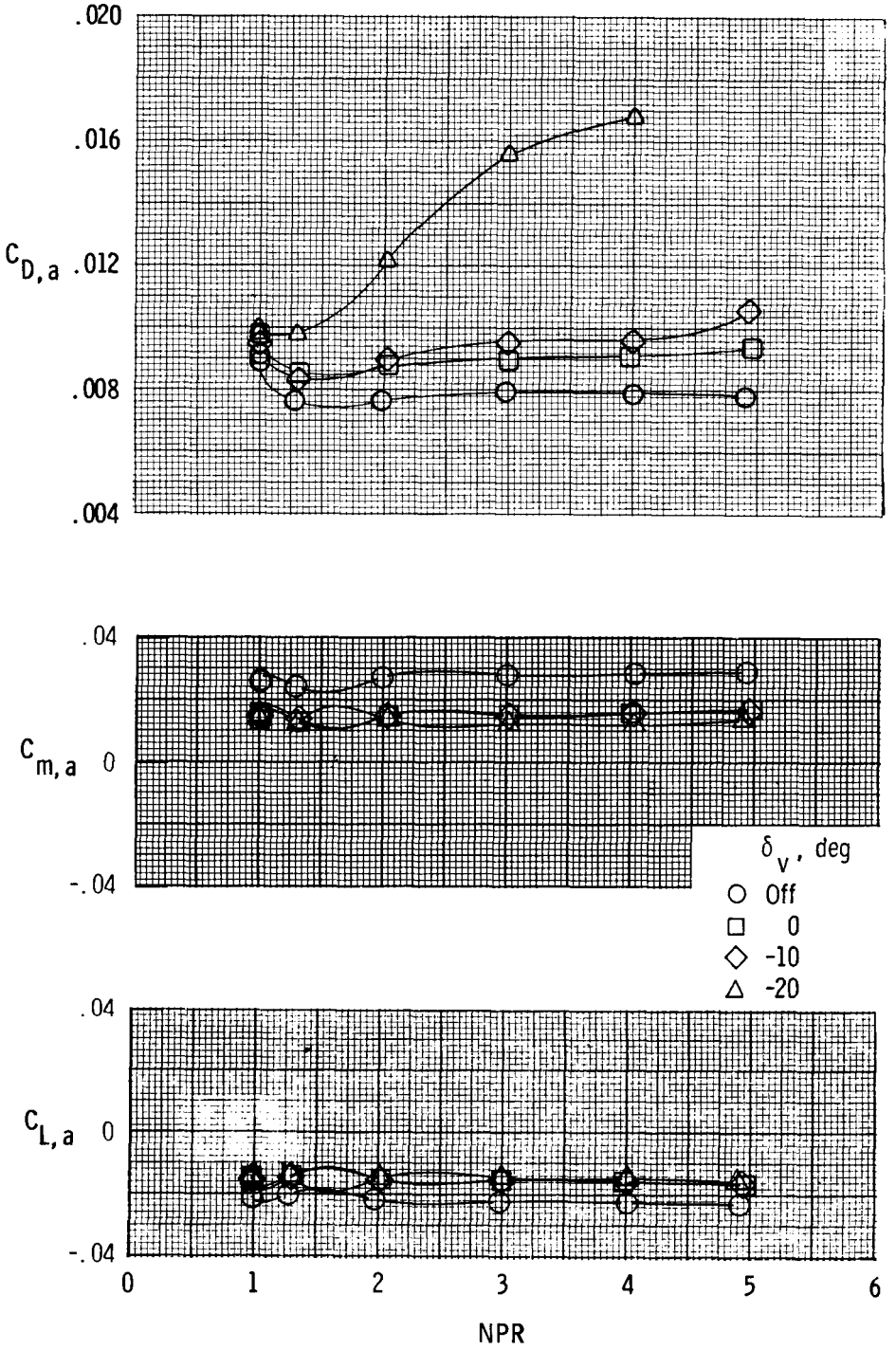

(b) Afterbody characteristics with $M = 0.70$ and $\alpha = 0°$.

Figure 6. Continued.

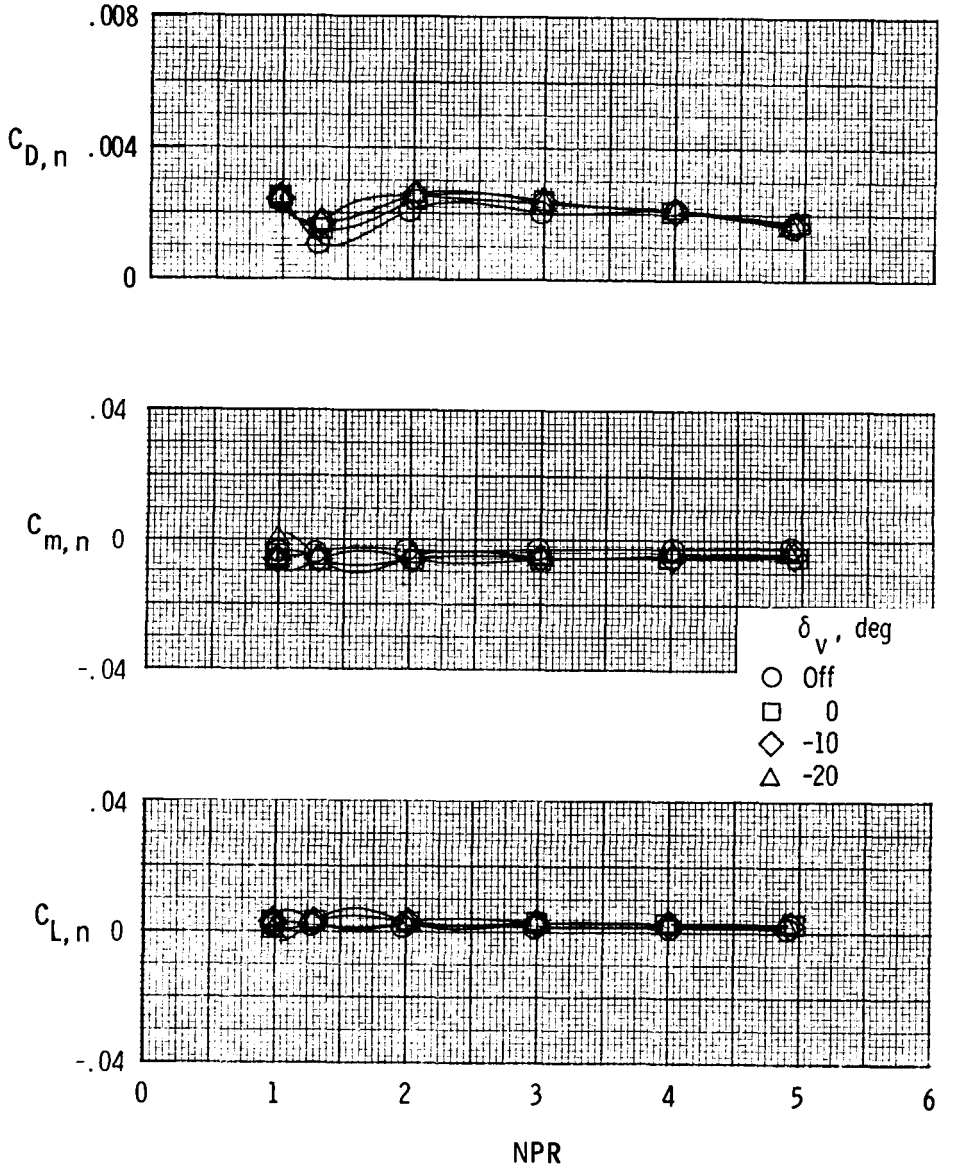

(c) Nozzle characteristics with $M = 0.70$ and $\alpha = 0°$.

Figure 6. Continued.

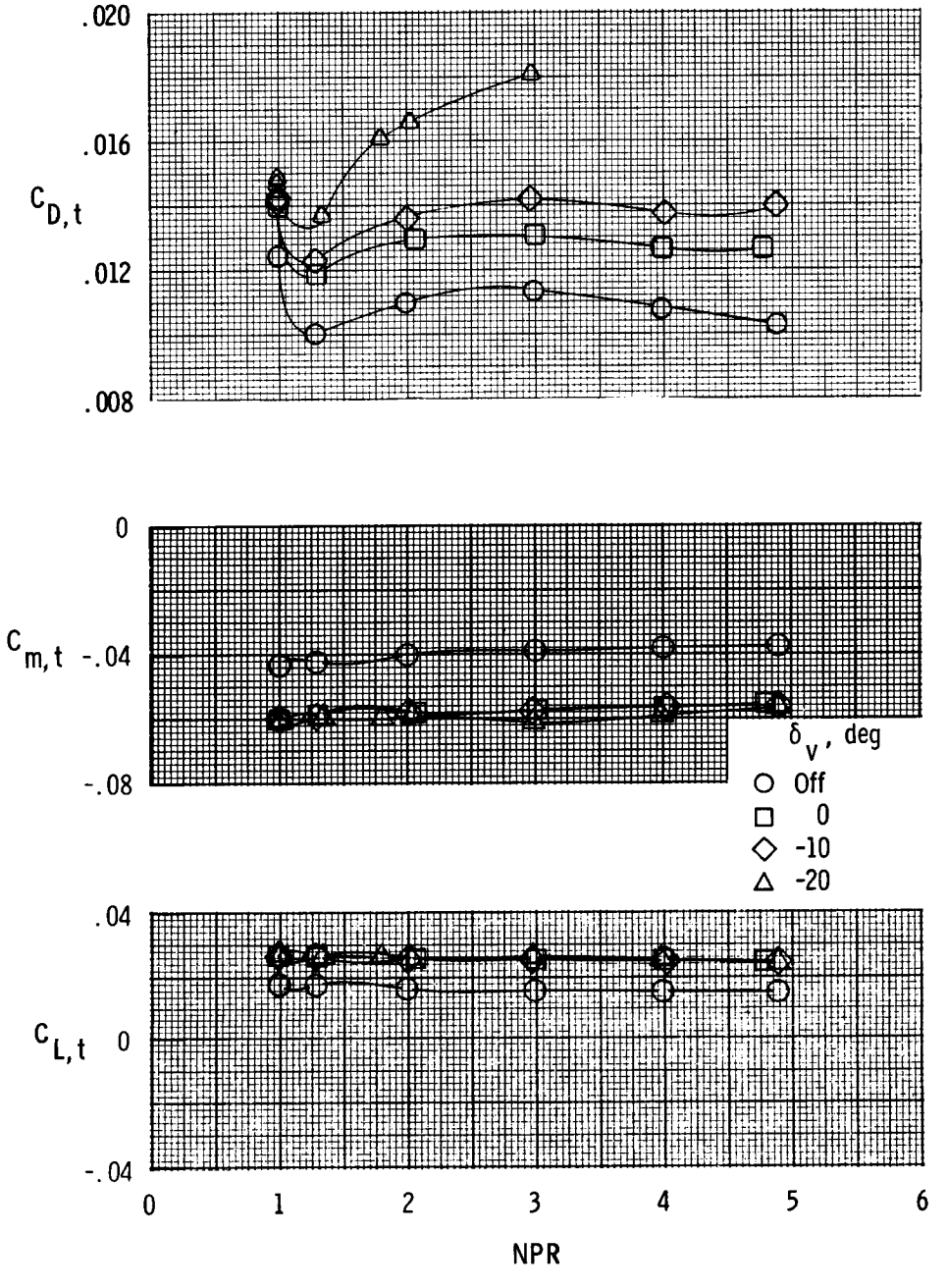

(d) Afterbody-nozzle characteristics with $M = 0.70$ and $\alpha = 4.3°$.

Figure 6. Continued.

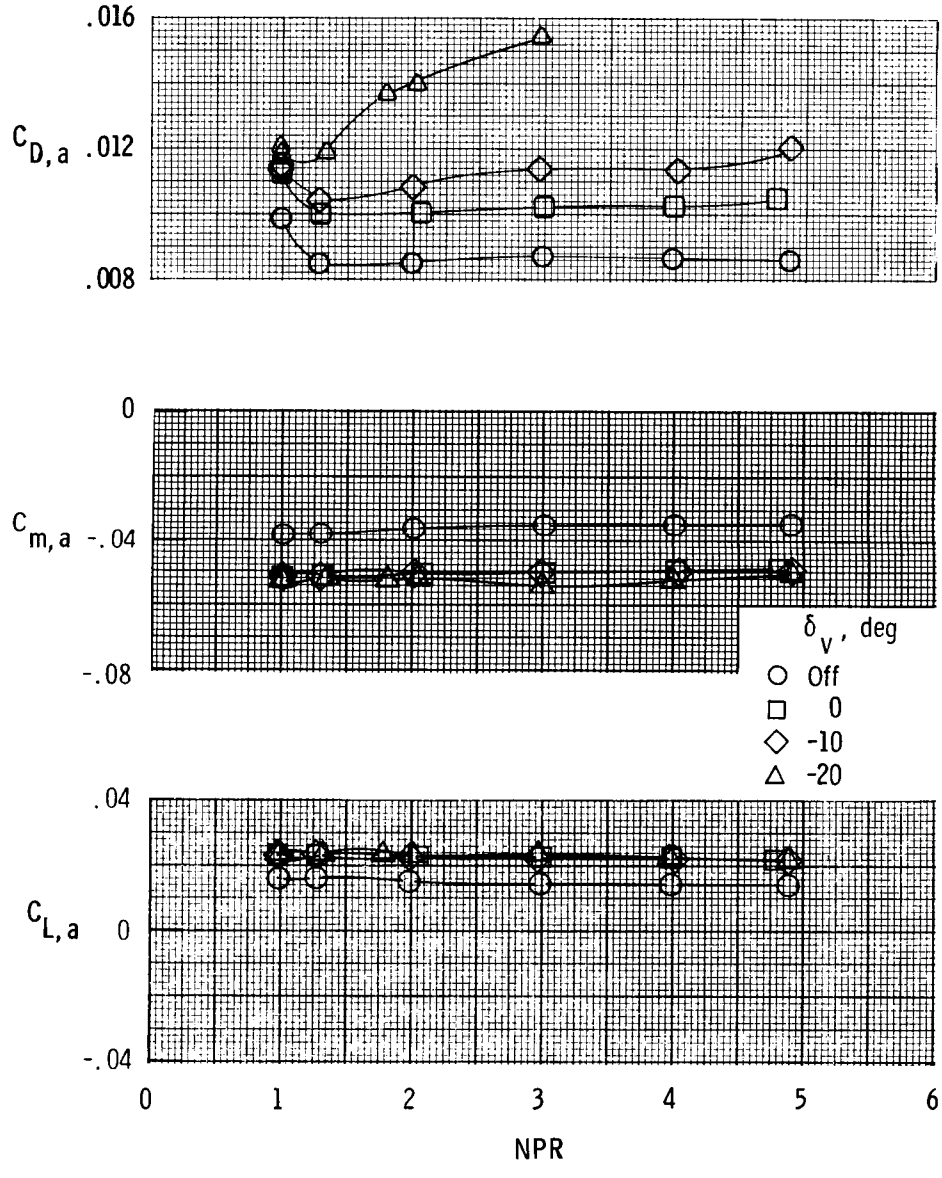

(e) Afterbody characteristics with $M = 0.70$ and $\alpha = 4.3°$.

Figure 6. Continued.

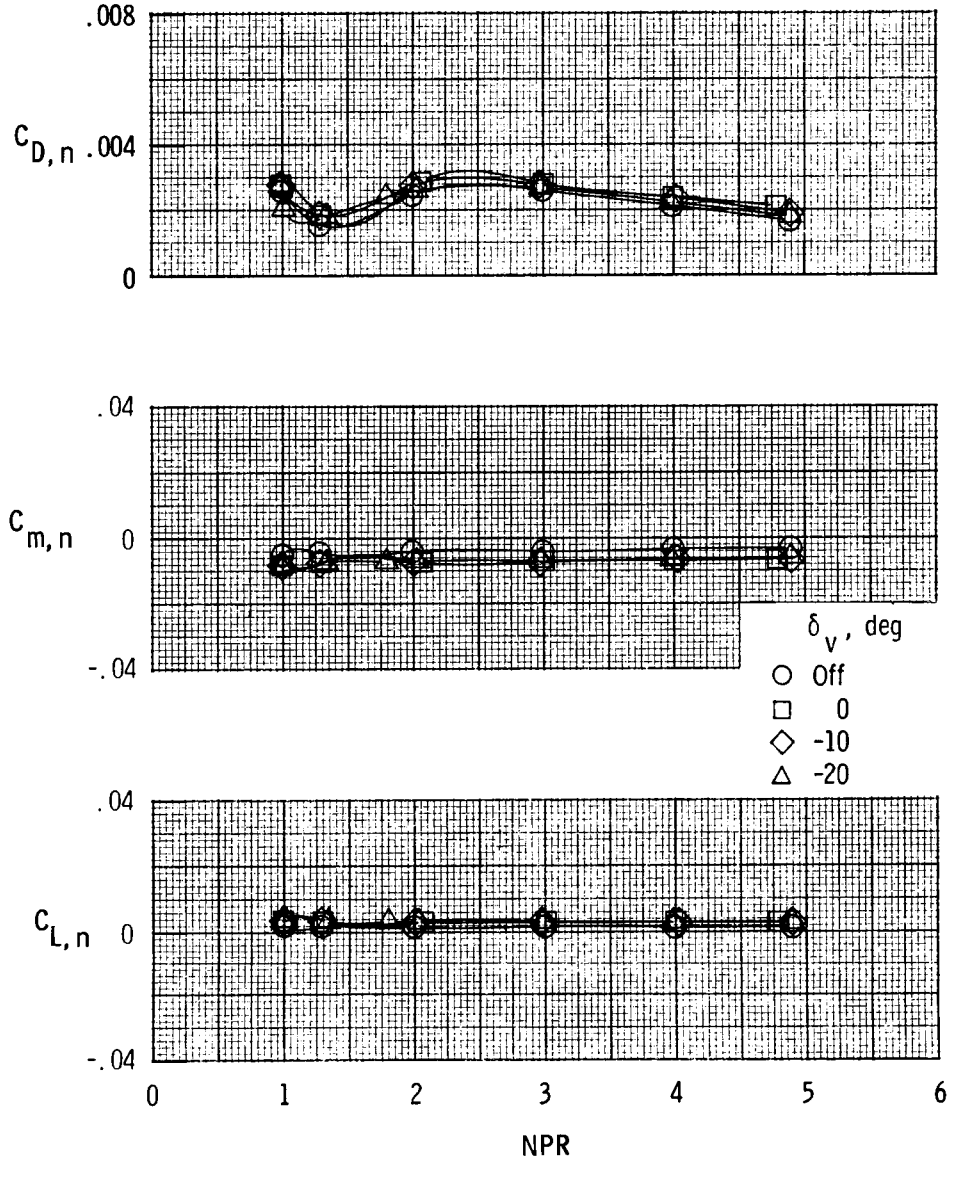

(f) Nozzle characteristics with $M = 0.70$ and $\alpha = 4.3°$.

Figure 6. Continued.

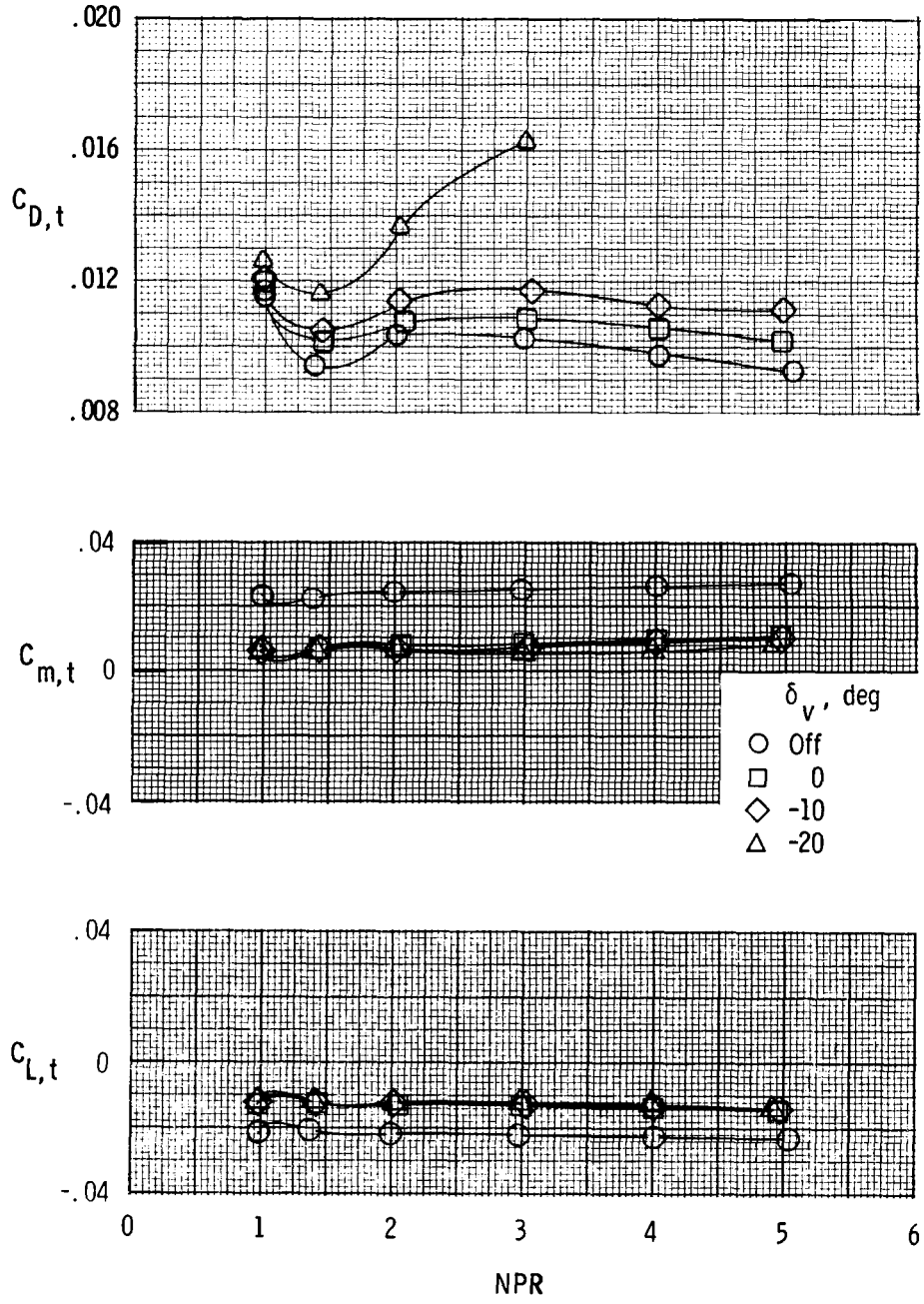

(g) Afterbody-nozzle characteristics with $M = 0.80$ and $\alpha = 0°$.

Figure 6. Continued.

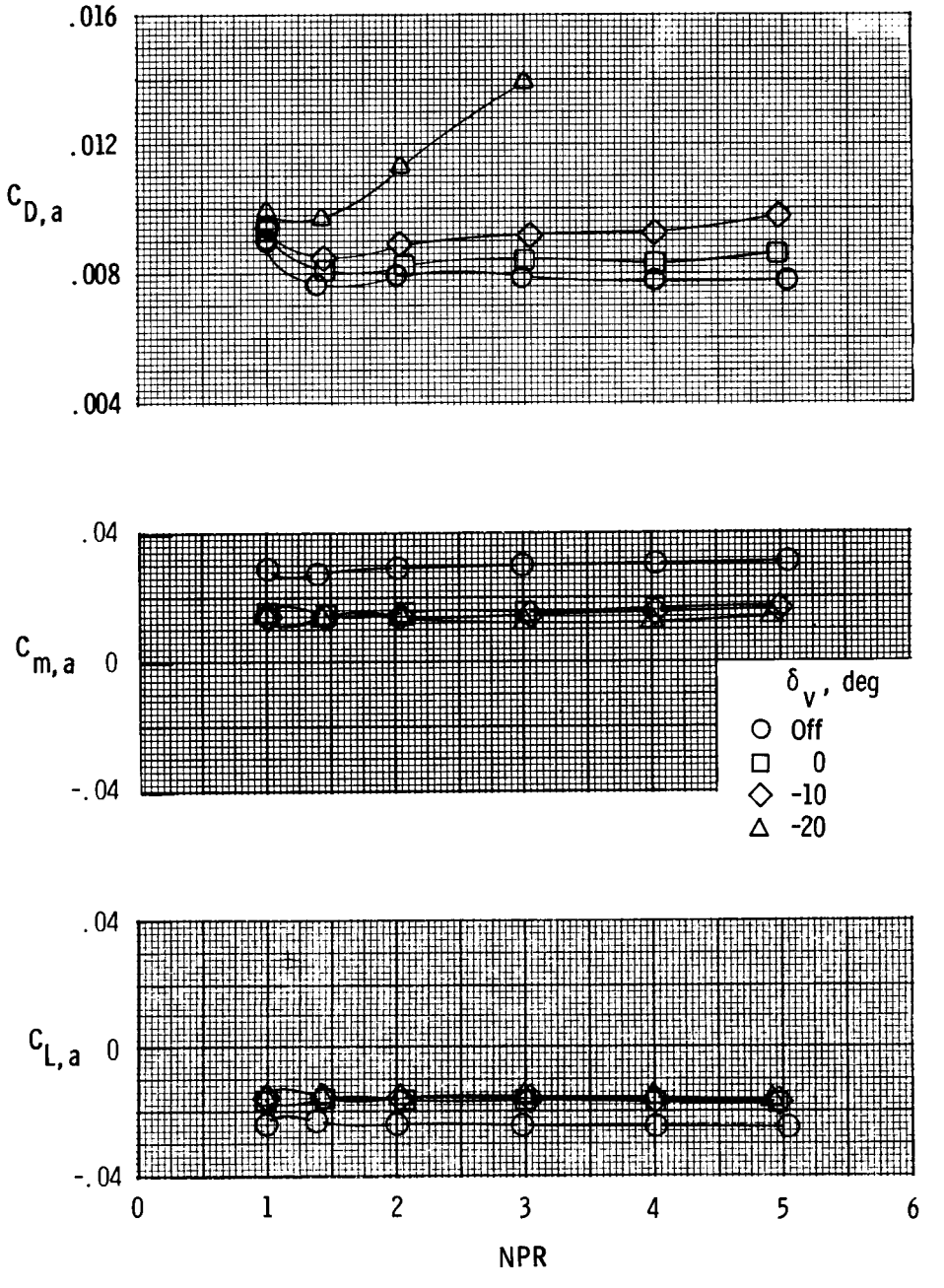

(h) Afterbody characteristics with $M = 0.80$ and $\alpha = 0°$.

Figure 6. Continued.

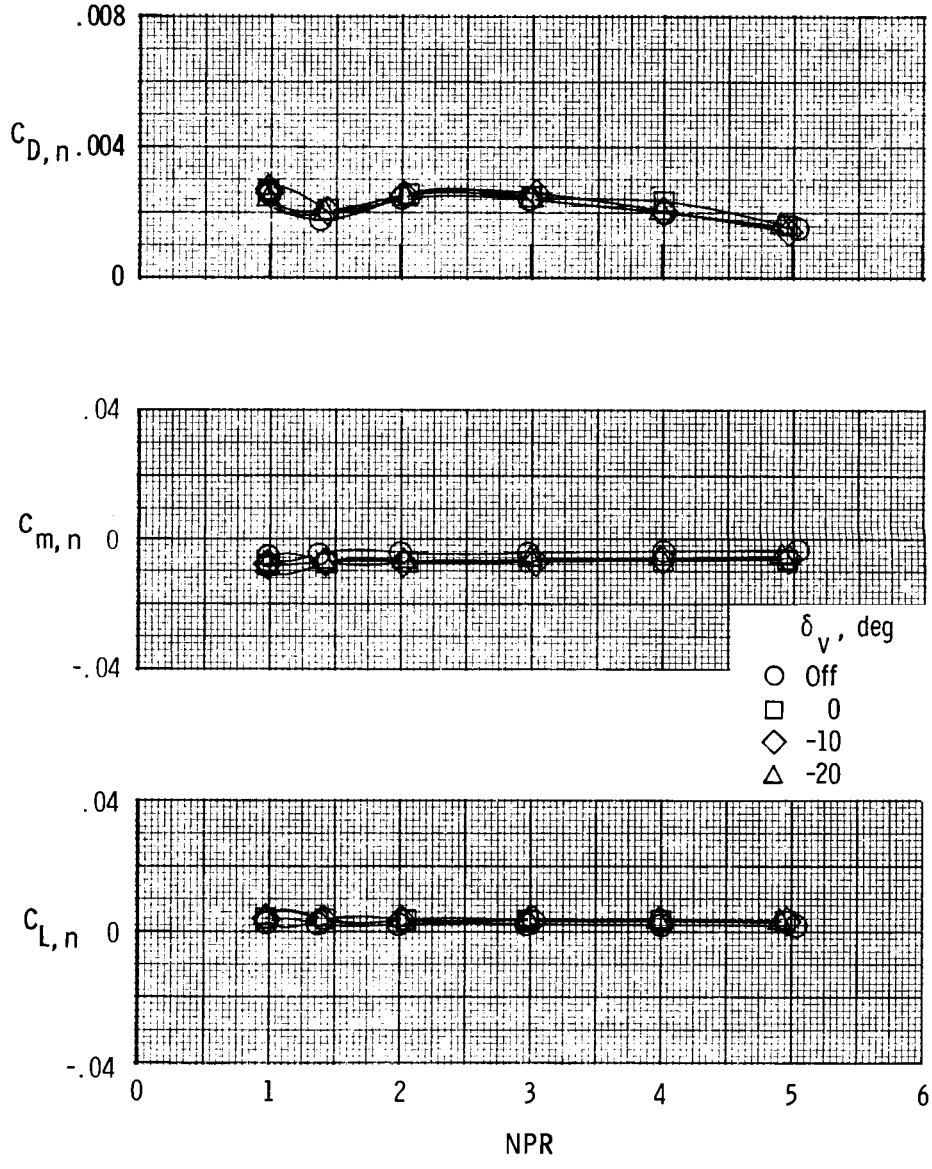

(i) Nozzle characteristics with $M = 0.80$ and $\alpha = 0°$.

Figure 6. Continued.

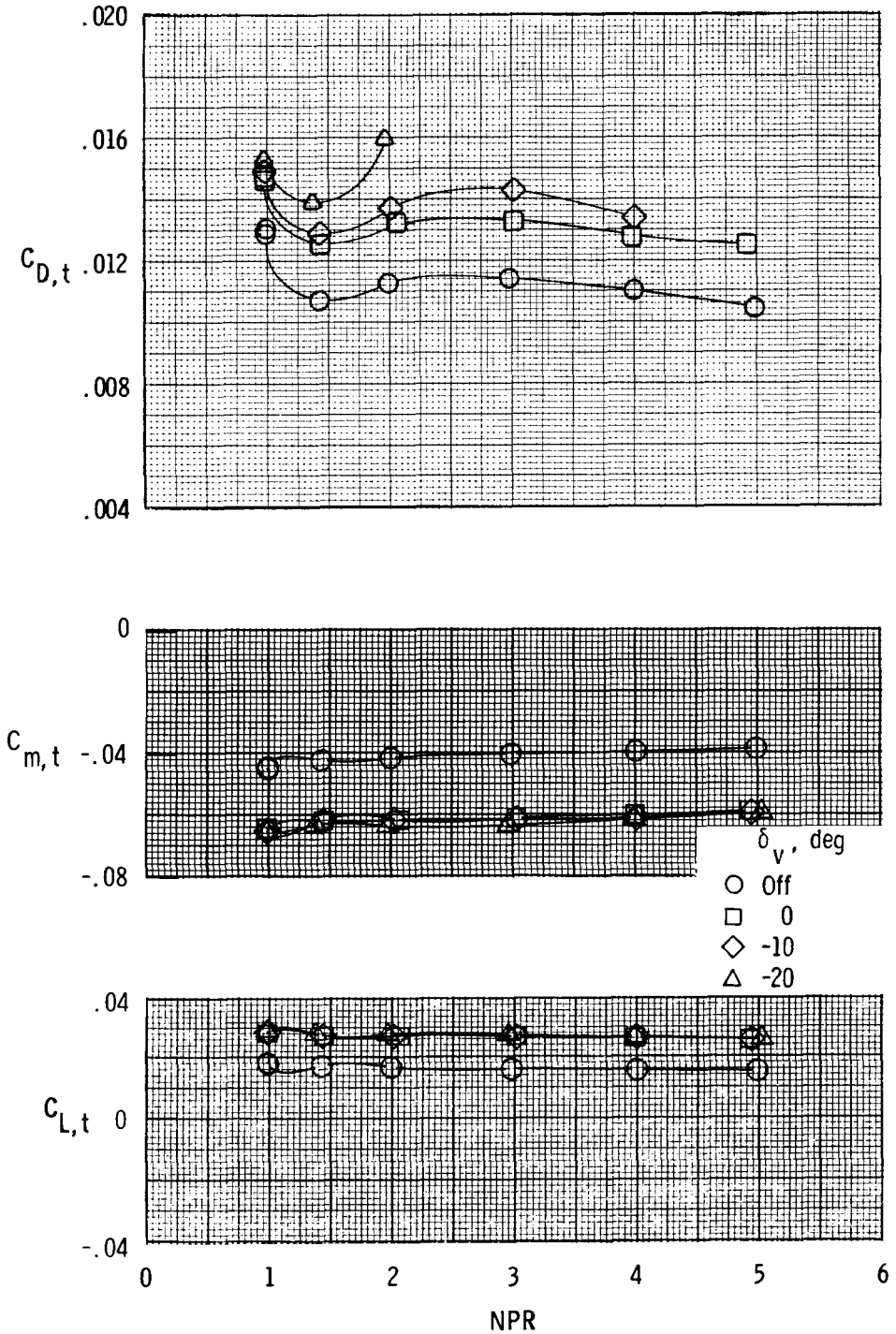

(j) Afterbody-nozzle characteristics with $M = 0.80$ and $\alpha = 4.3°$.

Figure 6. Continued.

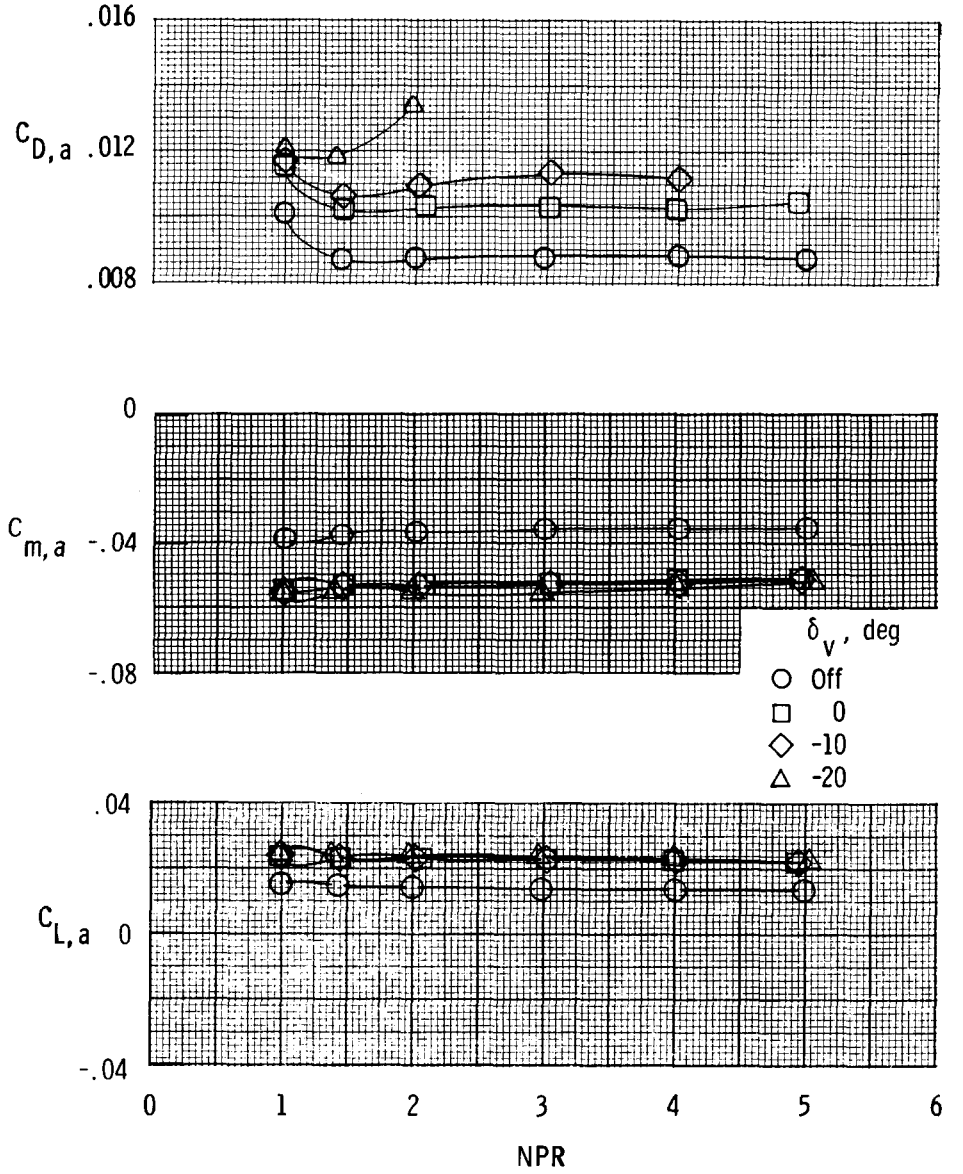

(k) Afterbody characteristics with $M = 0.80$ and $\alpha = 4.3°$.

Figure 6. Continued.

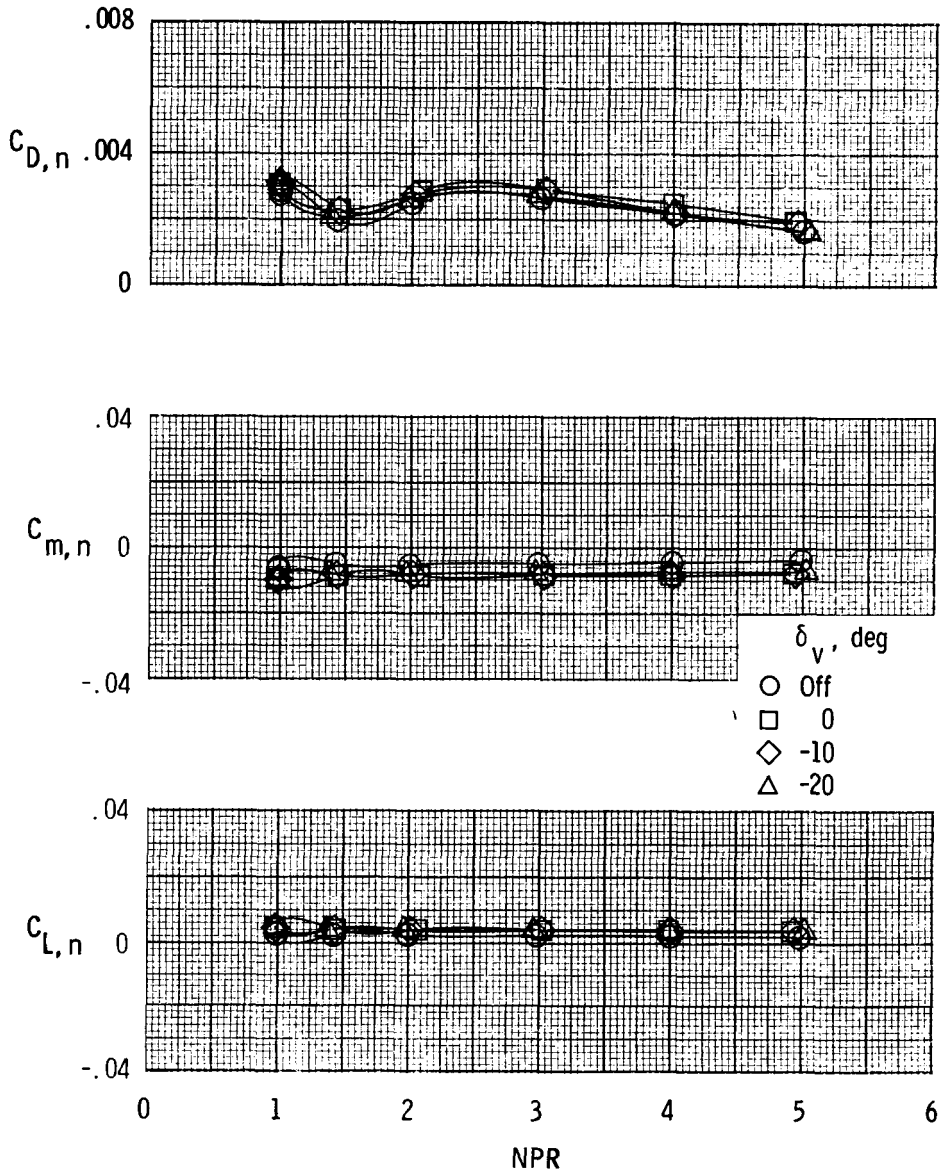

(l) Nozzle characteristics with $M = 0.80$ and $\alpha = 4.3°$.

Figure 6. Continued.

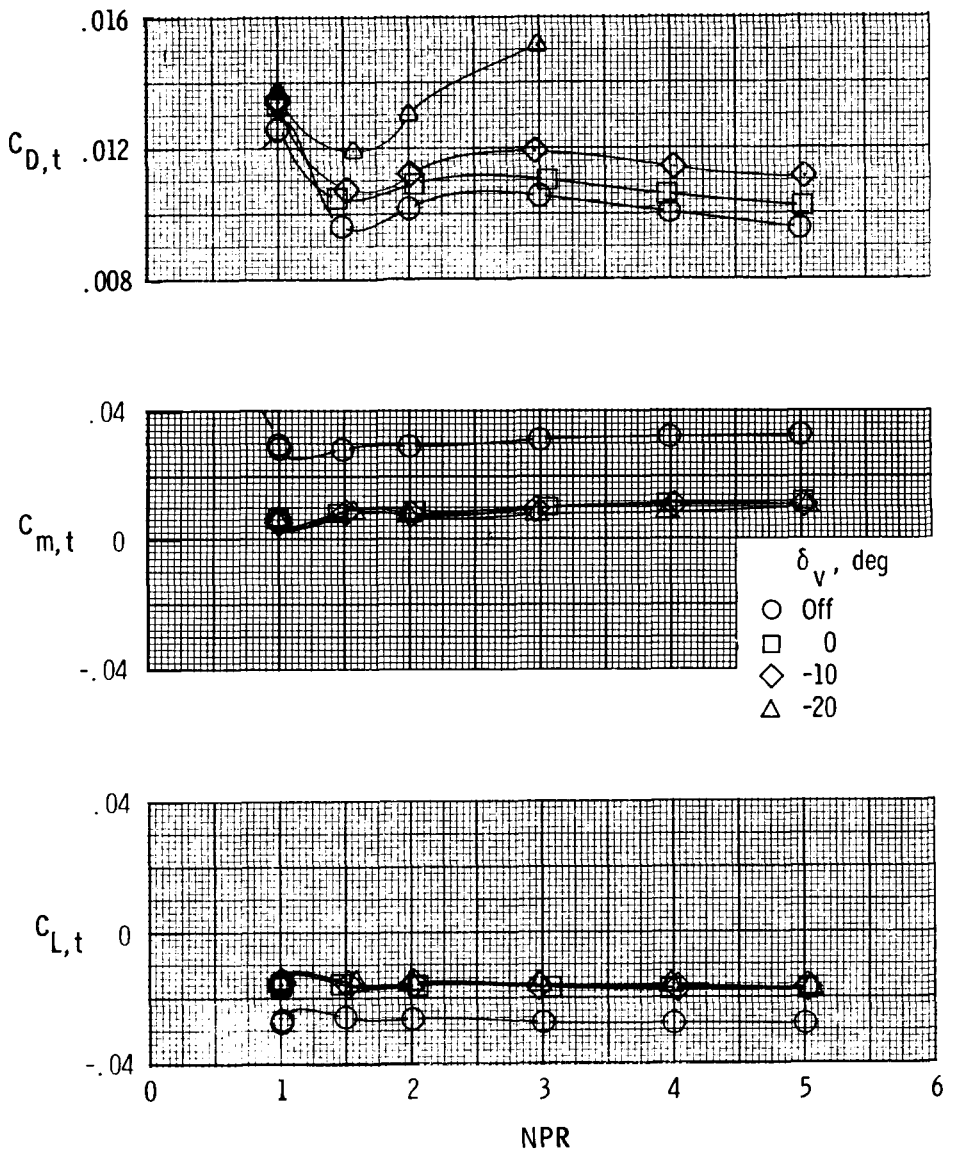

(m) Afterbody-nozzle characteristics with $M = 0.90$ and $\alpha = 0°$.

Figure 6. Continued.

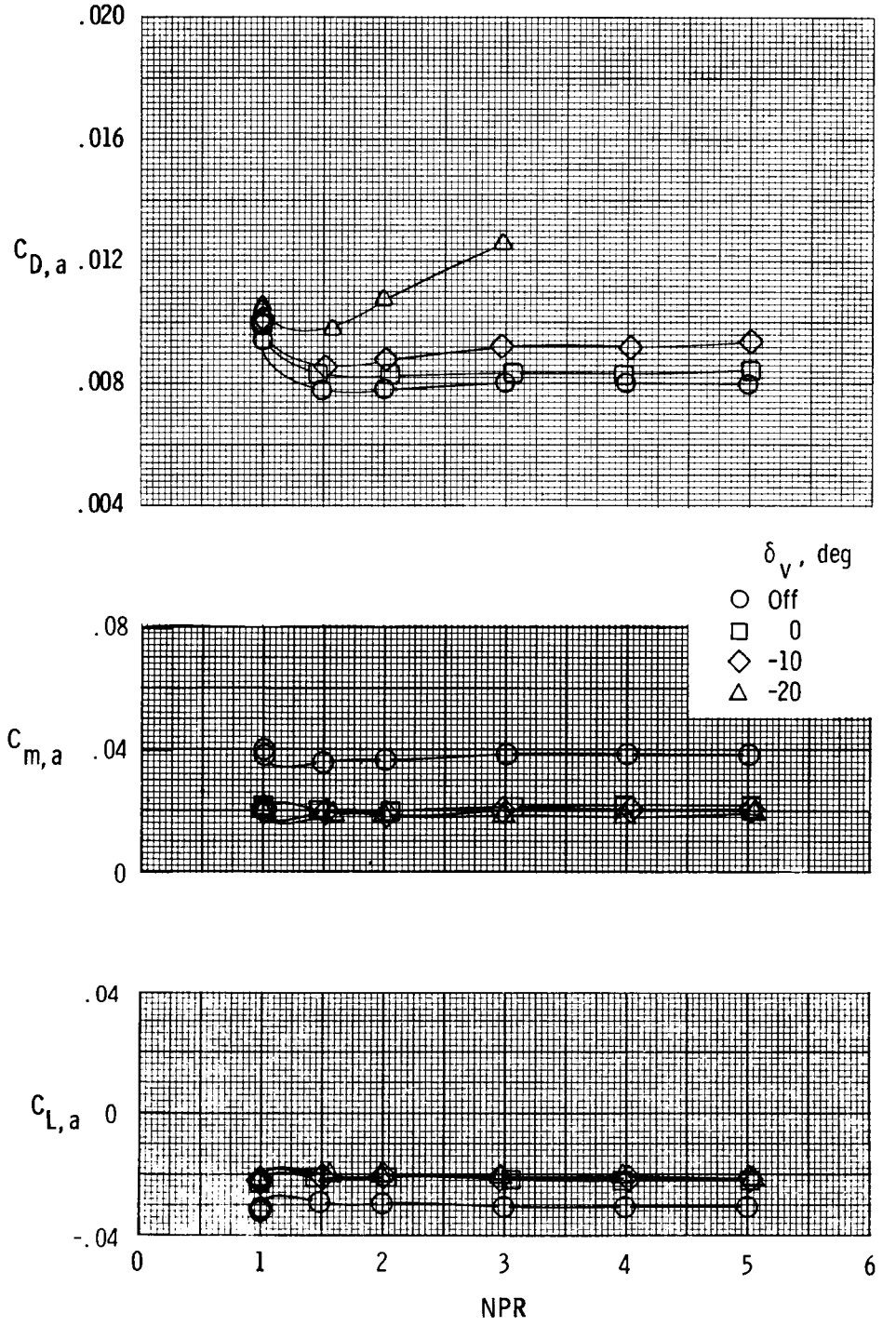

(n) Afterbody characteristics with $M = 0.90$ and $\alpha = 0°$.

Figure 6. Continued.

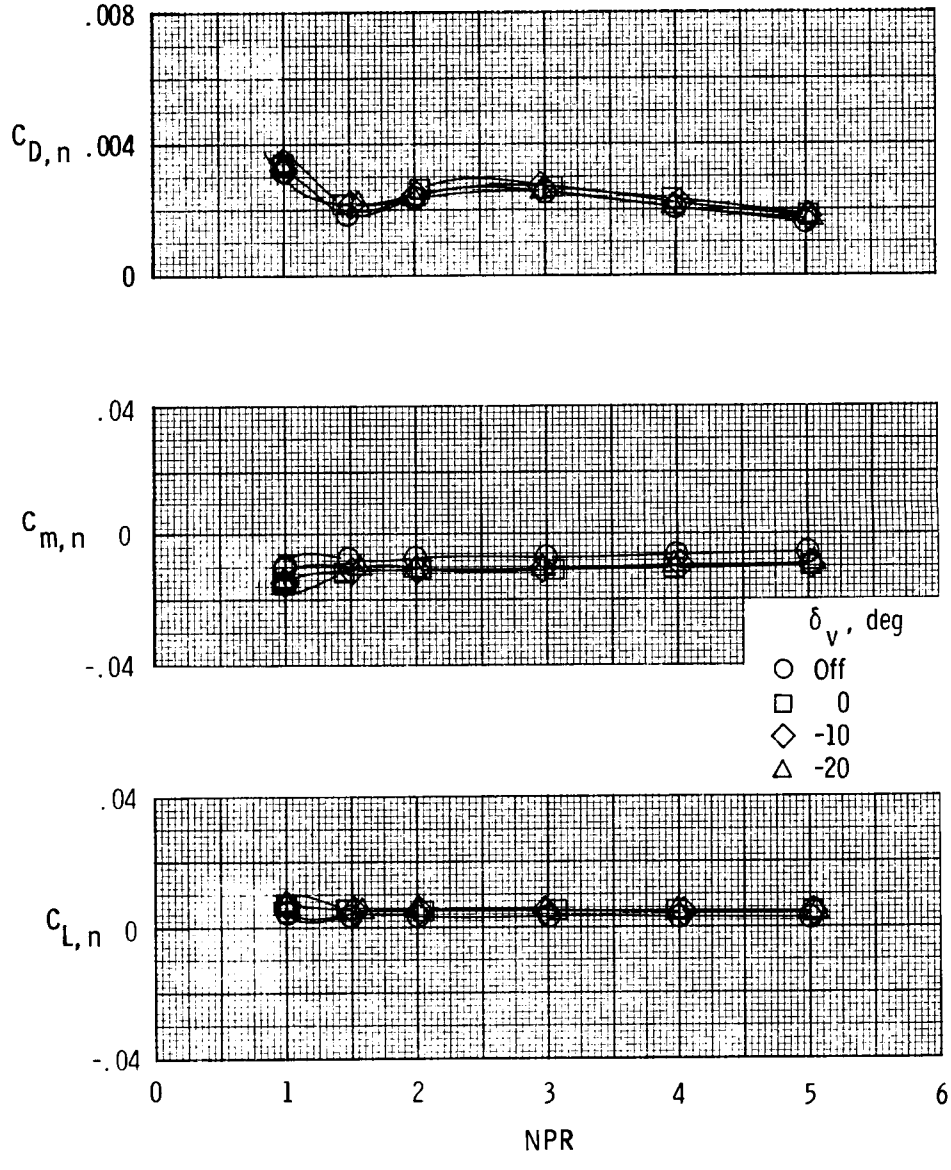

(o) Nozzle characteristics with $M = 0.90$ and $\alpha = 0°$.

Figure 6. Continued.

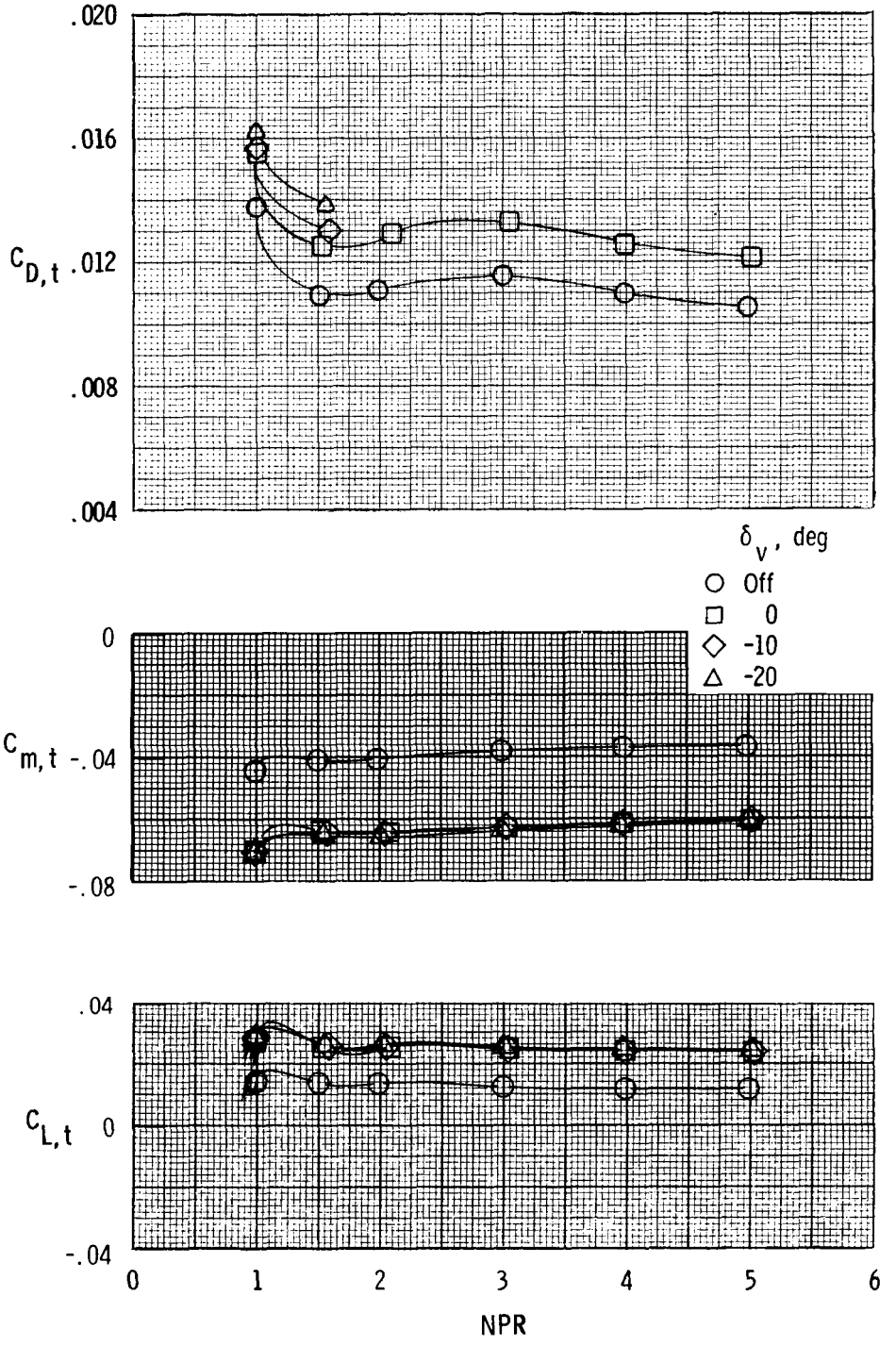

(p) Afterbody-nozzle characteristics with $M = 0.90$ and $\alpha = 4.3°$.

Figure 6. Continued.

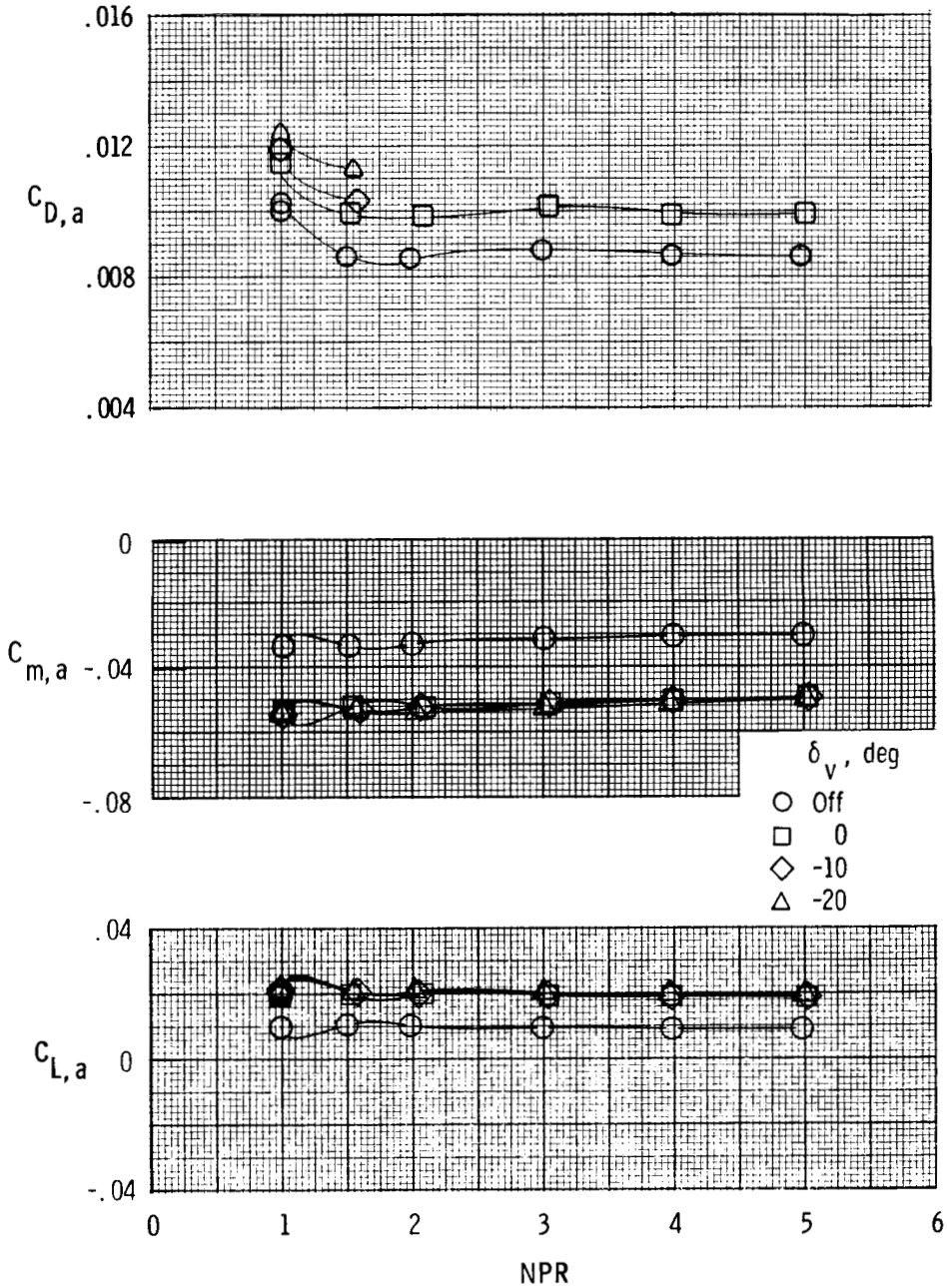

(q) Afterbody characteristics with $M = 0.90$ and $\alpha = 4.3°$.

Figure 6. Continued.

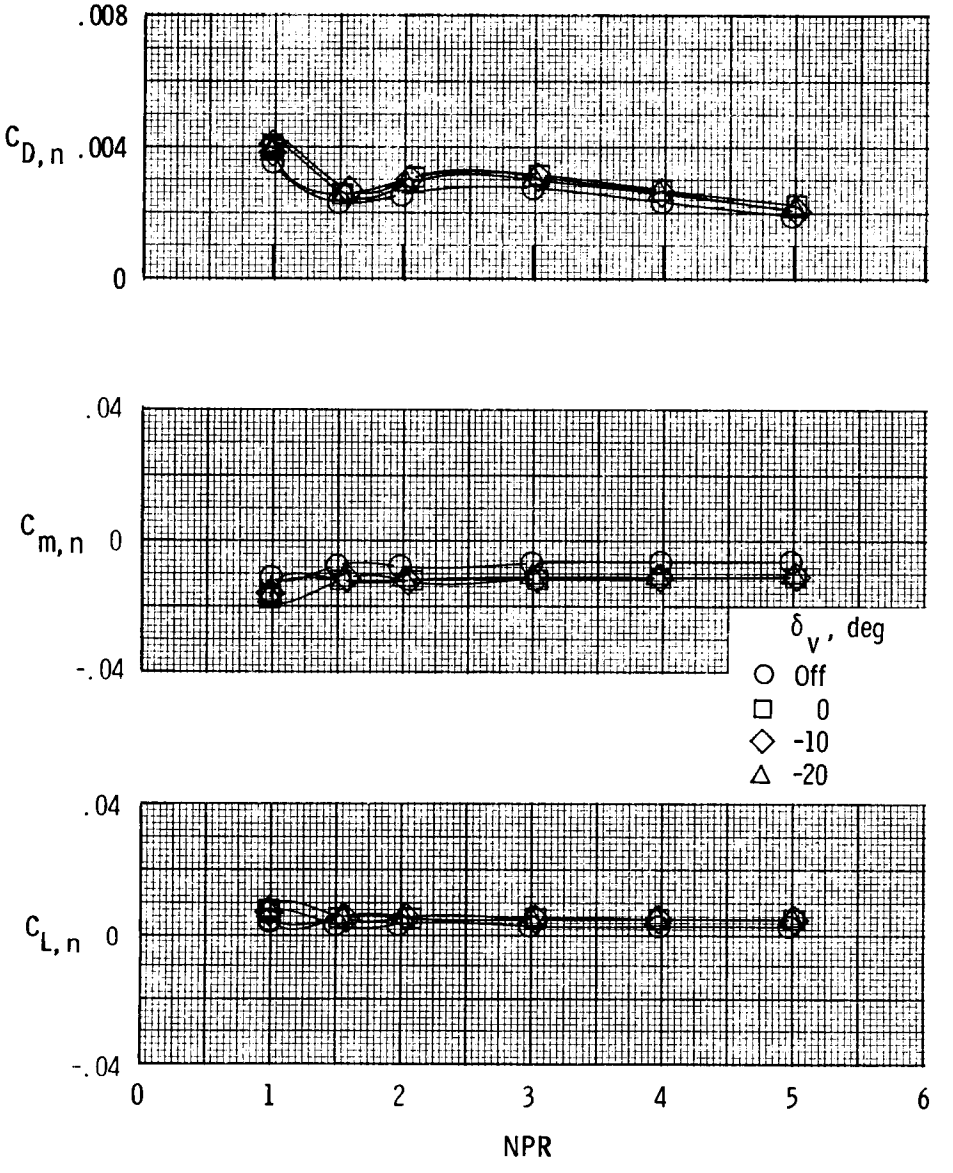

(r) Nozzle characteristics with $M = 0.90$ and $\alpha = 4.3°$.

Figure 6. Continued.

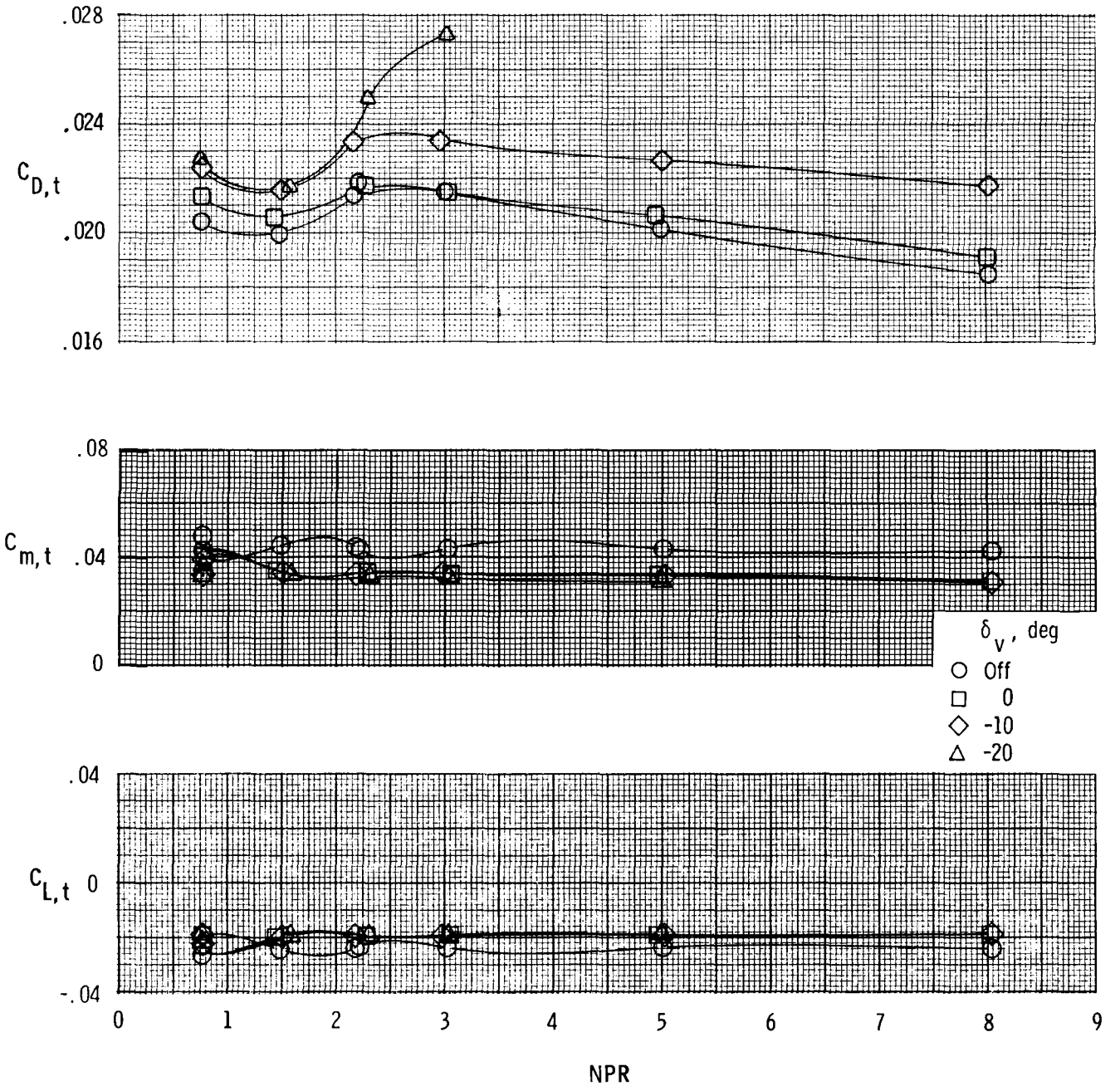

(s) Afterbody-nozzle characteristics with $M = 1.25$ and $\alpha = 0°$.

Figure 6. Continued.

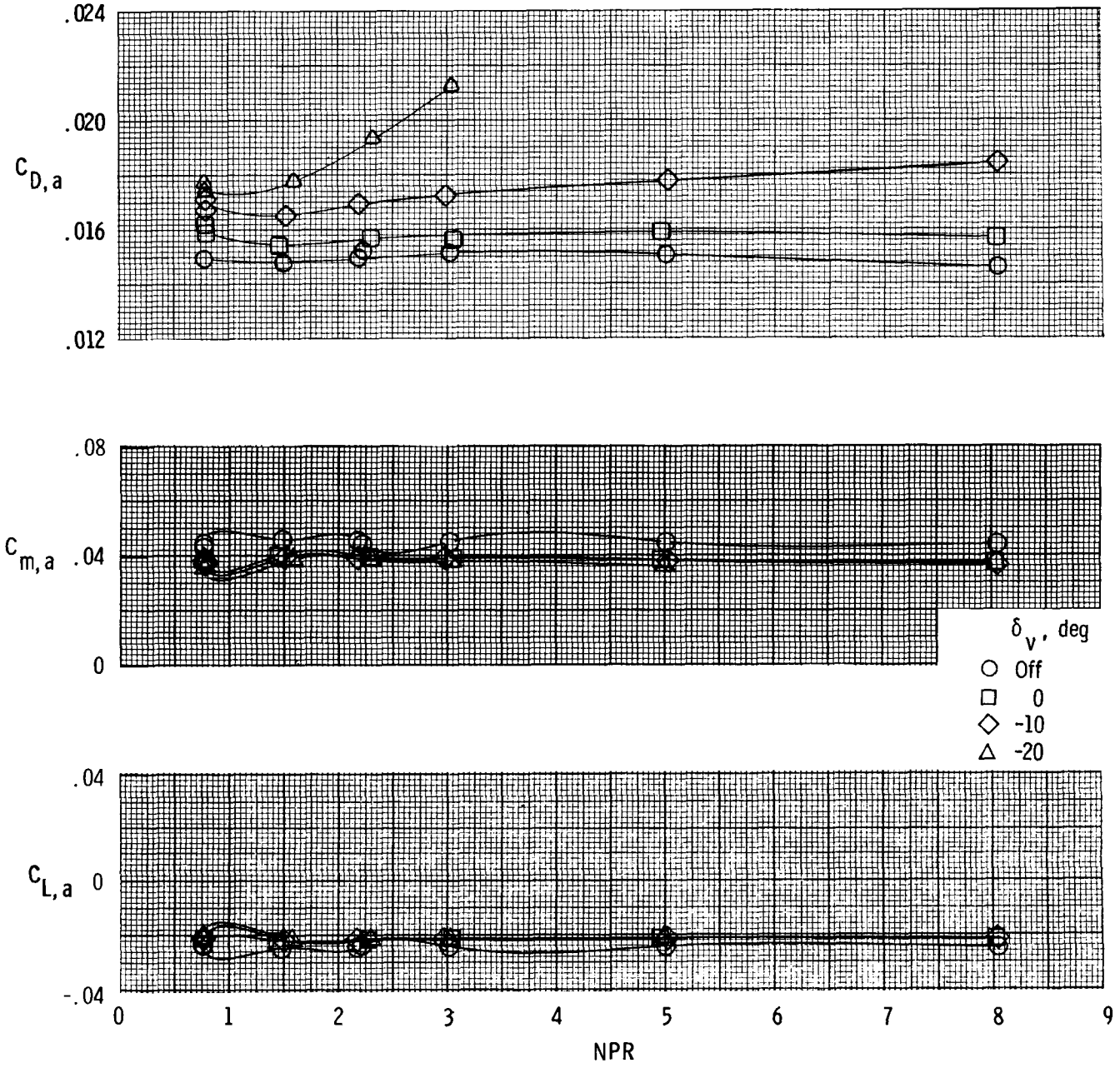

(t) Afterbody characteristics with $M = 1.25$ and $\alpha = 0°$.

Figure 6. Continued.

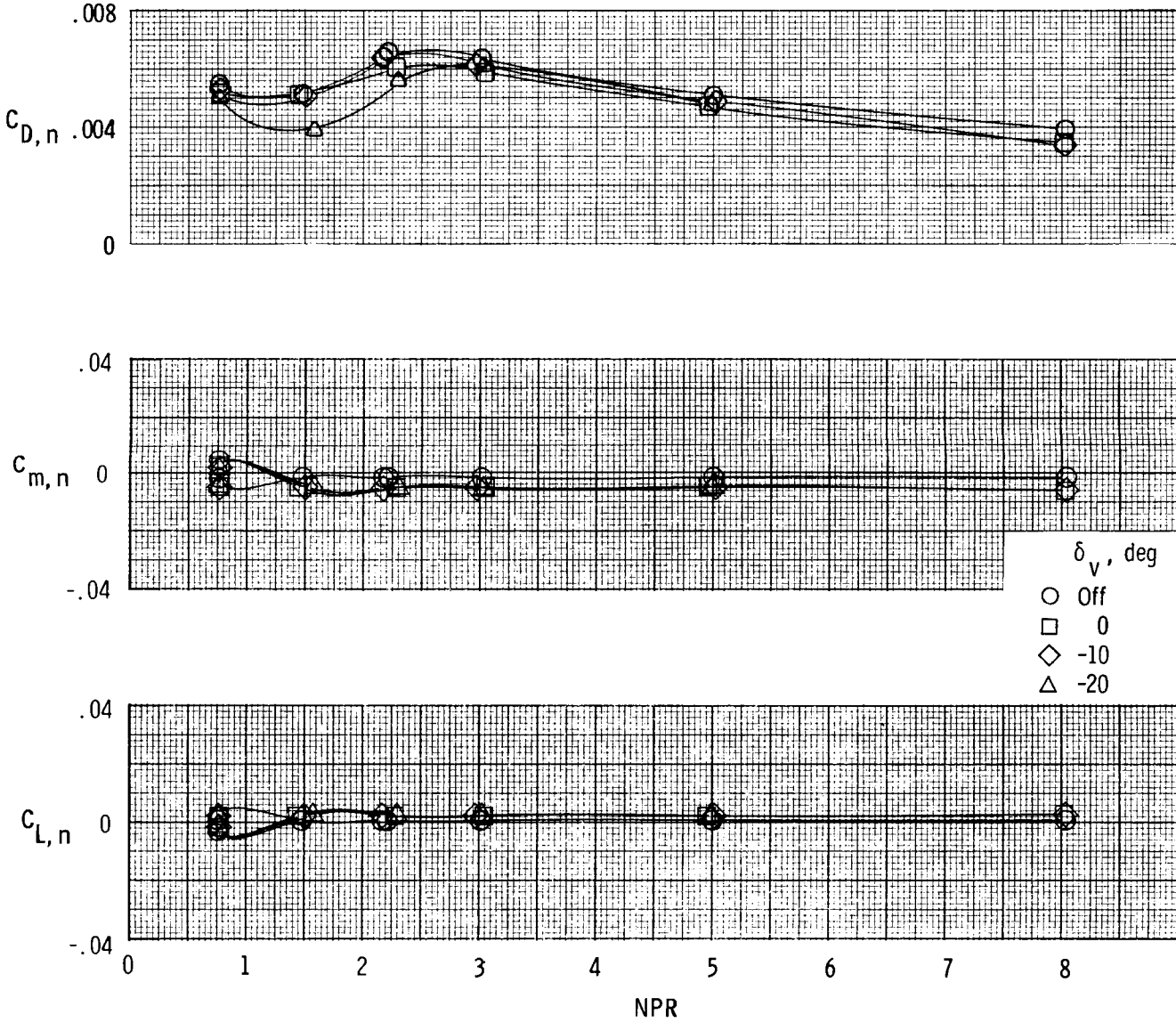

(u) Nozzle characteristics with $M = 1.25$ and $\alpha = 0°$.

Figure 6. Continued.

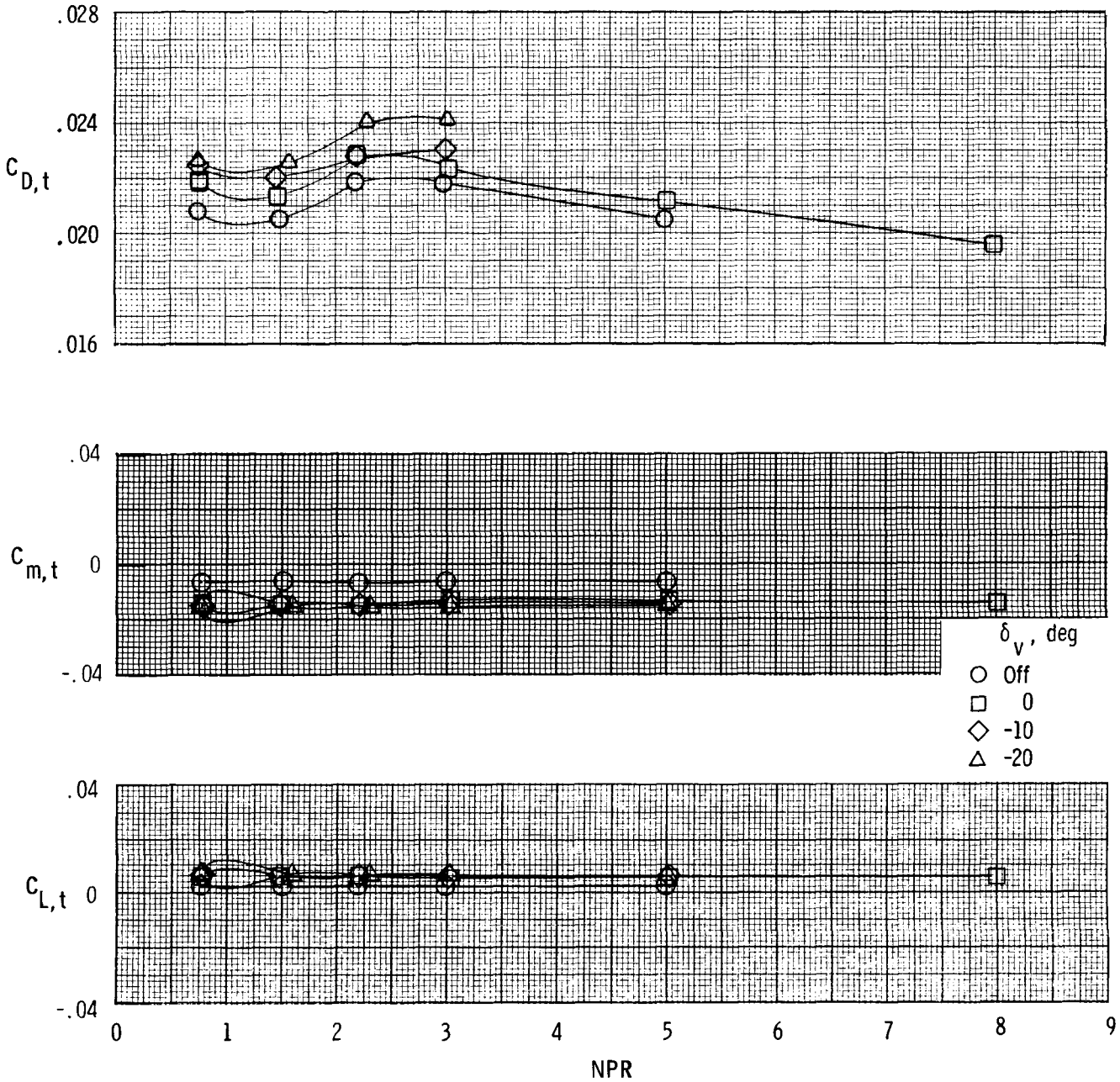

(v) Afterbody-nozzle characteristics with $M = 1.25$ and $\alpha = 2°$.

Figure 6. Continued.

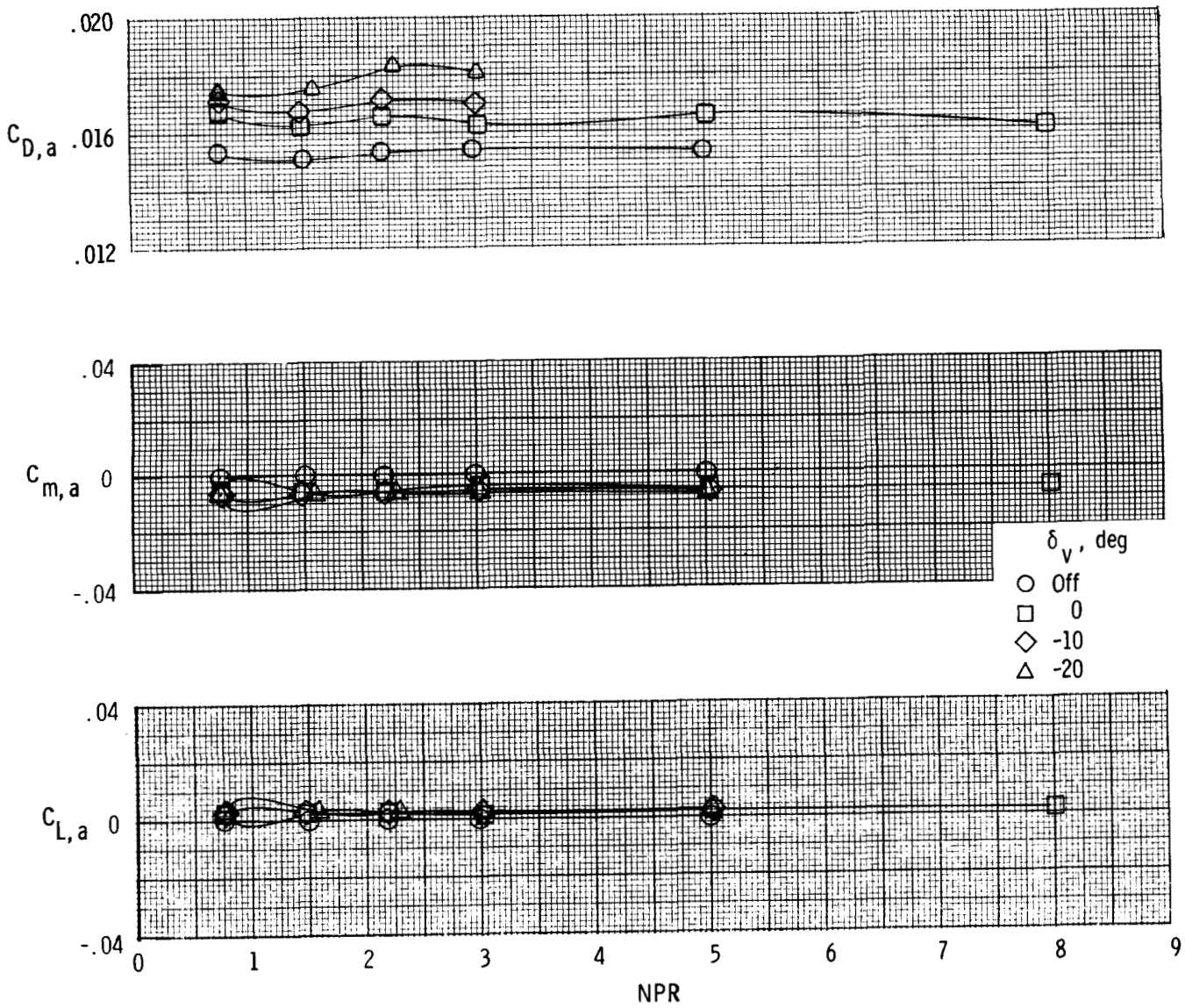

(w) Afterbody characteristics with $M = 1.25$ and $\alpha = 2°$.

Figure 6. Continued.

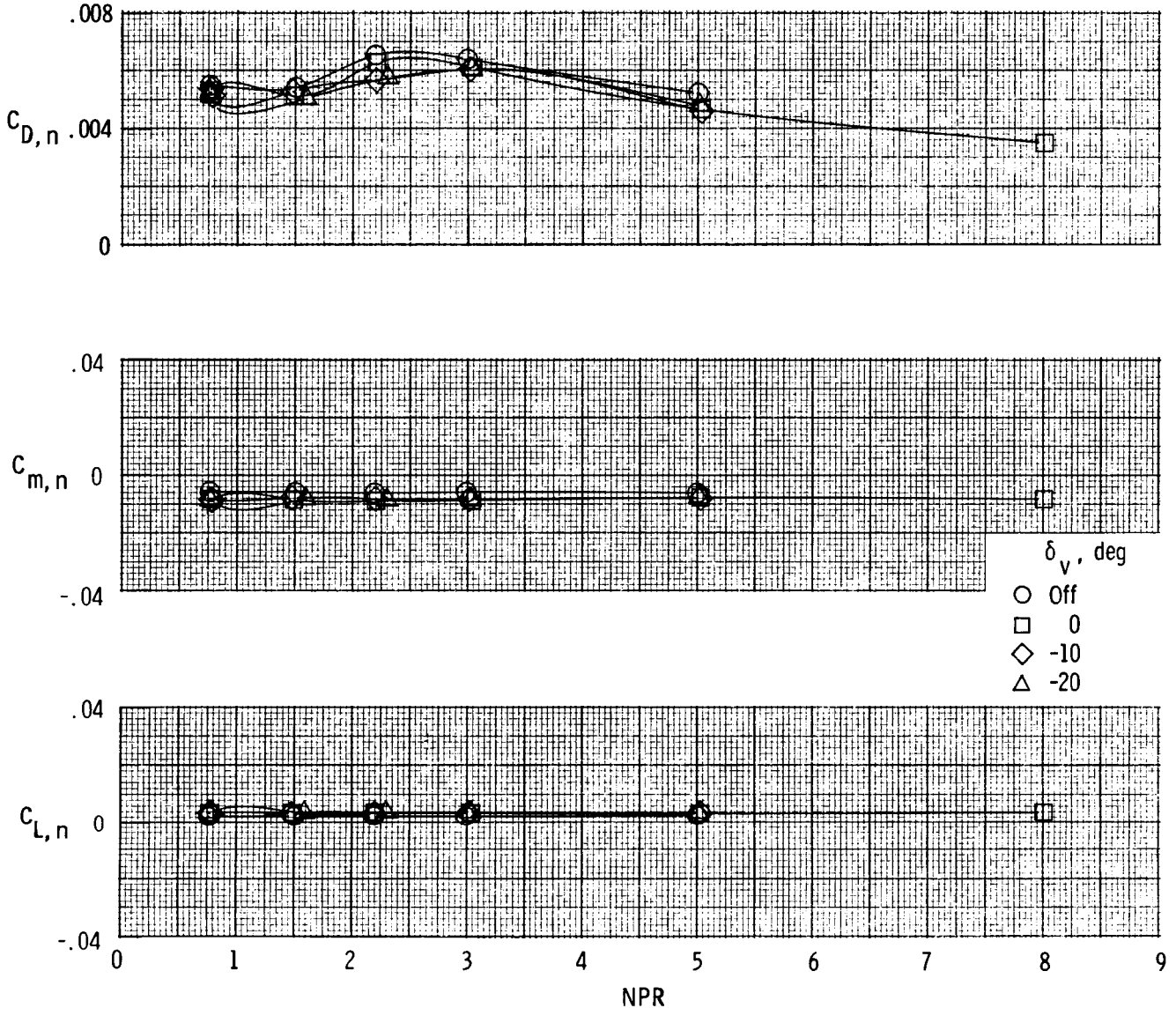

(x) Nozzle characteristics with $M = 1.25$ and $\alpha = 2°$.

Figure 6. Concluded.

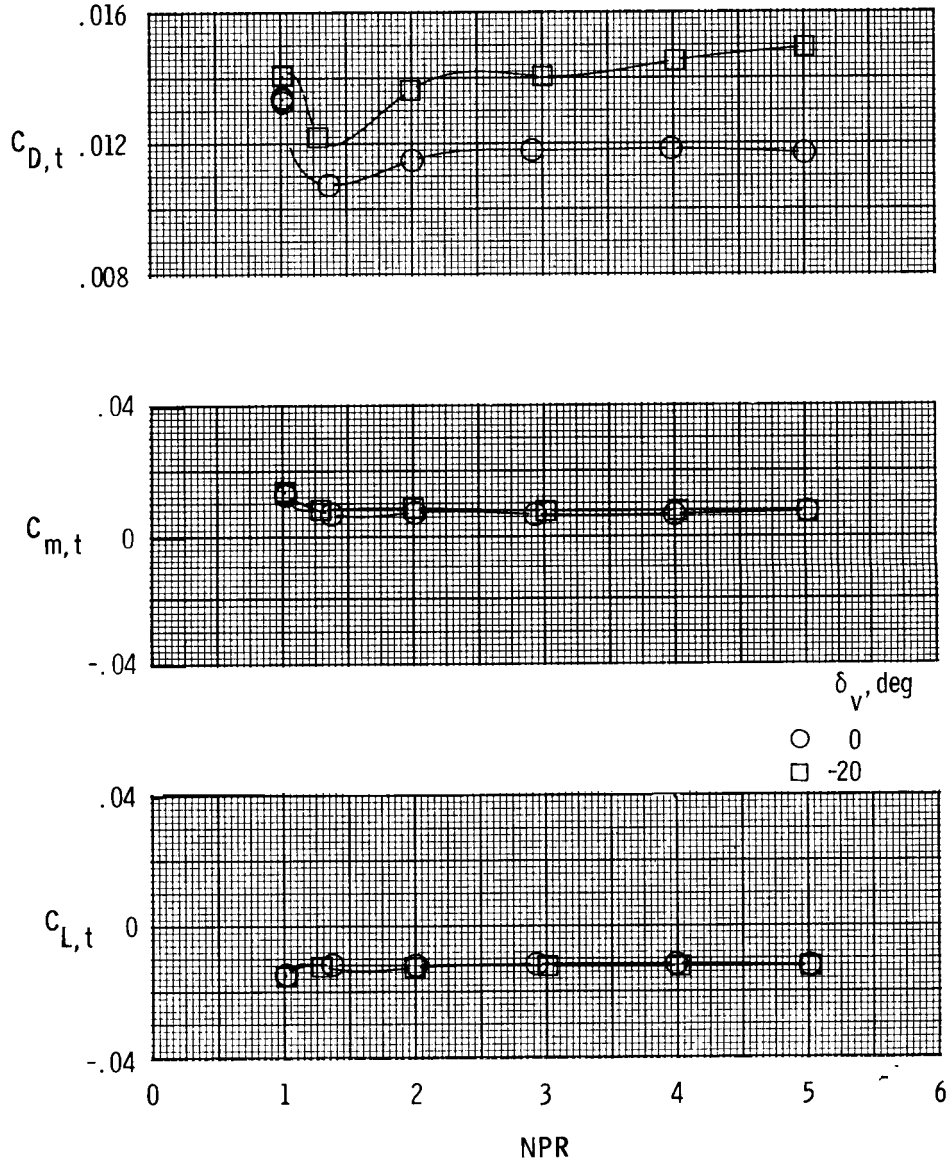

(a) Afterbody-nozzle characteristics with $M = 0.70$ and $\alpha = 0°$.

Figure 7. Afterbody and nozzle longitudinal characteristics for model with F110 cruise nozzles and yaw vanes installed. $\Lambda = 68°; \delta_h = 0°$.

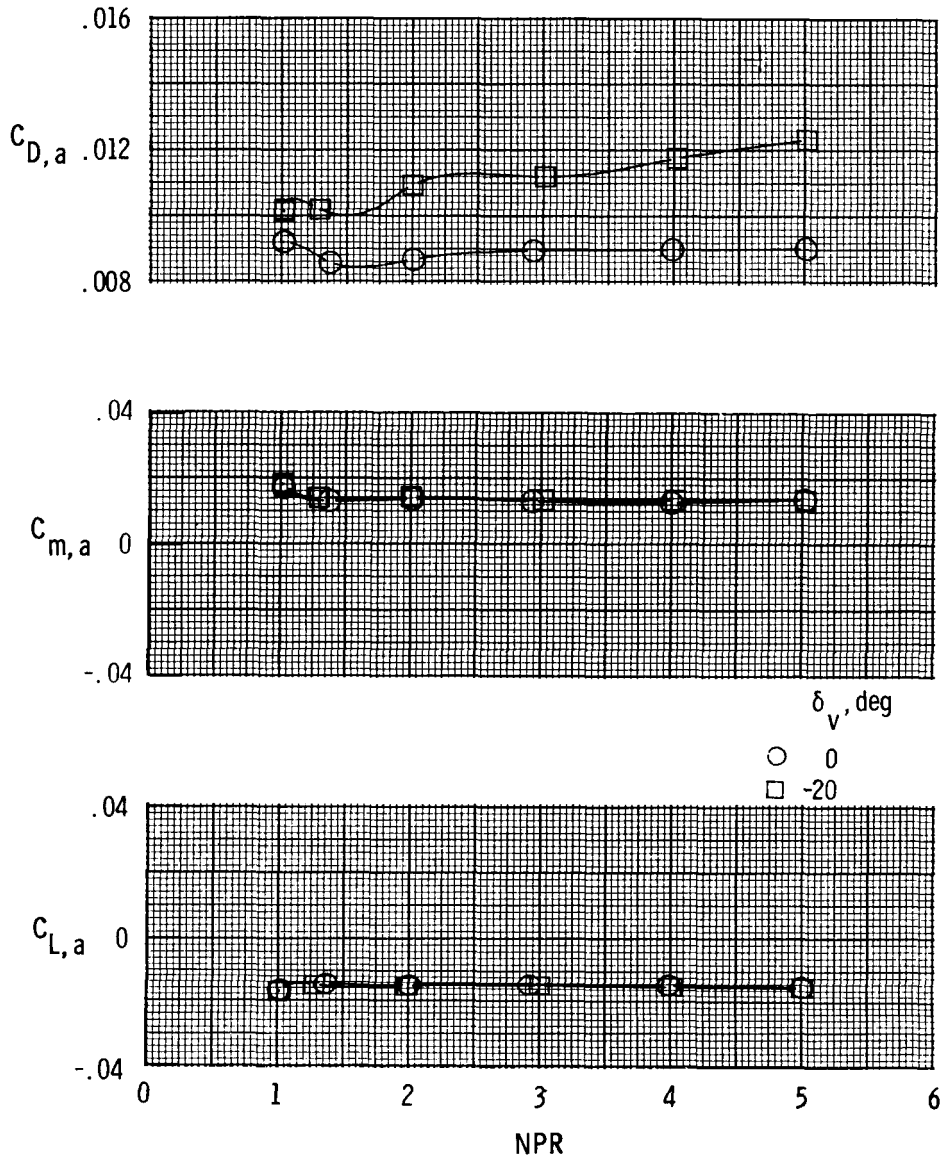

(b) Afterbody characteristics with $M = 0.70$ and $\alpha = 0°$.

Figure 7. Continued.

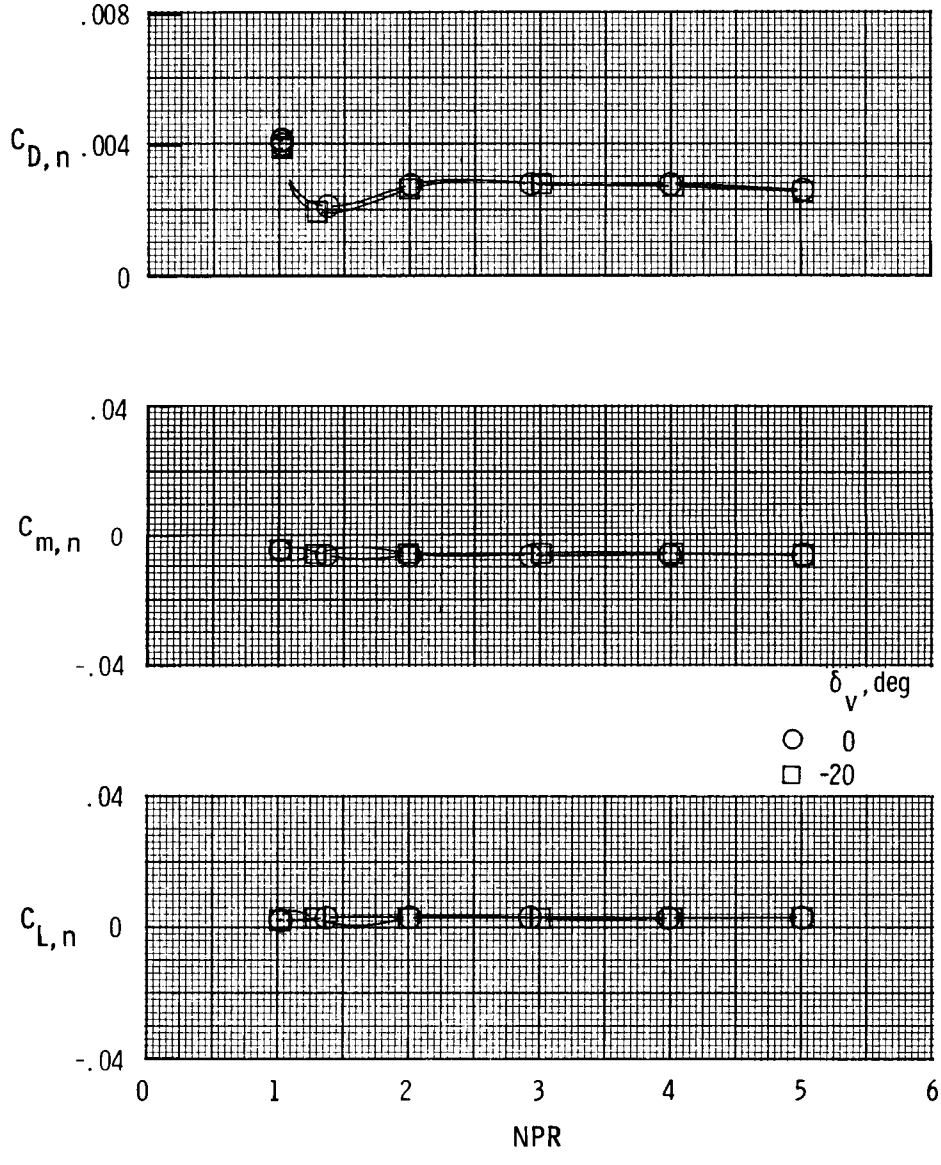

(c) Nozzle characteristics with $M = 0.70$ and $\alpha = 0°$.

Figure 7. Continued.

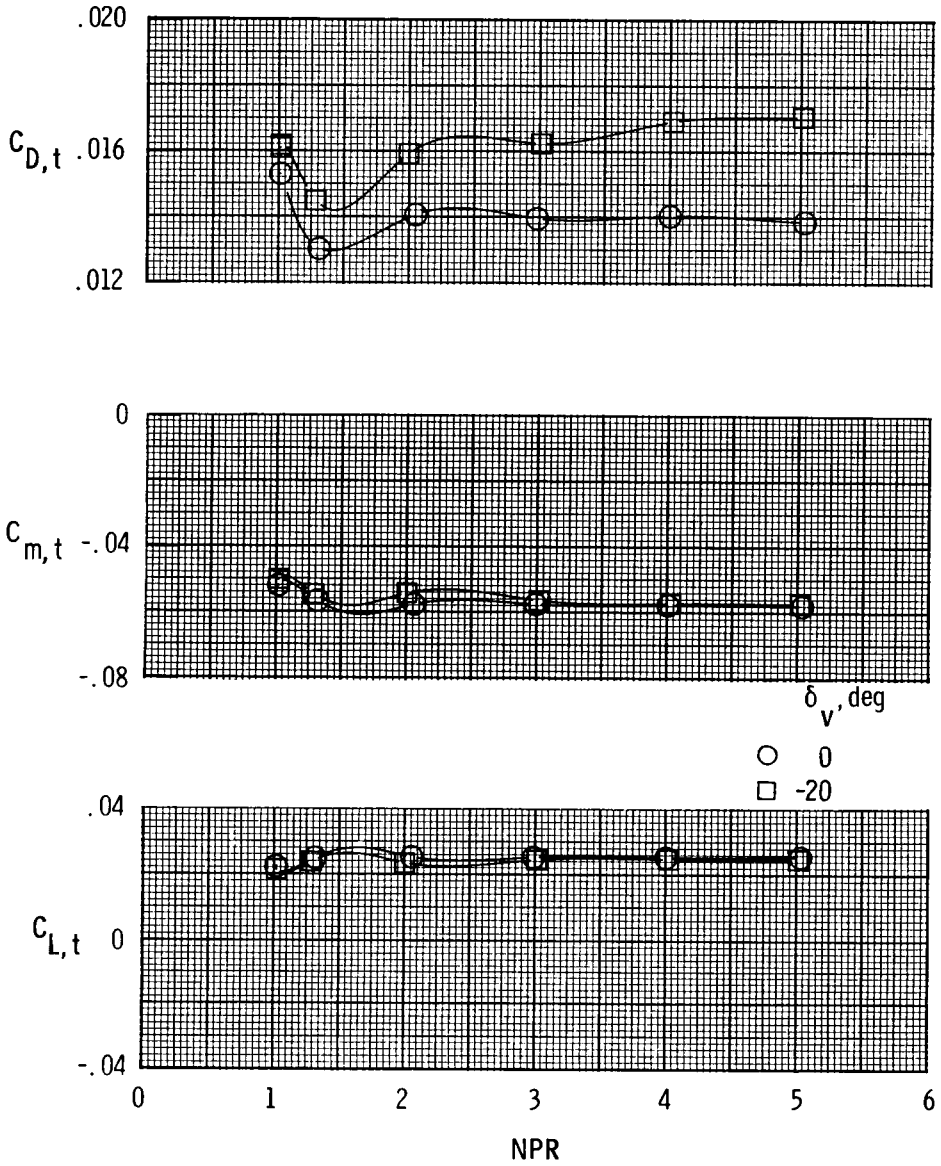

(d) Afterbody-nozzle characteristics with $M = 0.70$ and $\alpha = 4.3°$.

Figure 7. Continued.

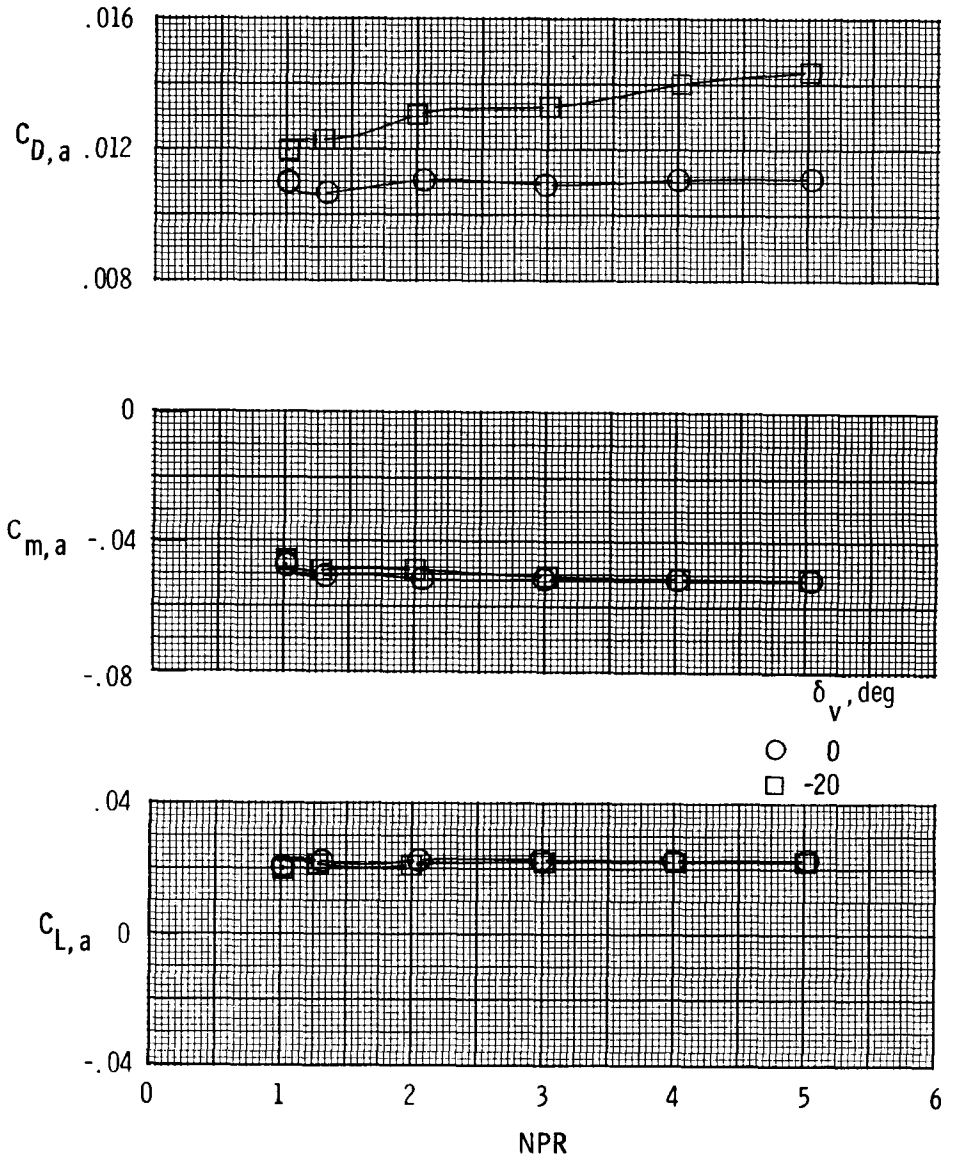

(e) Afterbody characteristics with $M = 0.70$ and $\alpha = 4.3°$.

Figure 7. Continued.

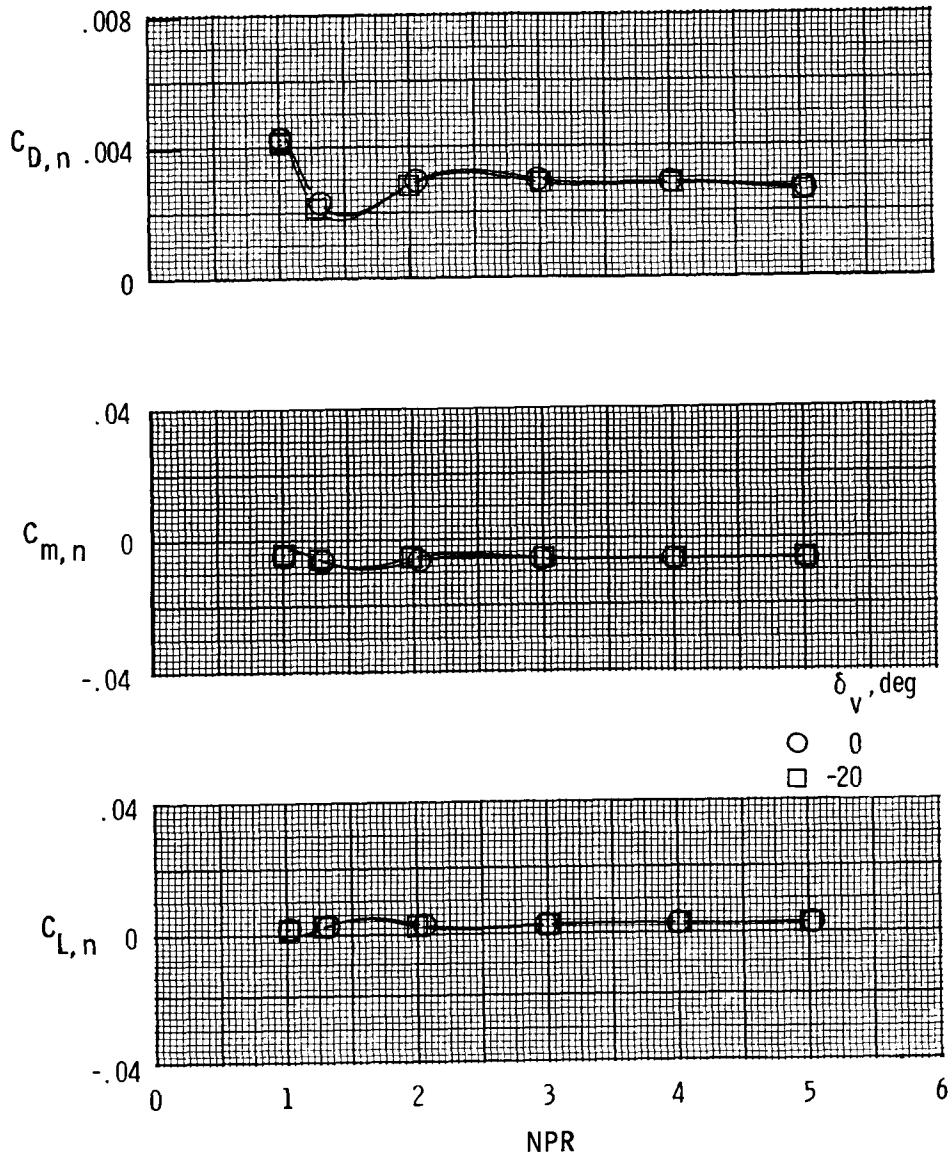

(f) Nozzle characteristics with $M = 0.70$ and $\alpha = 4.3°$.

Figure 7. Continued.

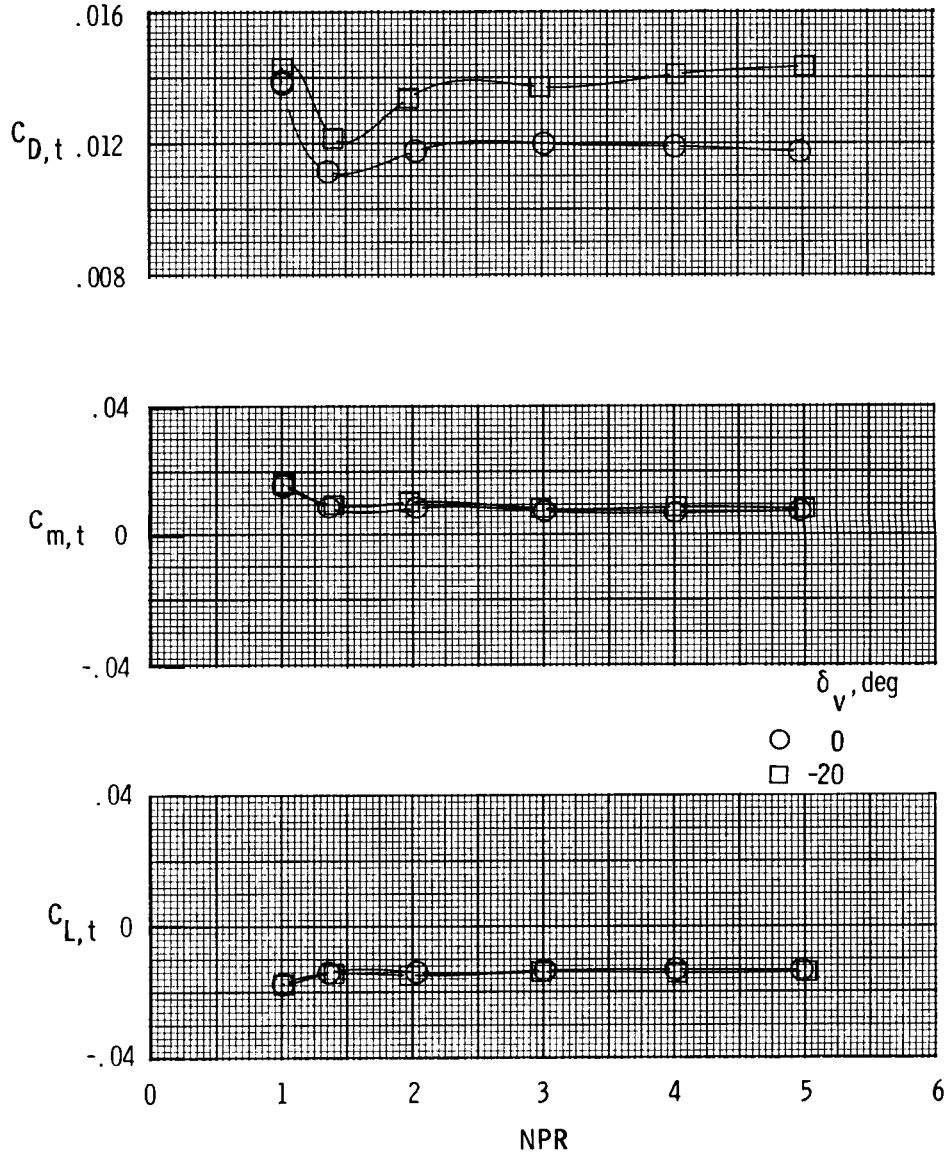

(g) Afterbody-nozzle characteristics with $M = 0.80$ and $\alpha = 0°$.

Figure 7. Continued.

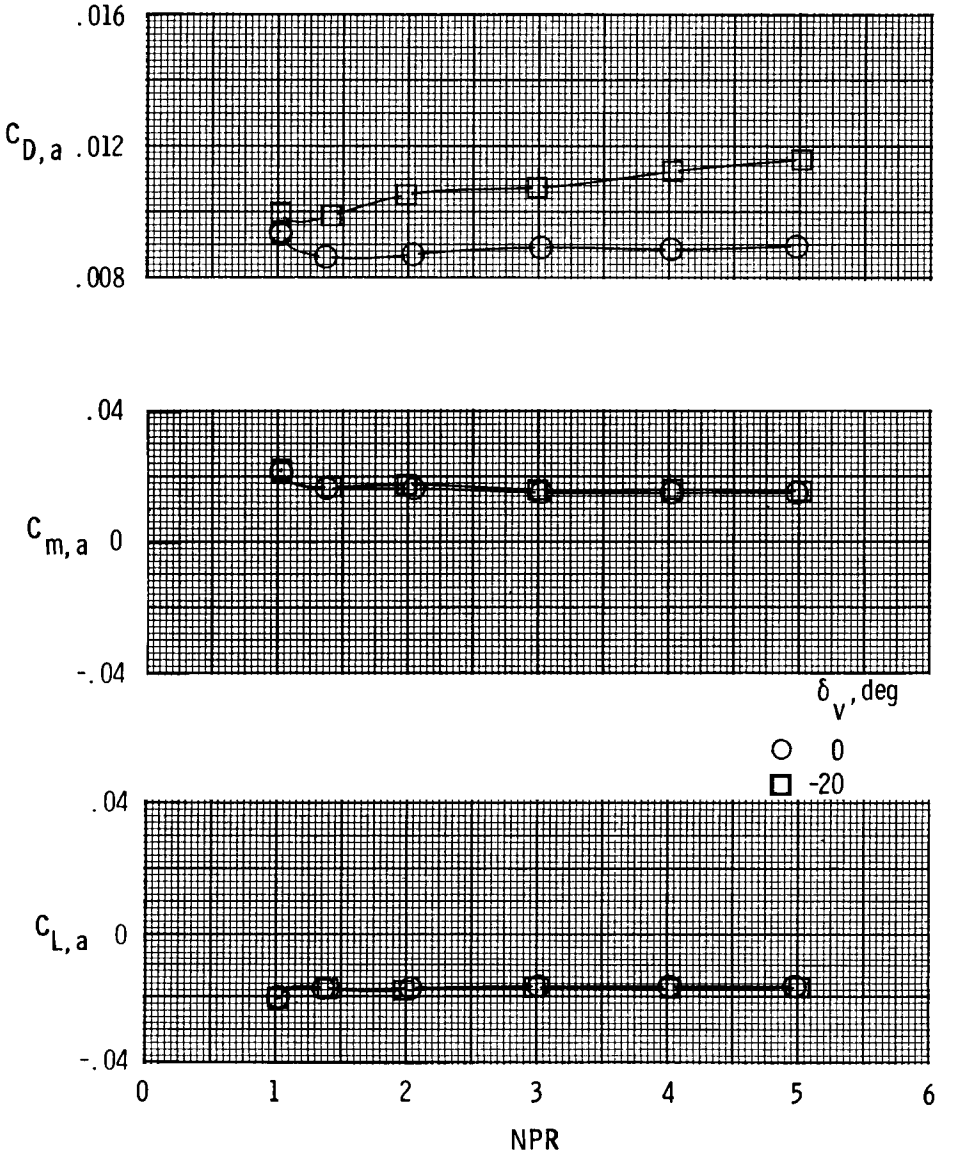

(h) Afterbody characteristics with $M = 0.80$ and $\alpha = 0°$.

Figure 7. Continued.

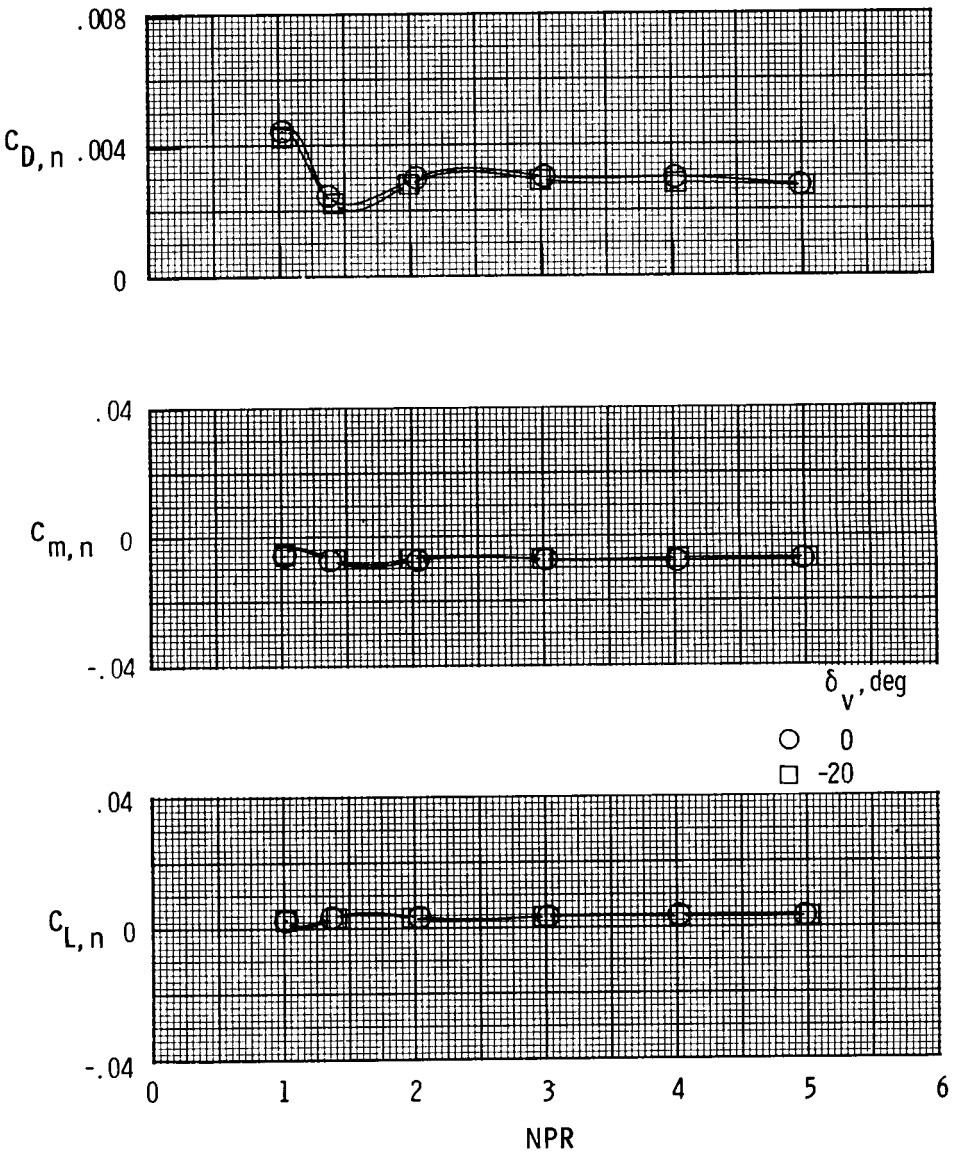

(i) Nozzle characteristics with $M = 0.80$ and $\alpha = 0°$.

Figure 7. Continued.

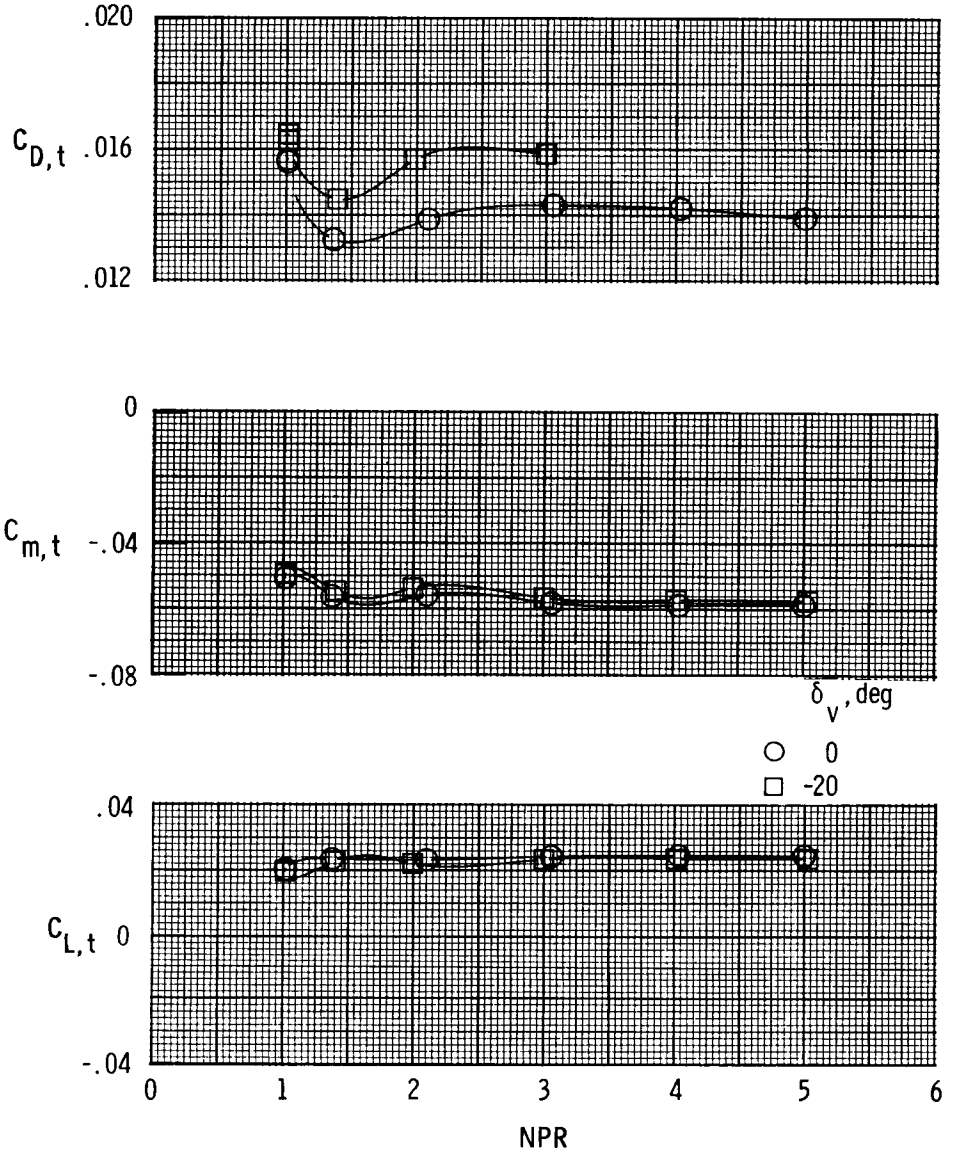

(j) Afterbody-nozzle characteristics with $M = 0.80$ and $\alpha = 4.3°$.

Figure 7. Continued.

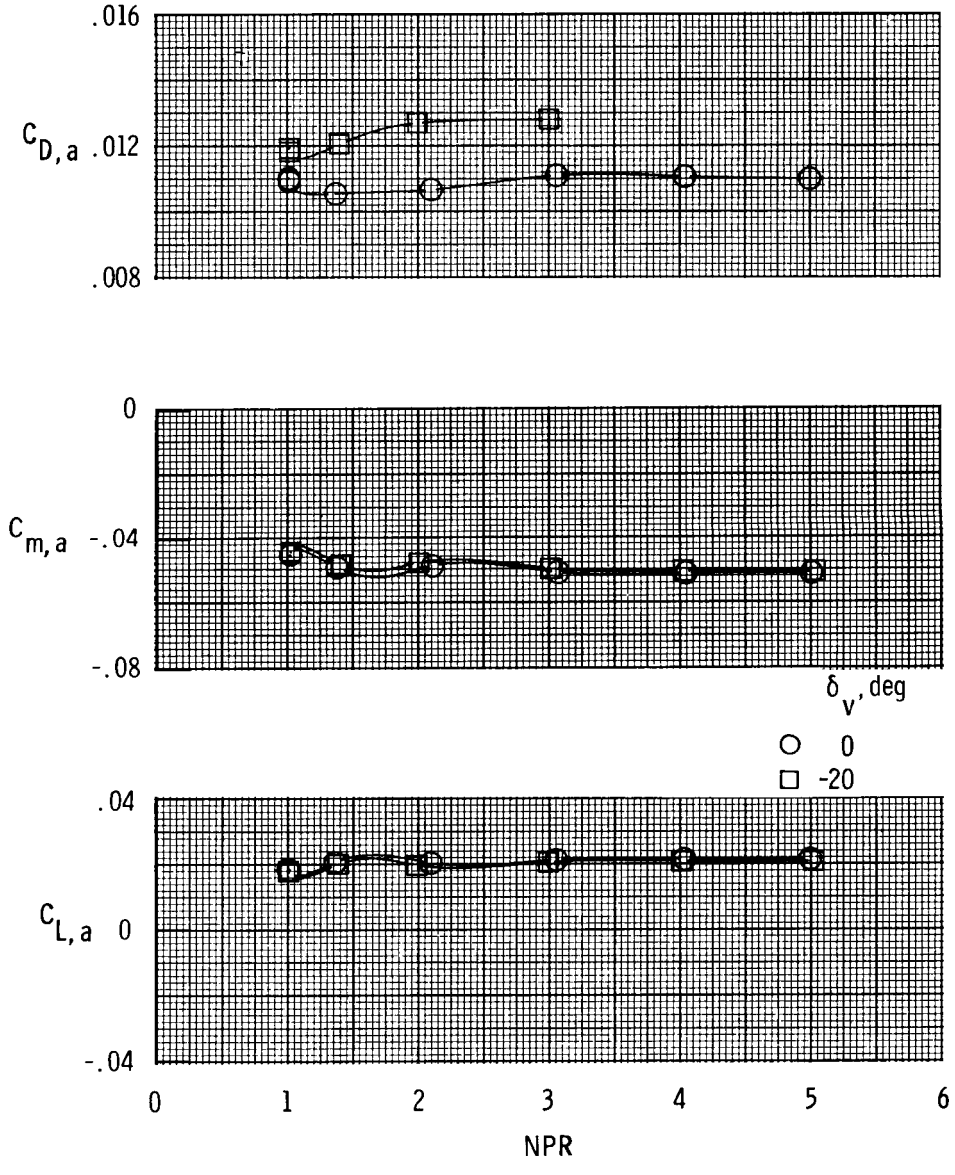

(k) Afterbody characteristics with $M = 0.80$ and $\alpha = 4.3°$.

Figure 7. Continued.

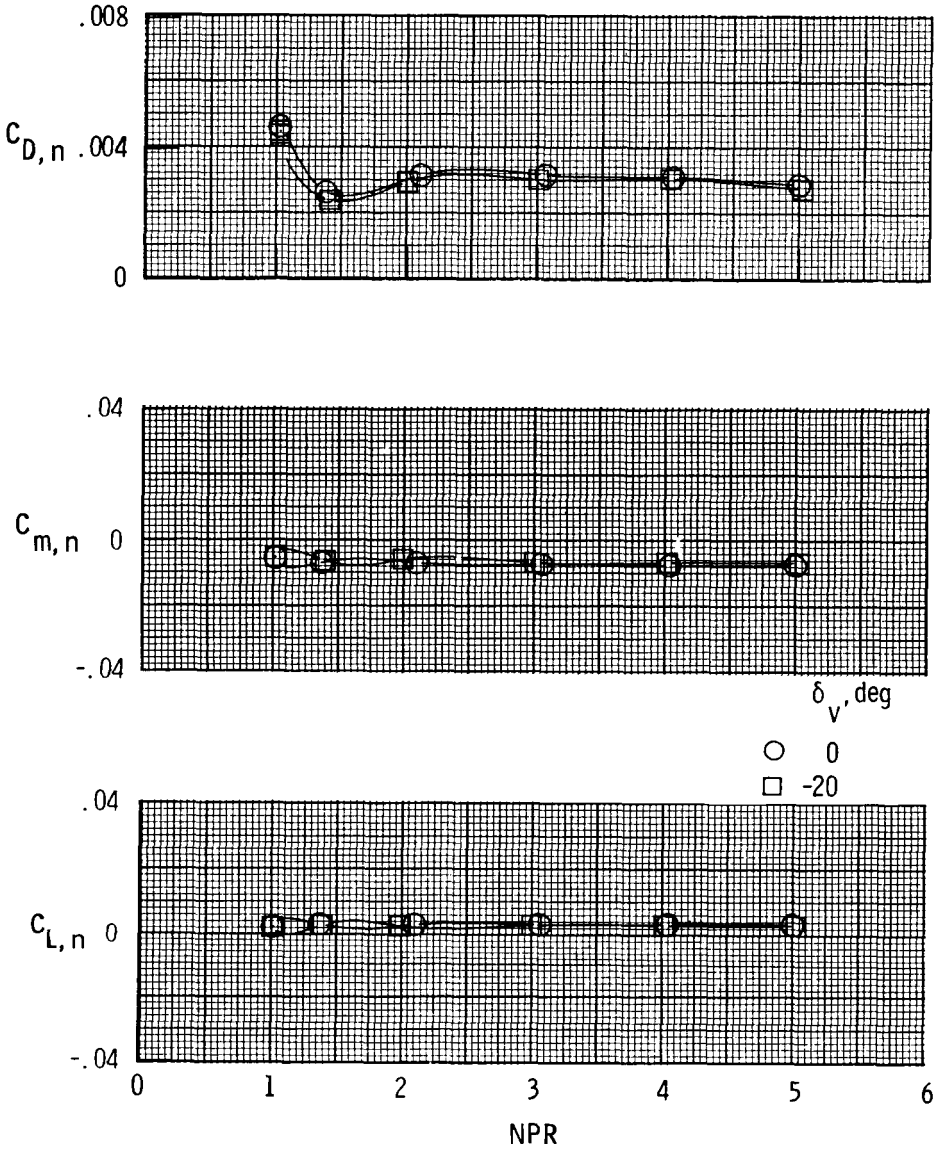

(l) Nozzle characteristics with $M = 0.80$ and $\alpha = 4.3°$.

Figure 7. Continued.

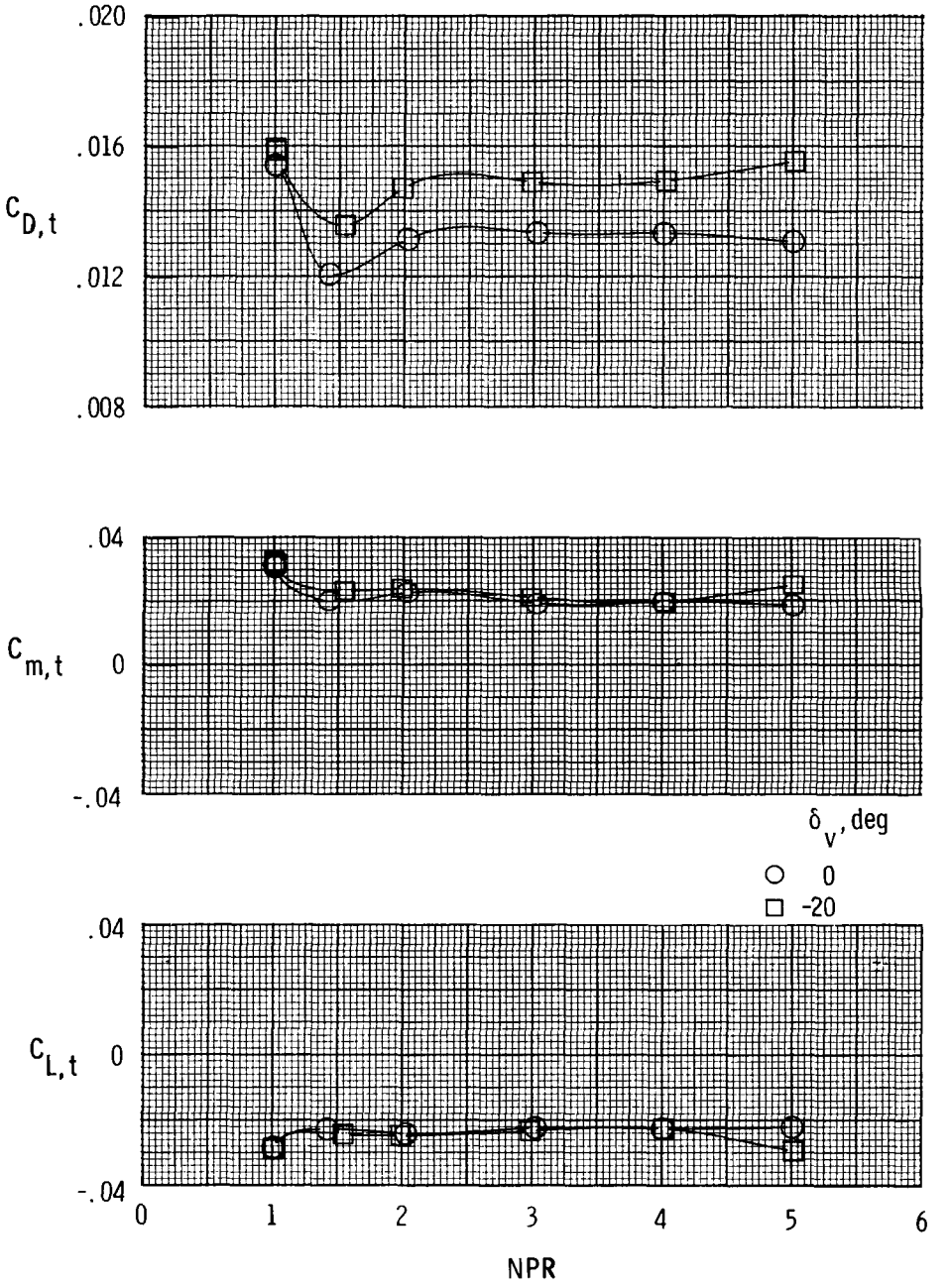

(m) Afterbody-nozzle characteristics with $M = 0.90$ and $\alpha = 0°$.

Figure 7. Continued.

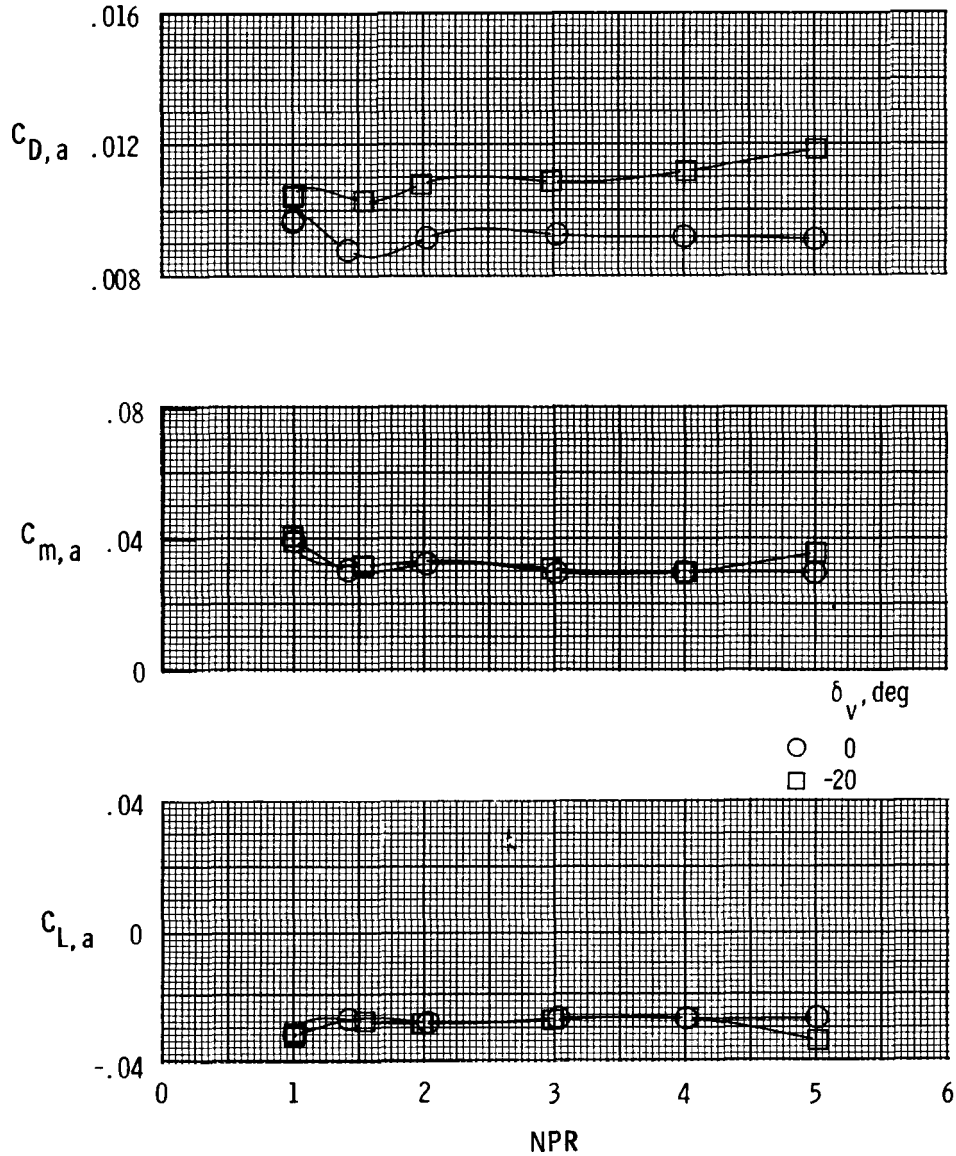

(n) Afterbody characteristics with $M = 0.90$ and $\alpha = 0°$.

Figure 7. Continued.

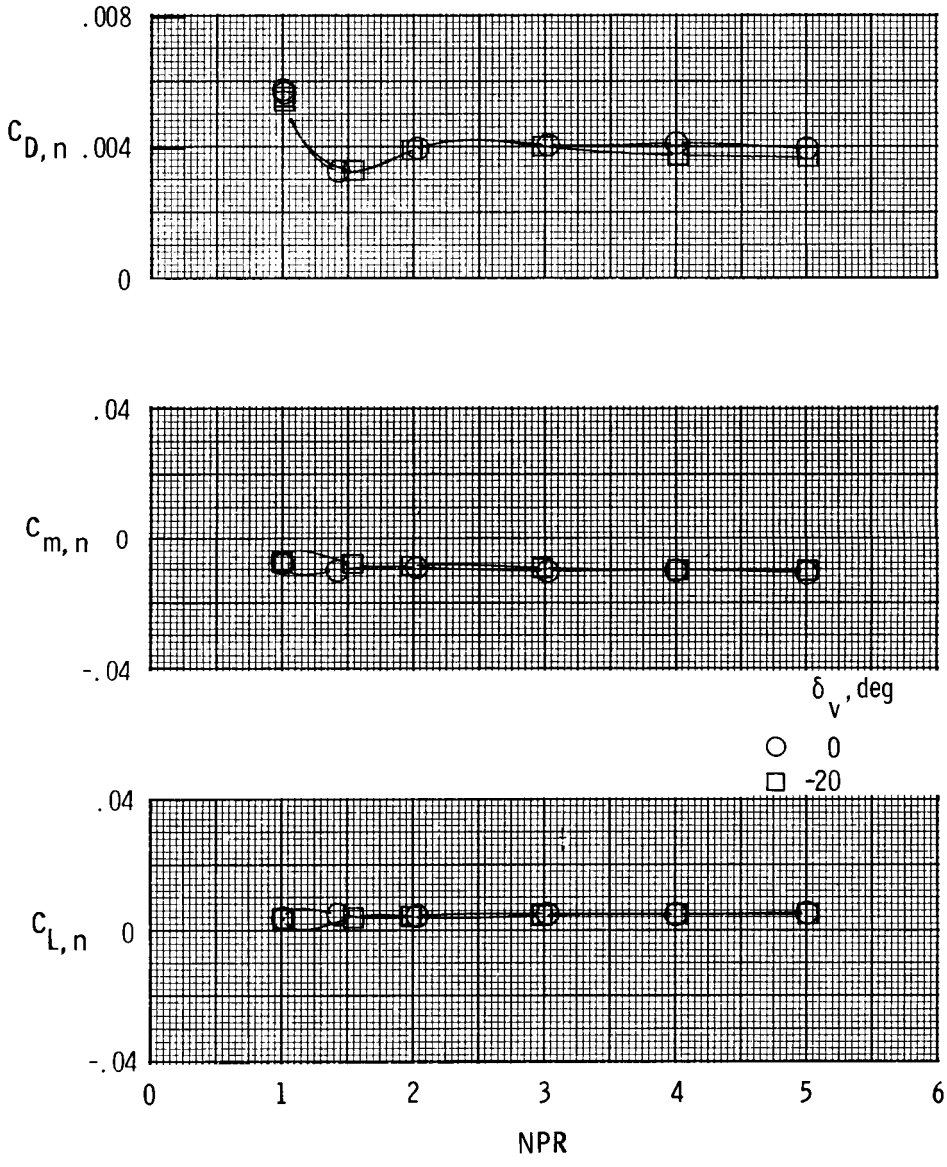

(o) Nozzle characteristics with $M = 0.90$ and $\alpha = 0°$.

Figure 7. Continued.

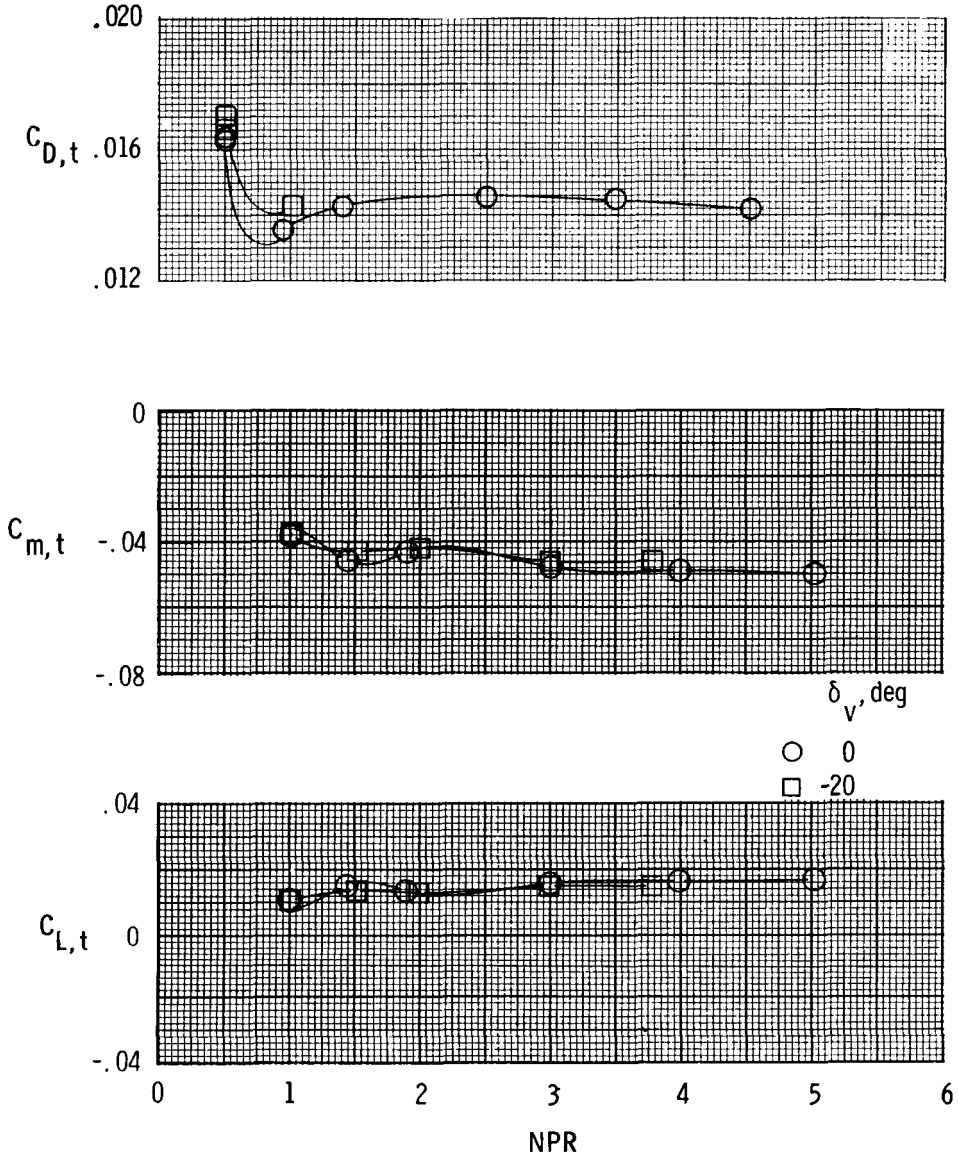

(p) Afterbody-nozzle characteristics with $M = 0.90$ and $\alpha = 4.3°$.

Figure 7. Continued.

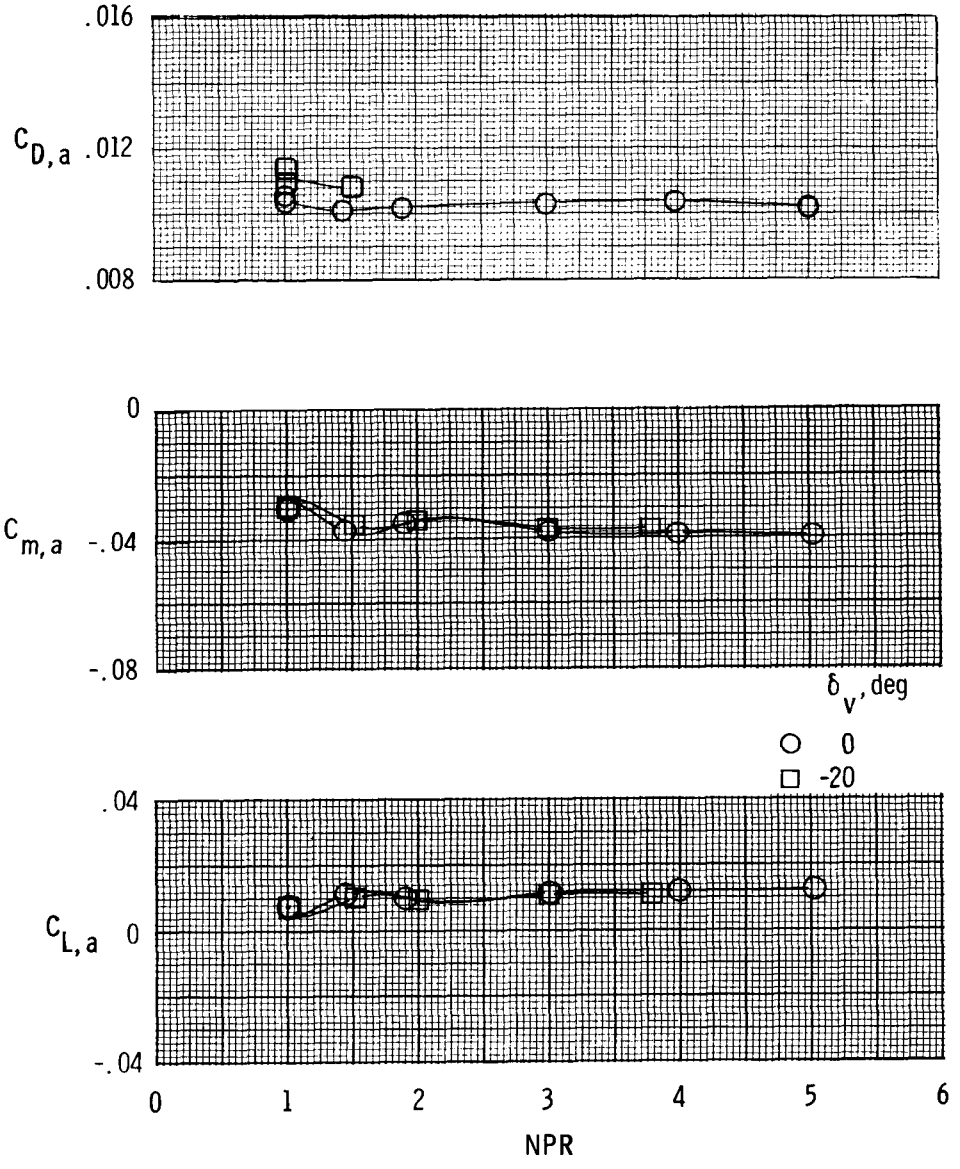

(q) Afterbody characteristics with $M = 0.90$ and $\alpha = 4.3°$.

Figure 7. Continued.

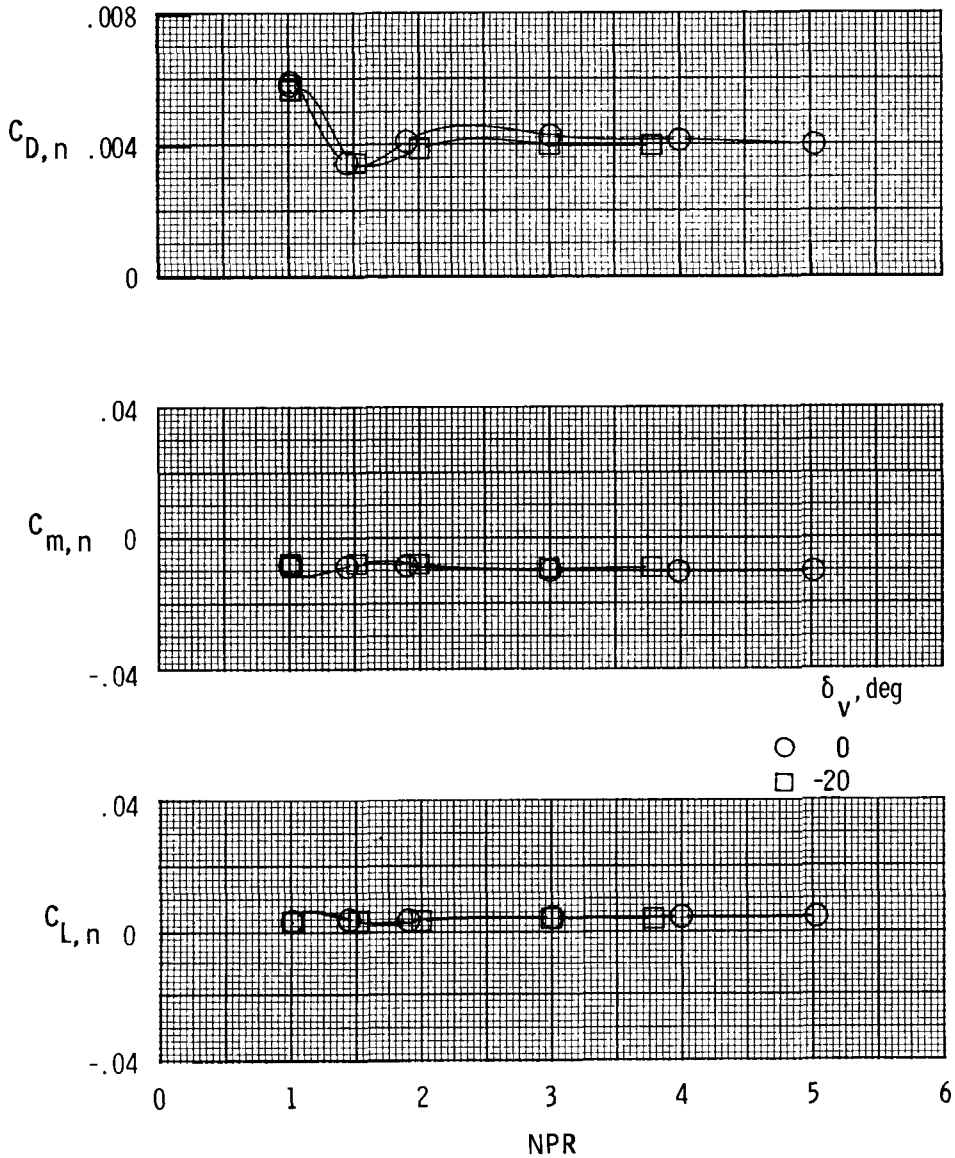

(r) Nozzle characteristics with $M = 0.90$ and $\alpha = 4.3°$.

Figure 7. Continued.

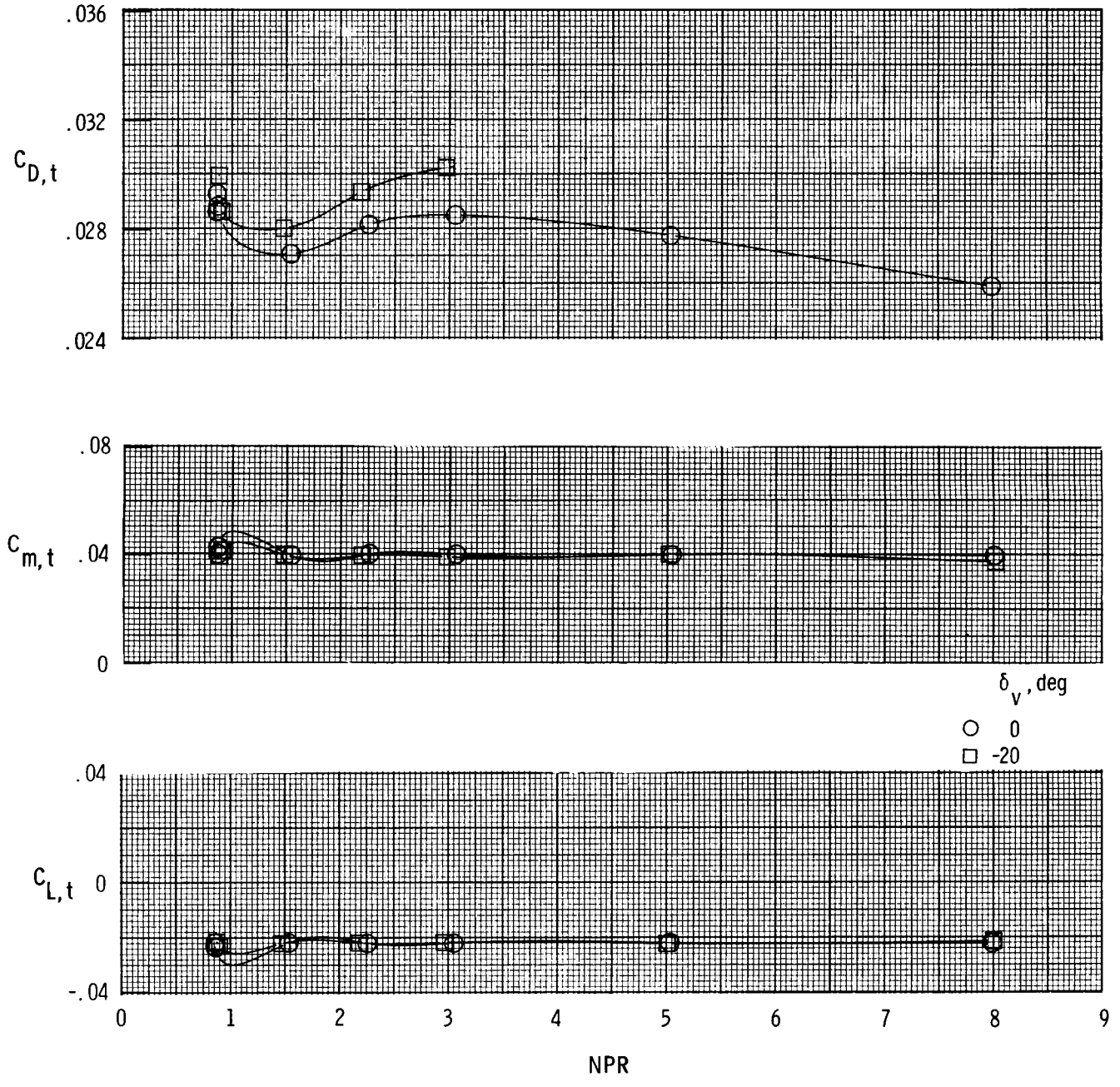

(s) Afterbody-nozzle characteristics with $M = 1.25$ and $\alpha = 0°$.

Figure 7. Continued.

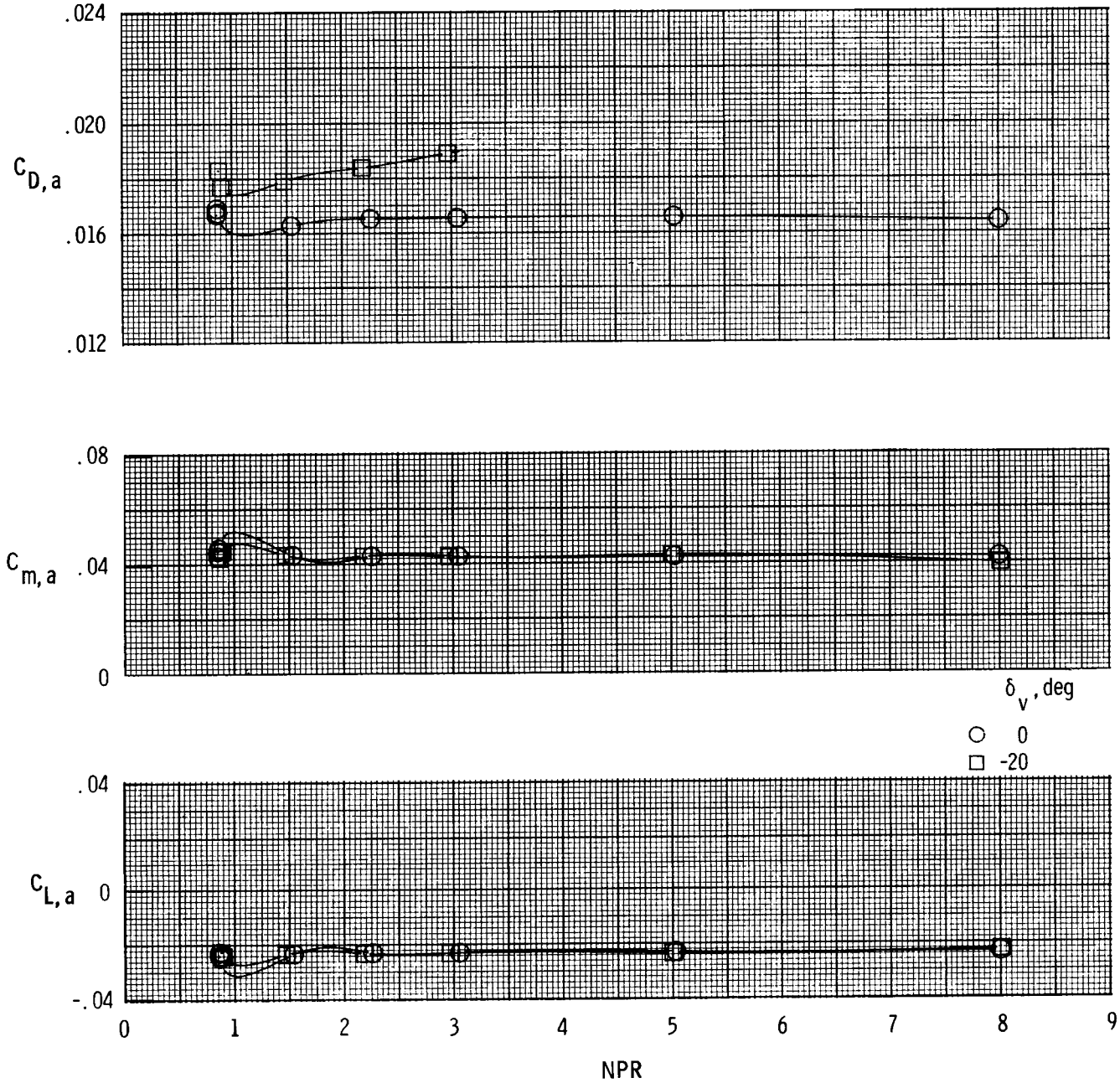

(t) Afterbody characteristics with $M = 1.25$ and $\alpha = 0°$.

Figure 7. Continued.

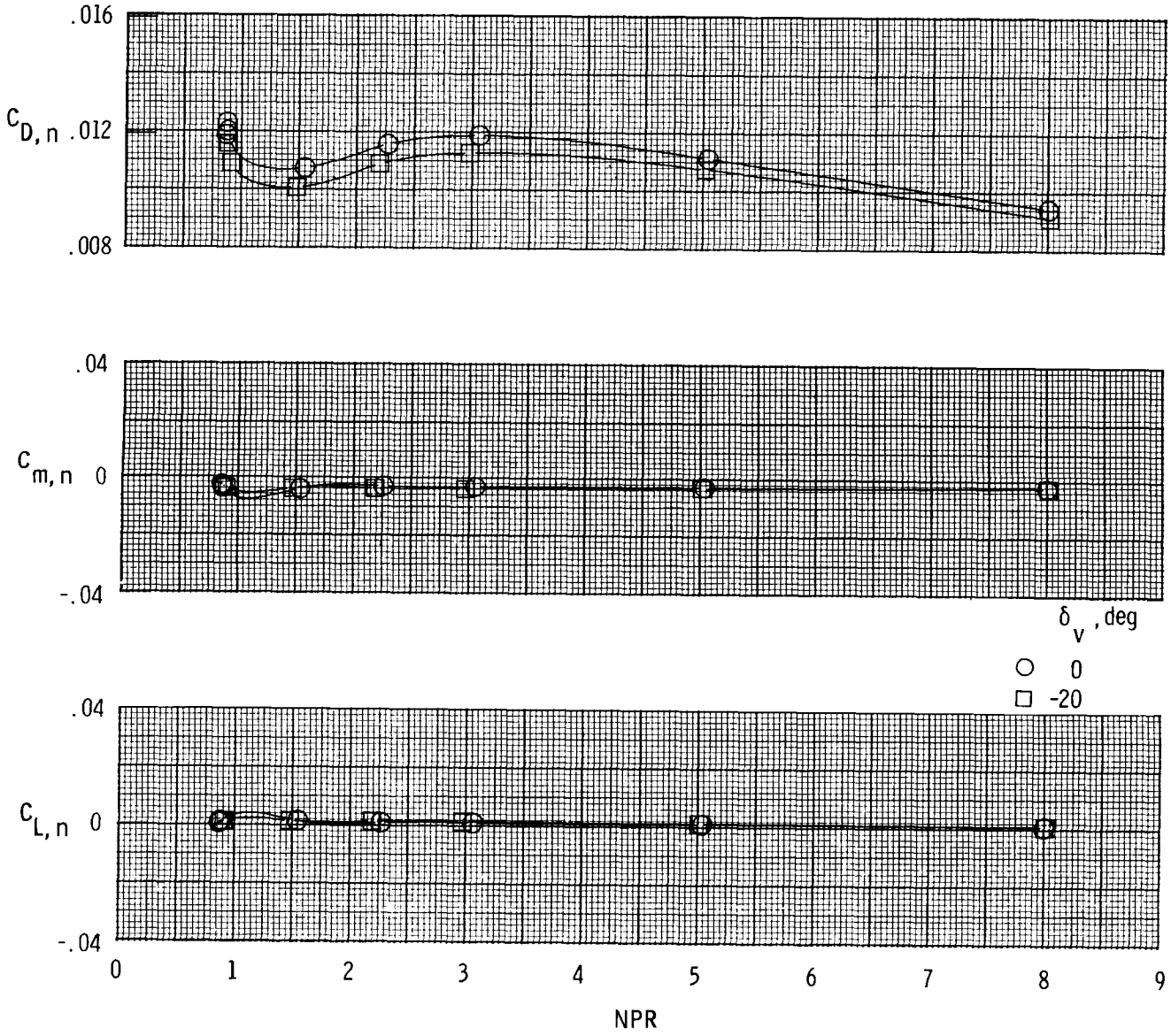

(u) Nozzle characteristics with $M = 1.25$ and $\alpha = 0°$.

Figure 7. Continued.

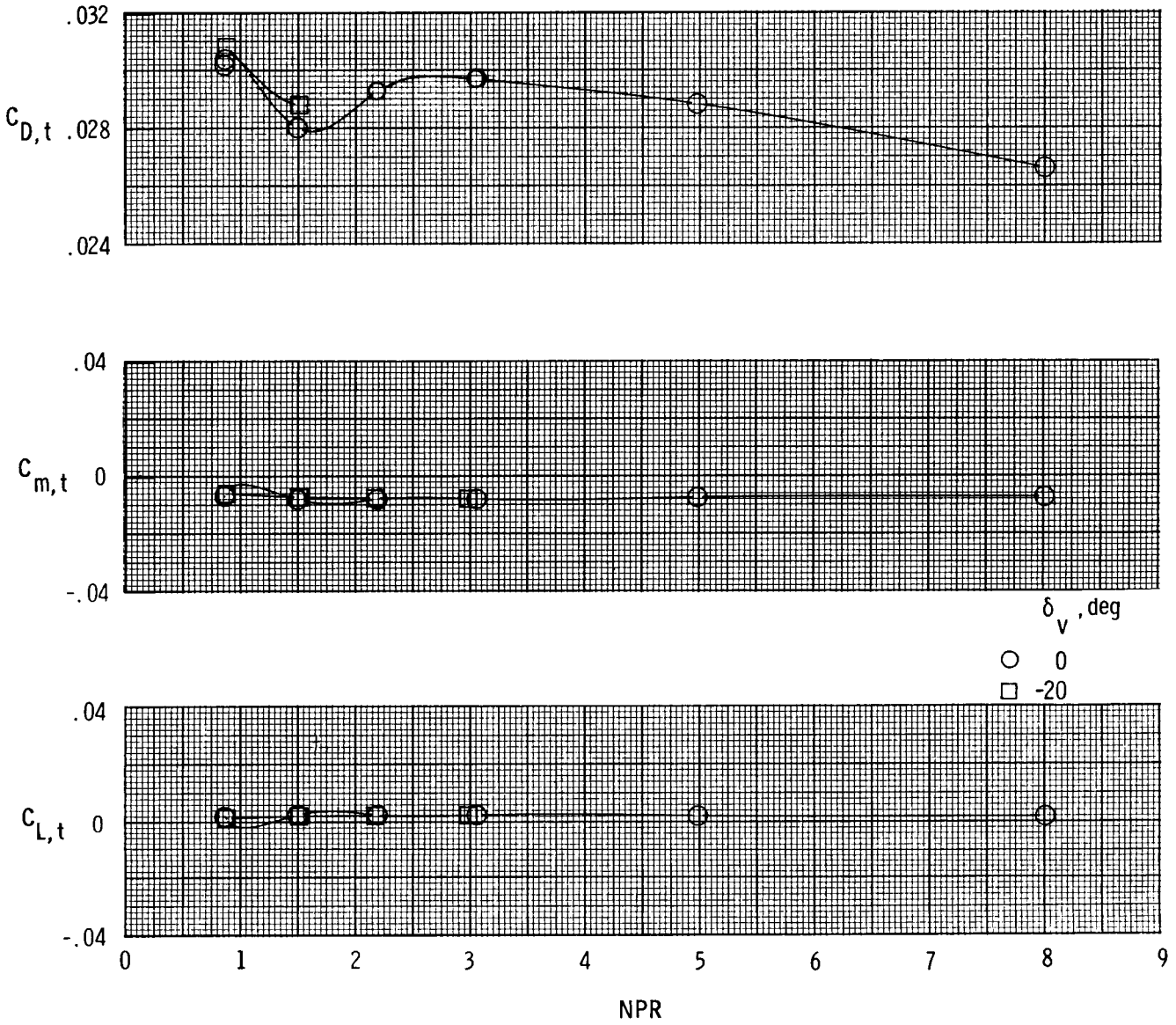

(v) Afterbody-nozzle characteristics with $M = 1.25$ and $\alpha = 2°$.

Figure 7. Continued.

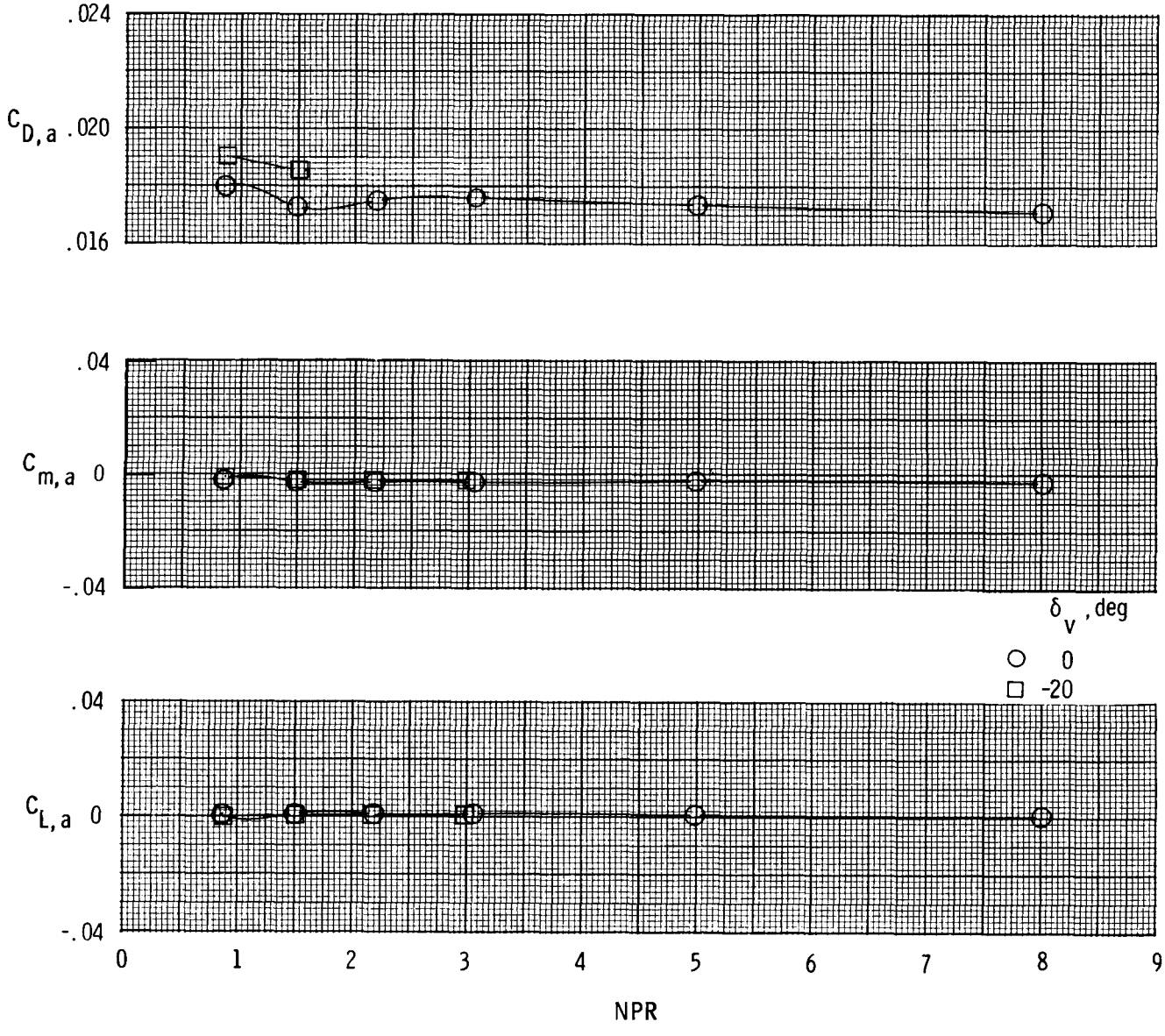

(w) Afterbody characteristics with $M = 1.25$ and $\alpha = 2°$.

Figure 7. Continued.

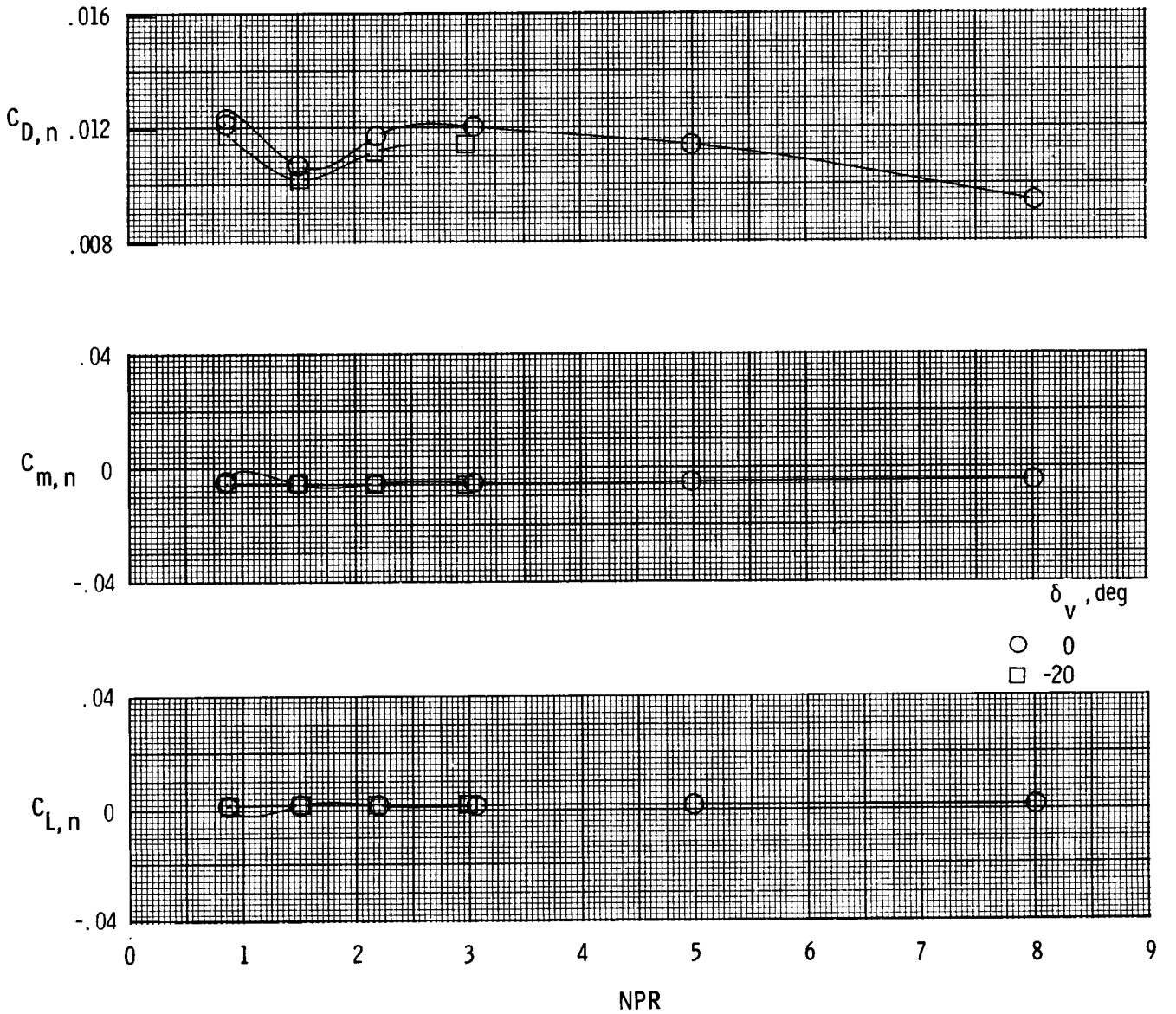

(x) Nozzle characteristics with $M = 1.25$ and $\alpha = 2°$.

Figure 7. Concluded.

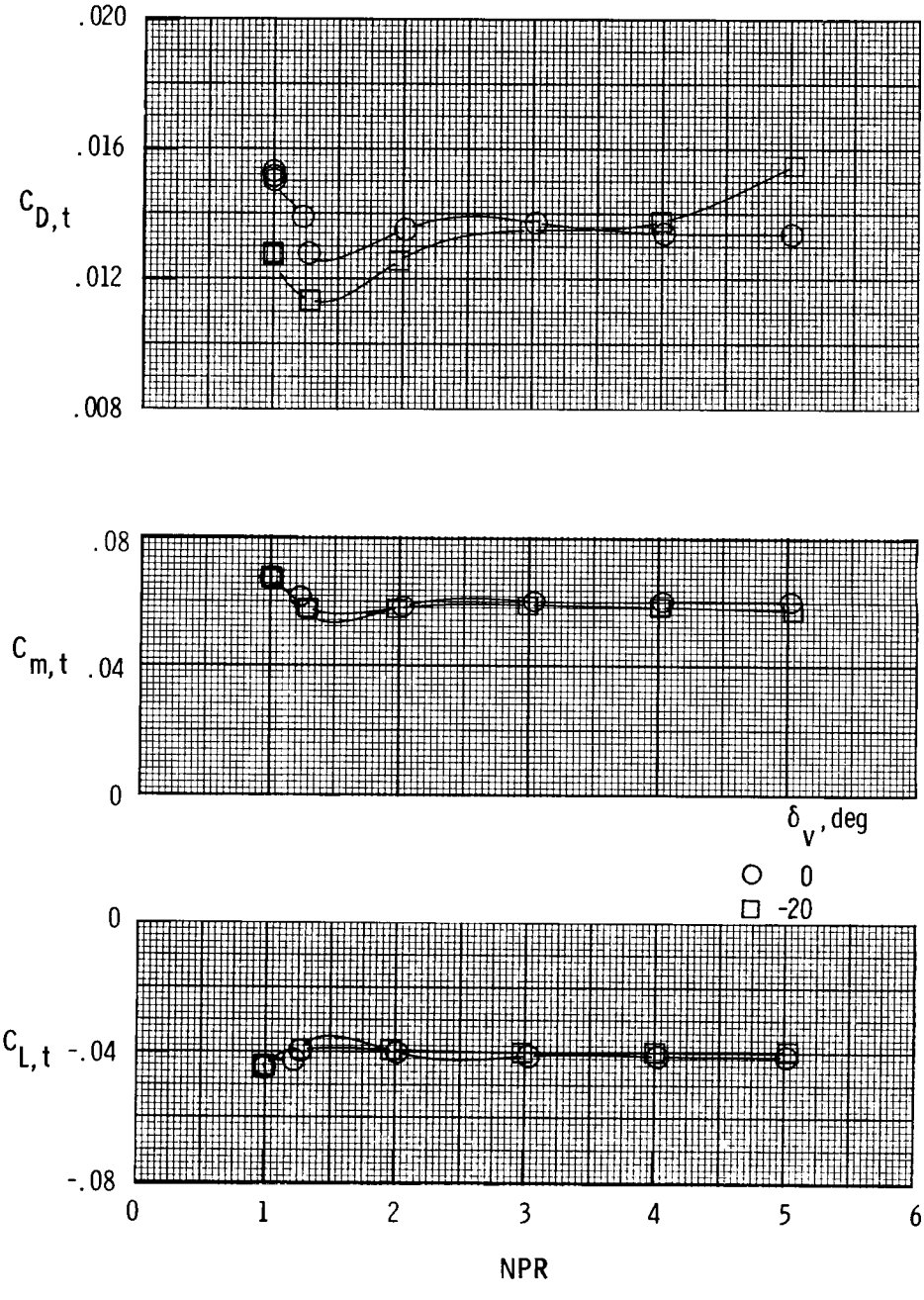

(a) Afterbody-nozzle characteristics with $M = 0.70$ and $\alpha = 0°$.

Figure 8. Afterbody and nozzle longitudinal characteristics for model with TF30 cruise nozzles and yaw vanes installed. $\Lambda = 68°$; $\delta_h = -2°$.

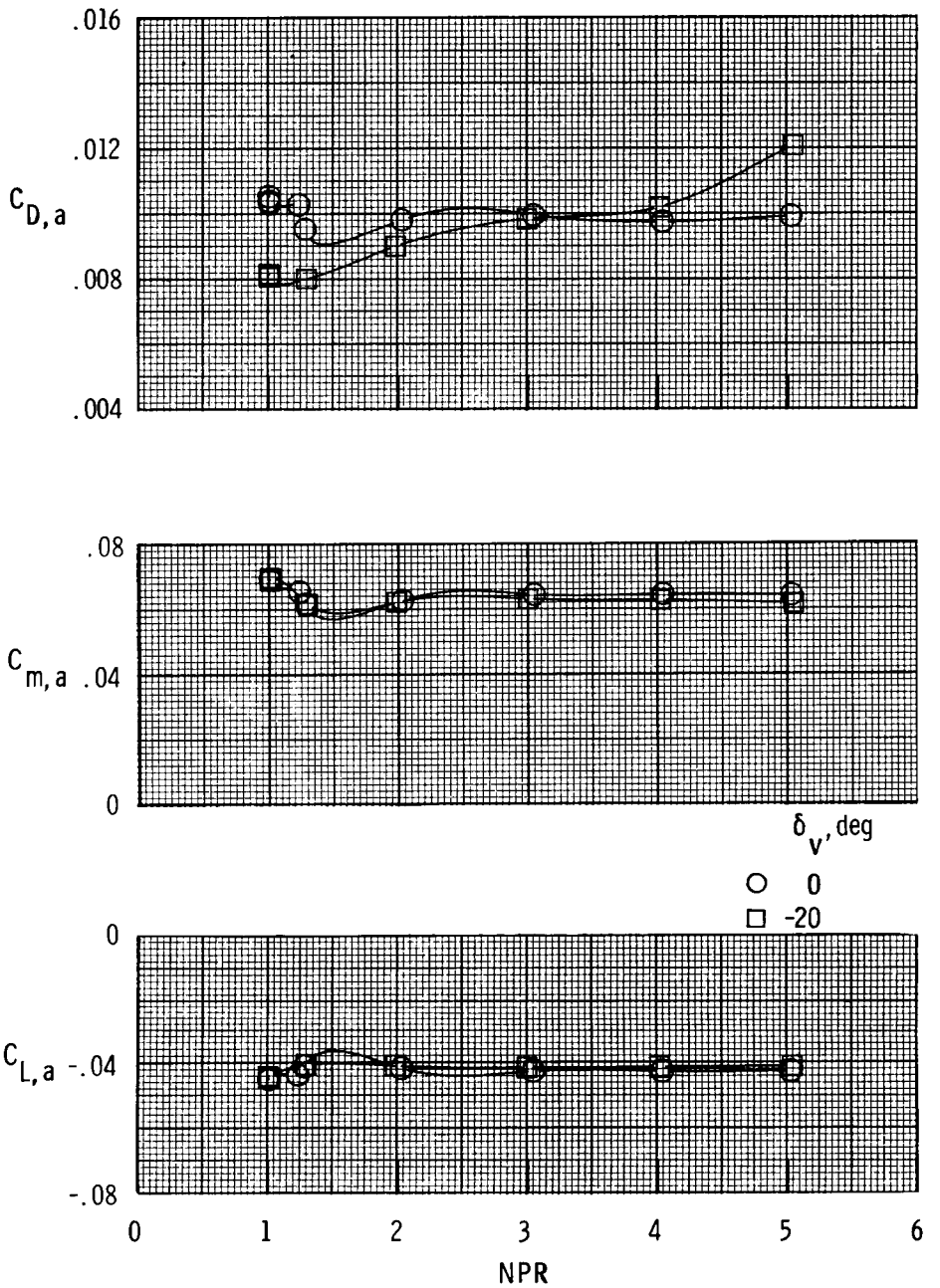

(b) Afterbody characteristics with $M = 0.70$ and $\alpha = 0°$.

Figure 8. Continued.

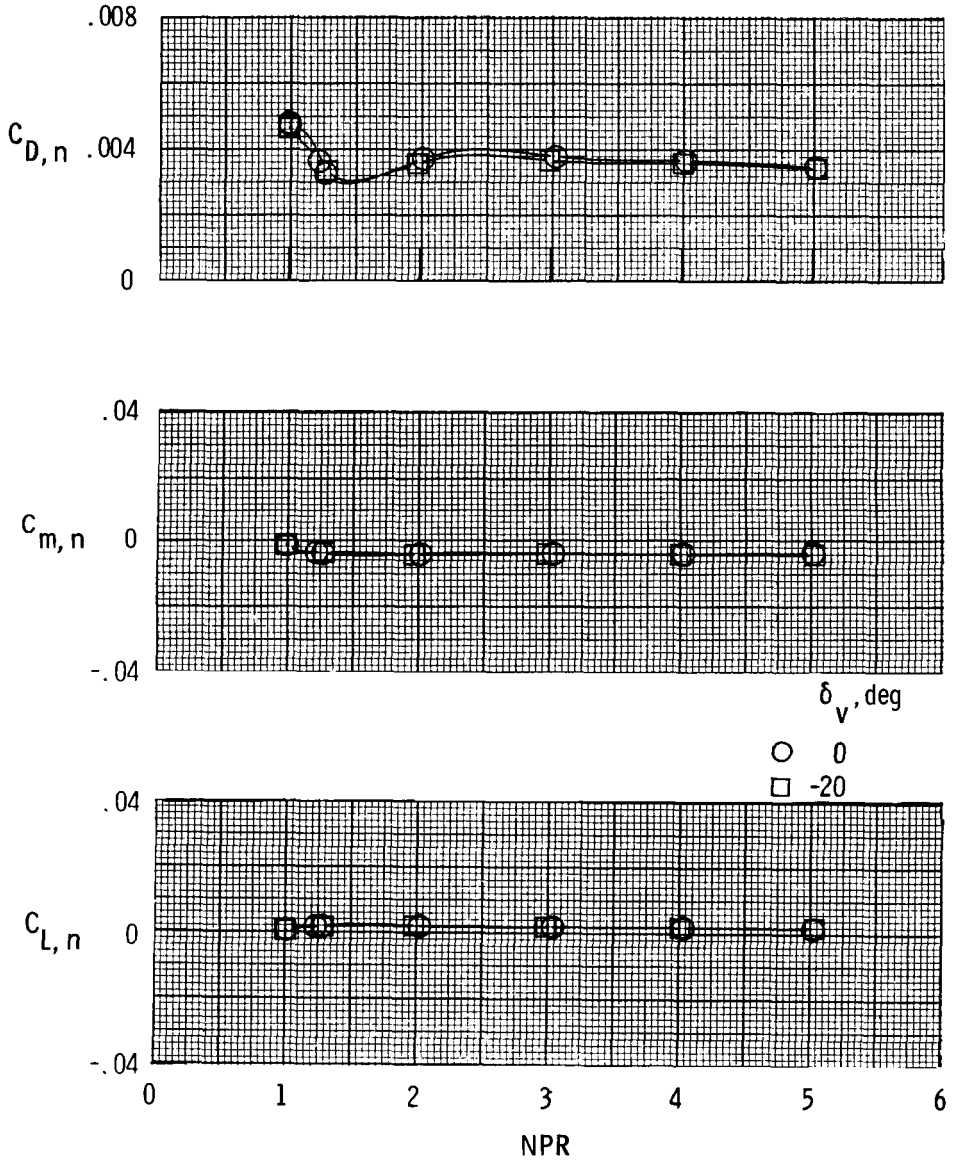

(c) Nozzle characteristics with $M = 0.70$ and $\alpha = 0°$.

Figure 8. Continued.

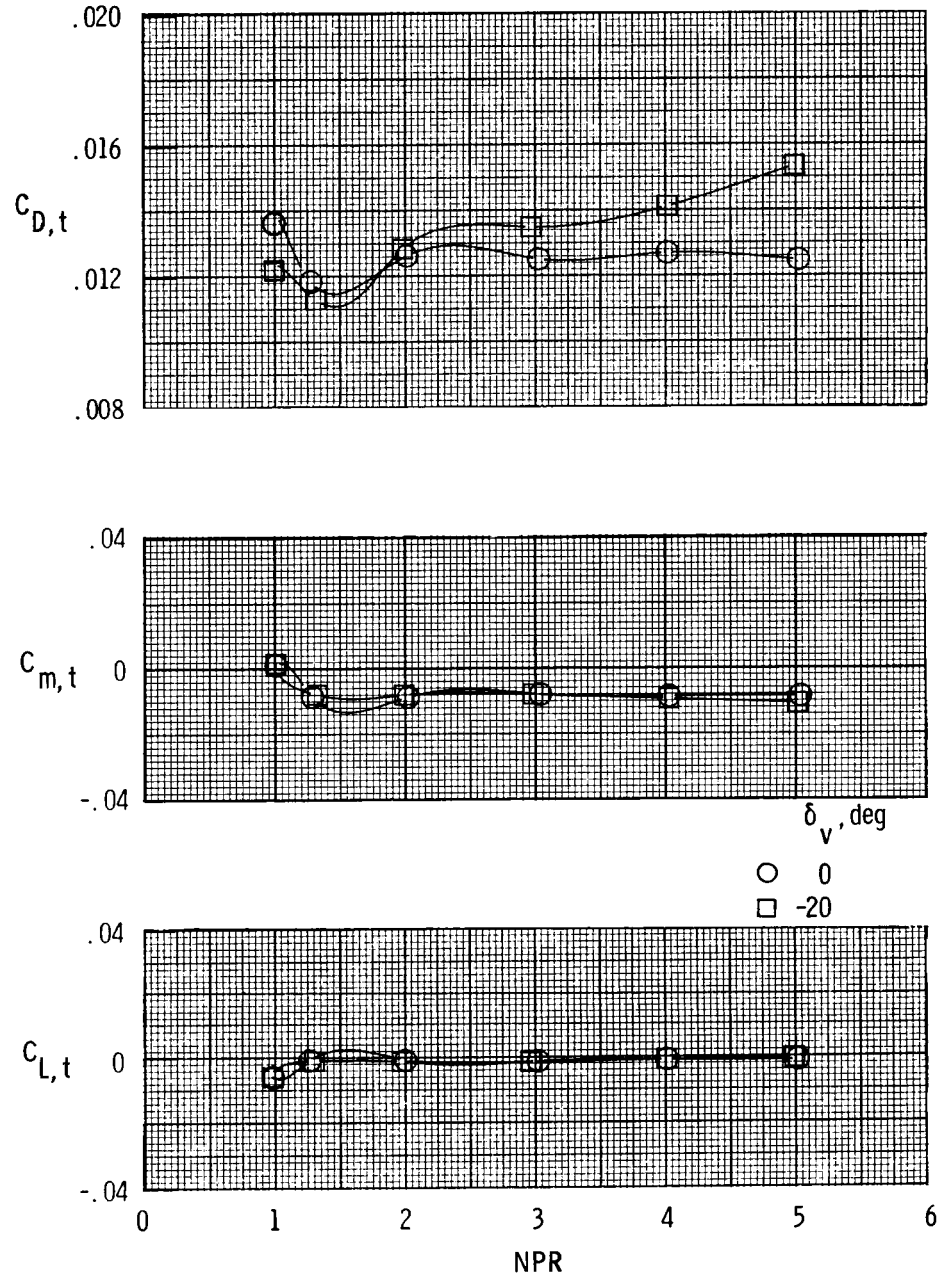

(d) Afterbody-nozzle characteristics with $M = 0.70$ and $\alpha = 4.3°$.

Figure 8. Continued.

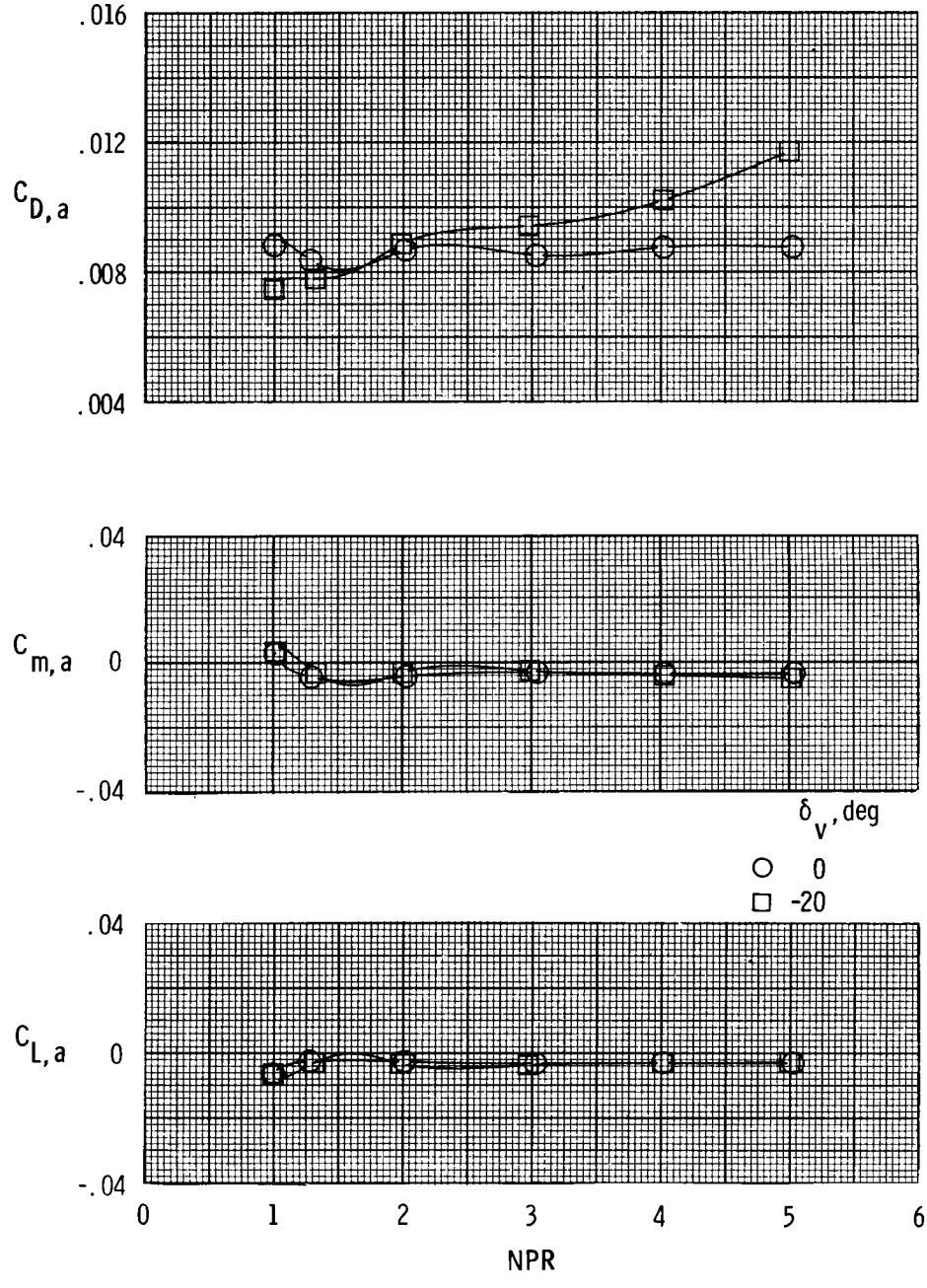

(e) Afterbody characteristics with $M = 0.70$ and $\alpha = 4.3°$.

Figure 8. Continued.

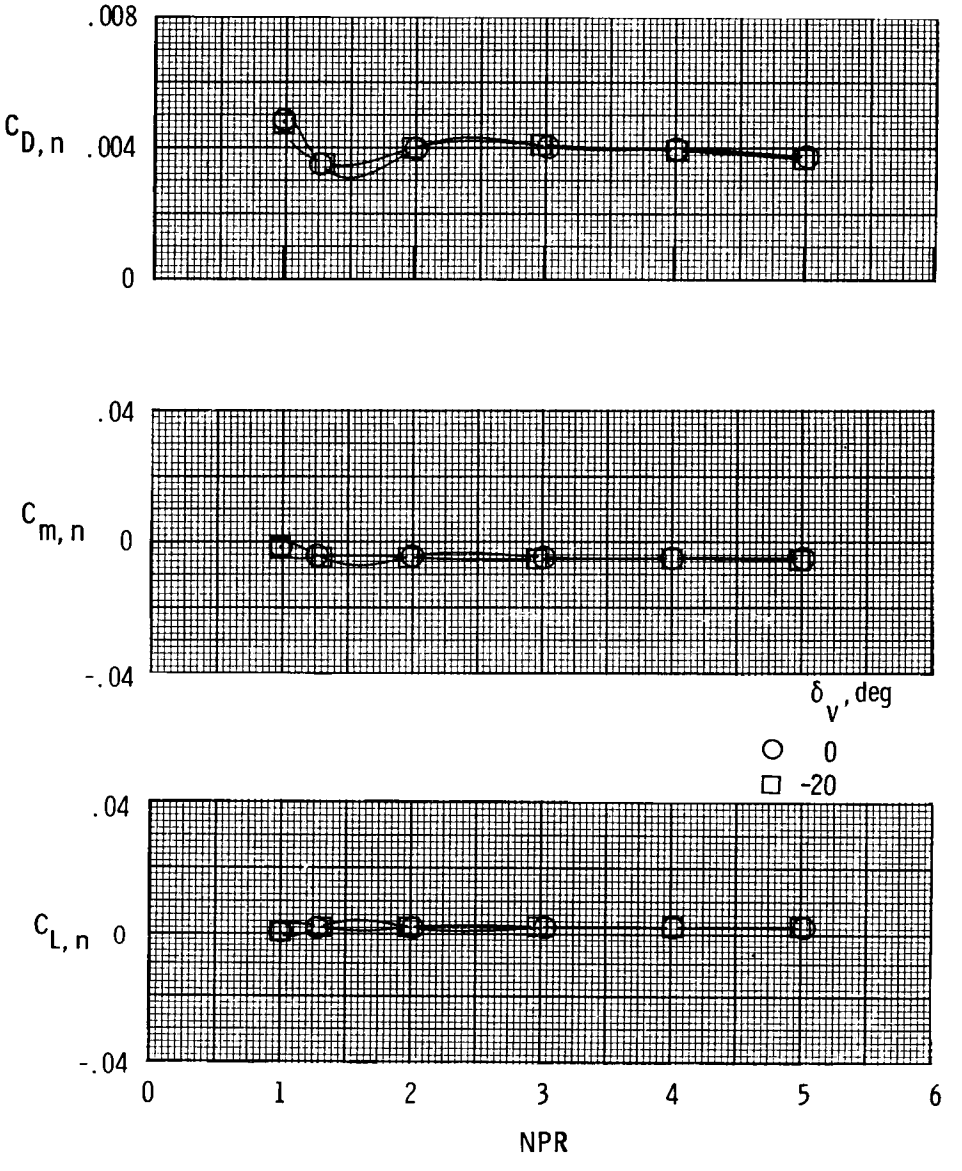

(f) Nozzle characteristics with $M = 0.70$ and $\alpha = 4.3°$.

Figure 8. Continued.

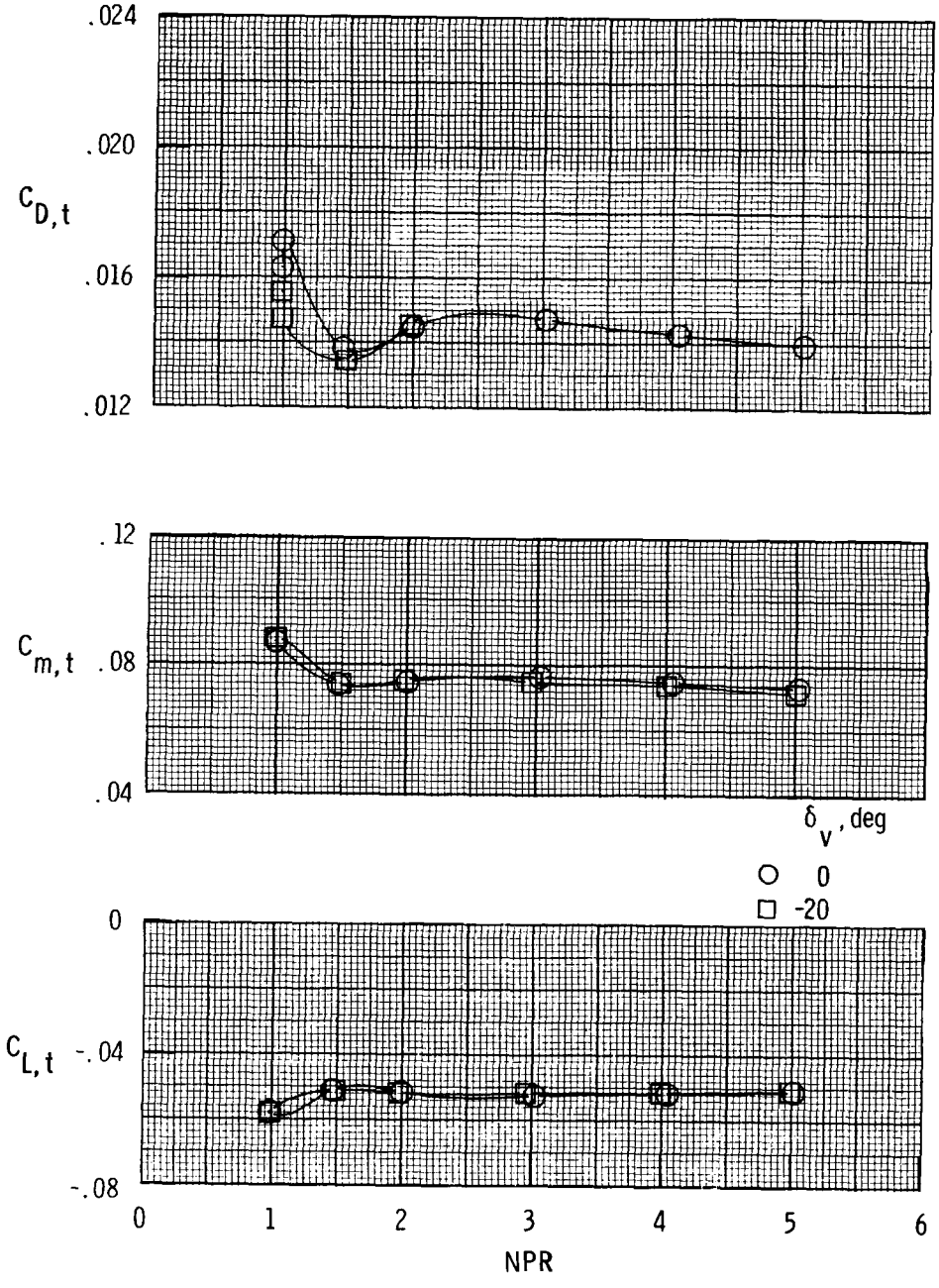

(g) Afterbody-nozzle characteristics with $M = 0.90$ and $\alpha = 0°$.

Figure 8. Continued.

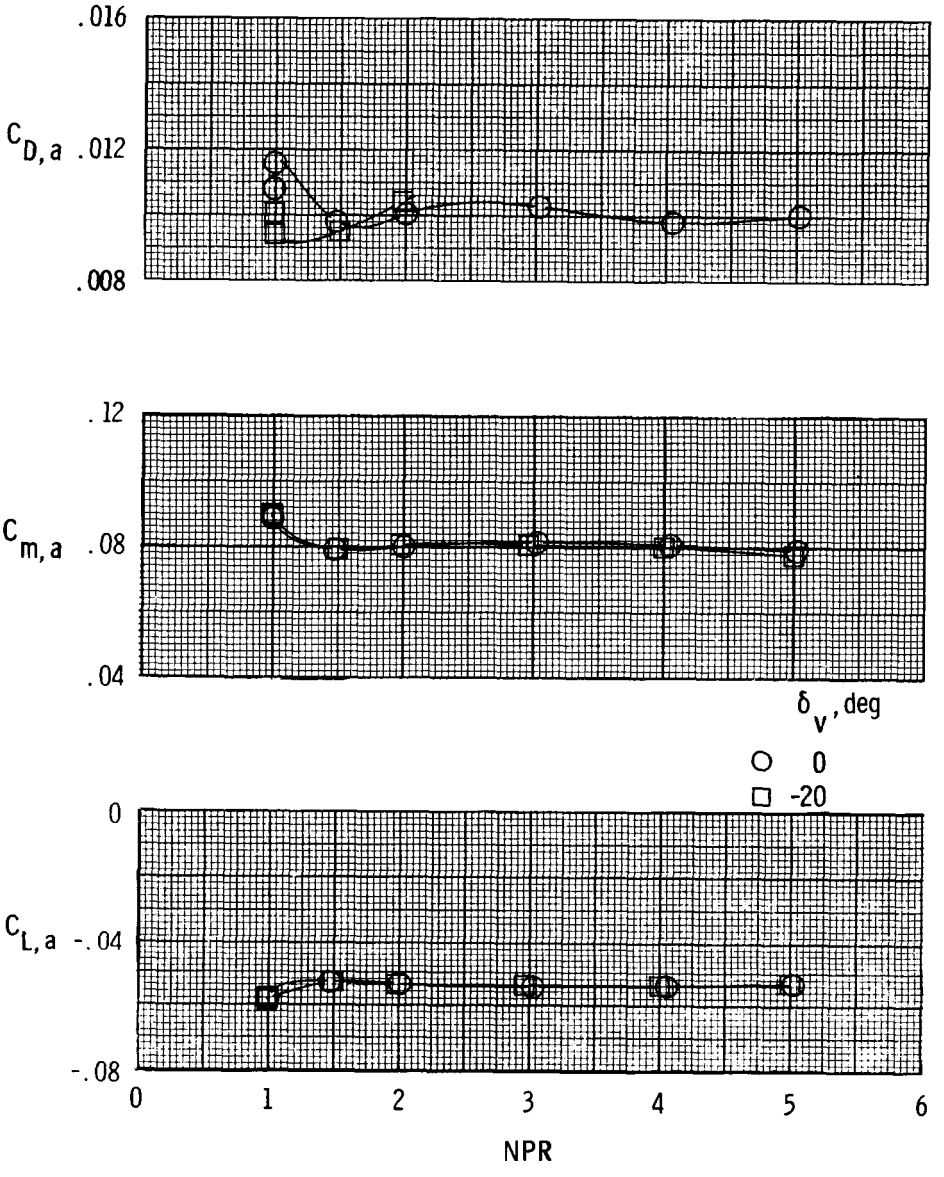

(h) Afterbody characteristics with $M = 0.90$ and $\alpha = 0°$.

Figure 8. Continued.

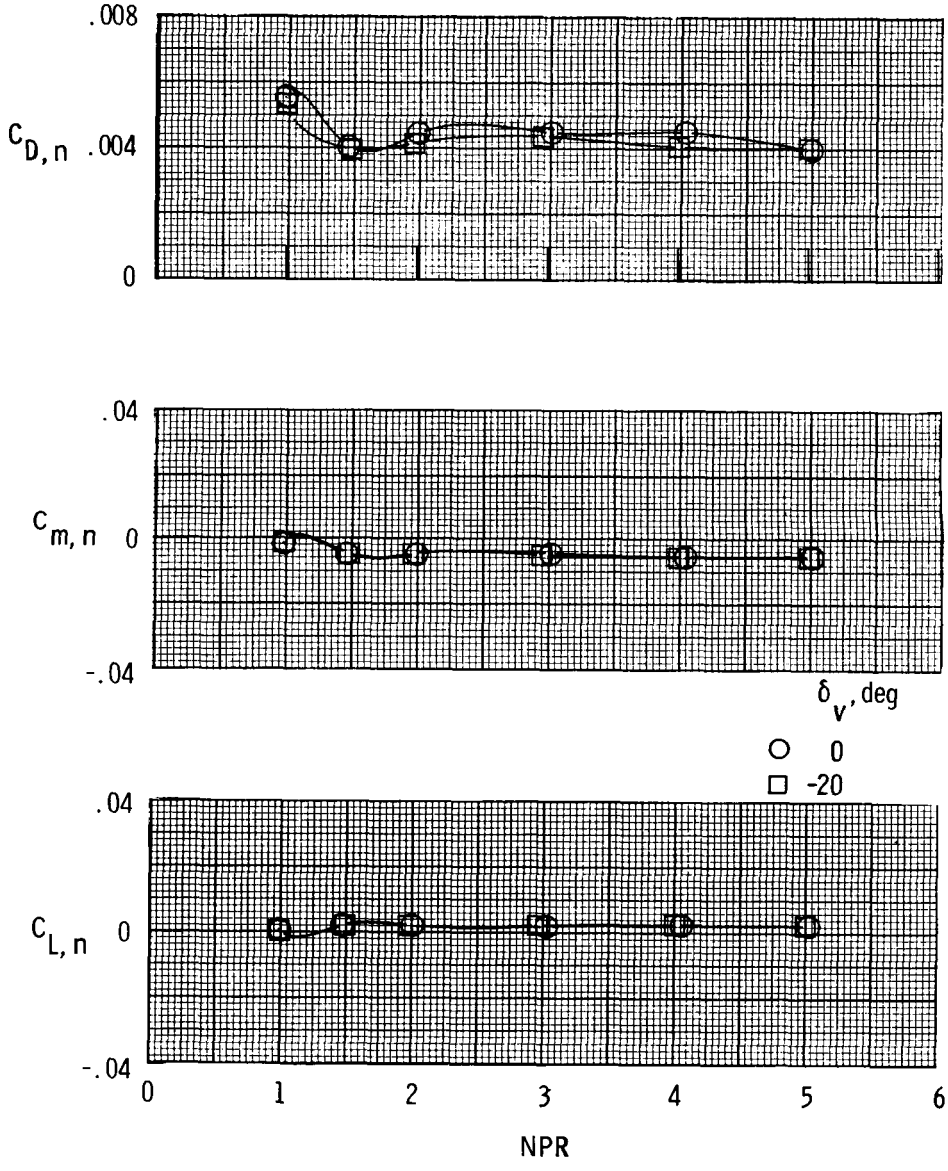

(i) Nozzle characteristics with $M = 0.90$ and $\alpha = 0°$.

Figure 8. Continued.

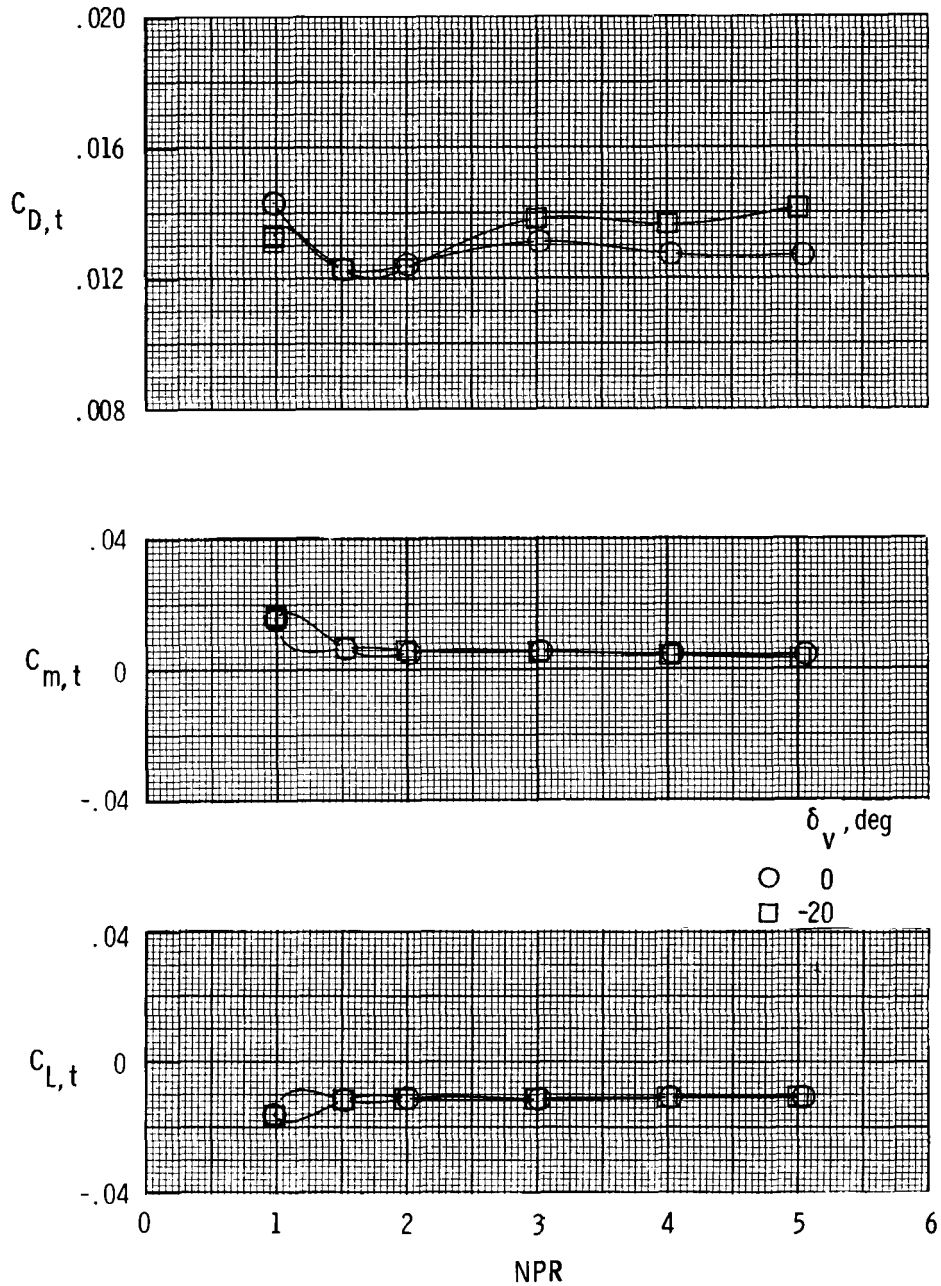

(j) Afterbody-nozzle characteristics with $M = 0.90$ and $\alpha = 4.3°$.

Figure 8. Continued.

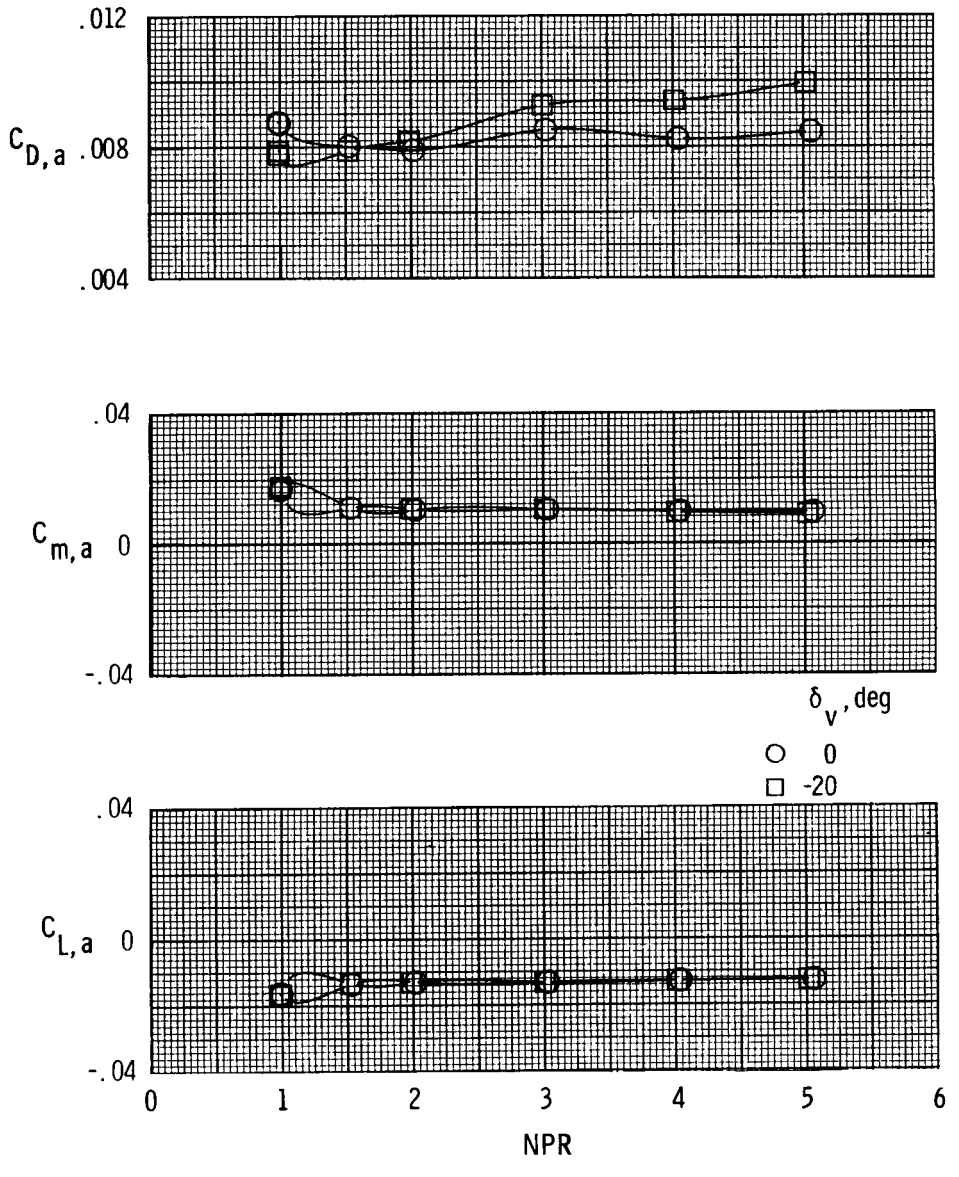

(k) Afterbody characteristics with $M = 0.90$ and $\alpha = 4.3°$.

Figure 8. Continued.

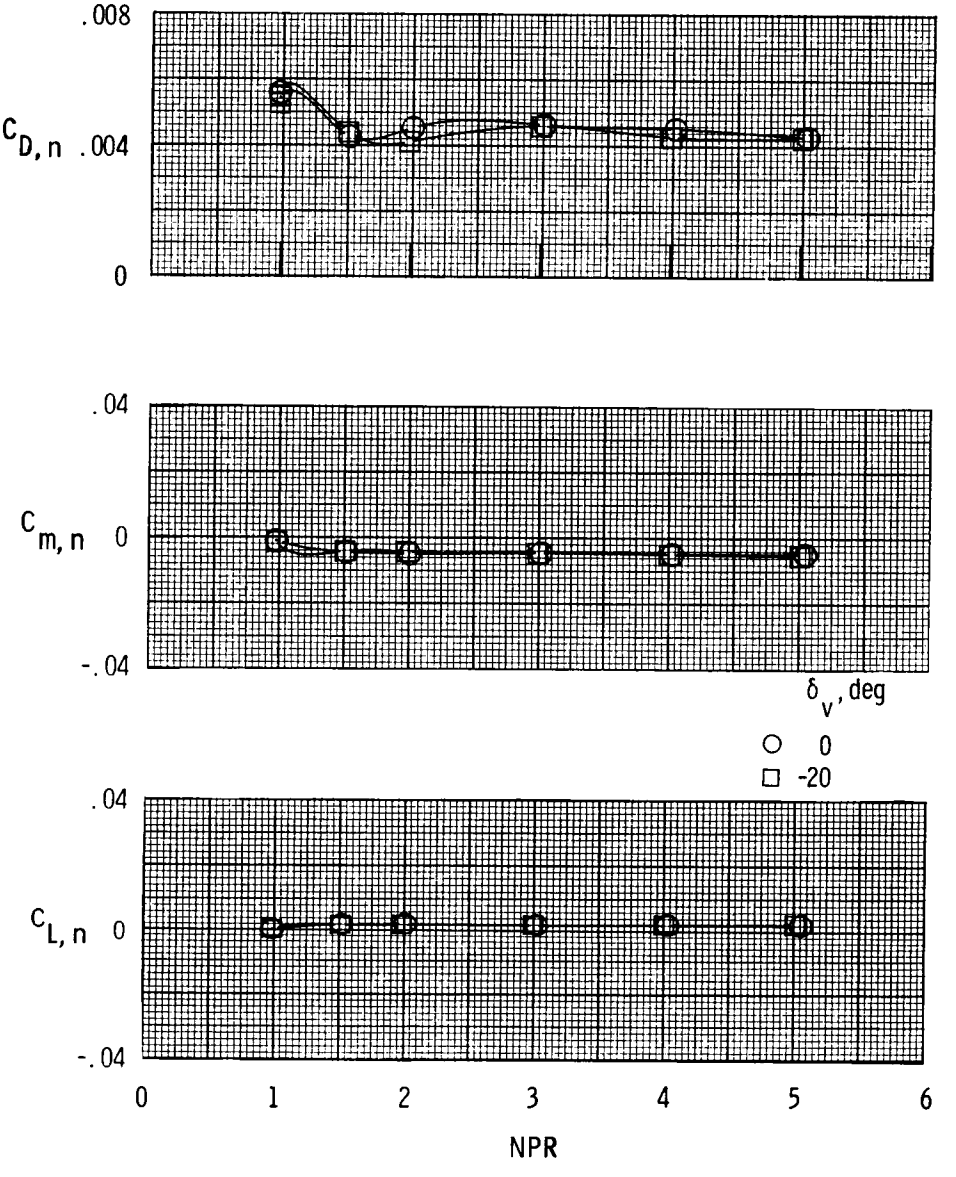

(l) Nozzle characteristics with $M = 0.90$ and $\alpha = 4.3°$.

Figure 8. Continued.

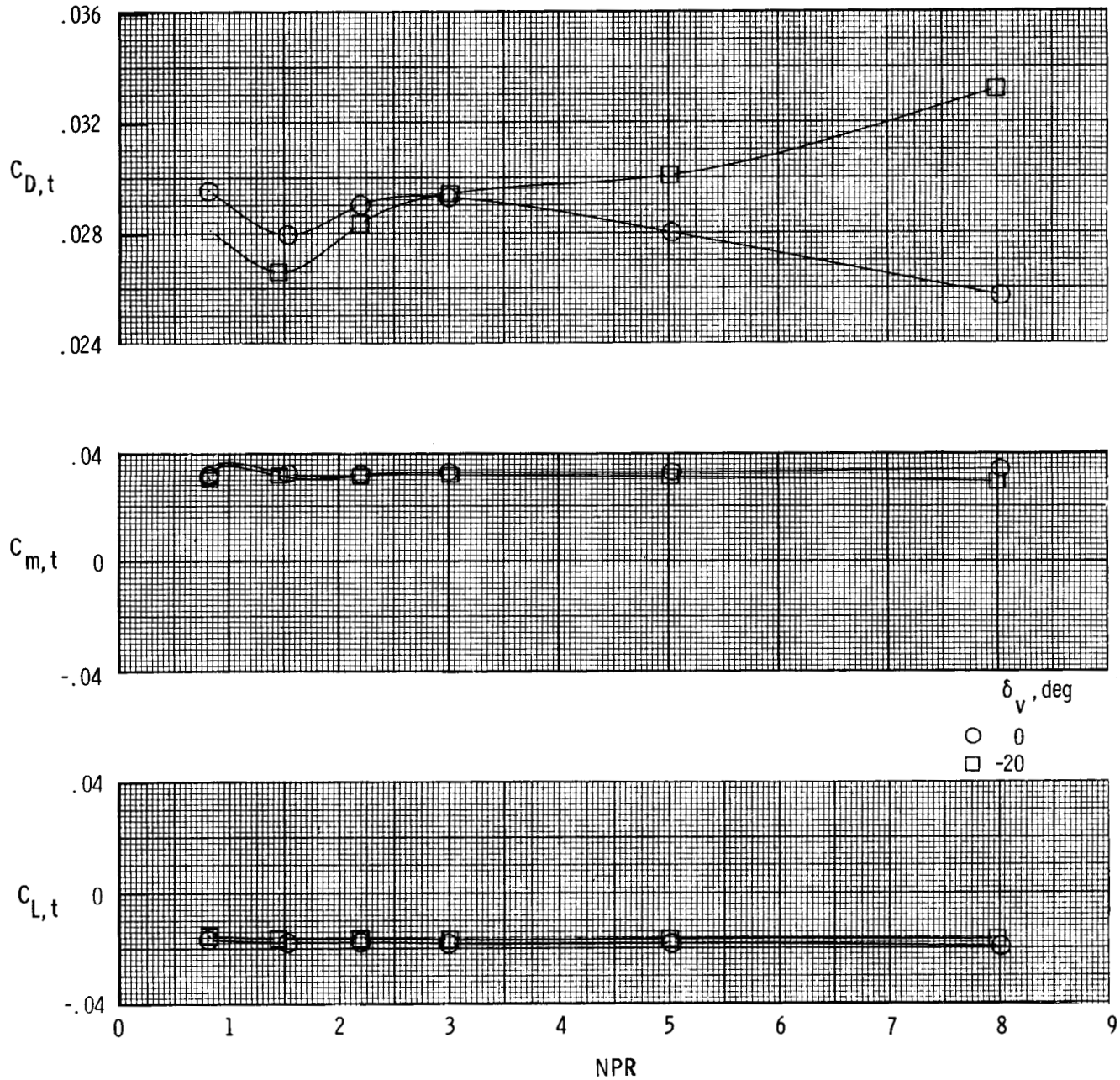

(m) Afterbody-nozzle characteristics with $M = 1.25$ and $\alpha = 2°$.

Figure 8. Continued.

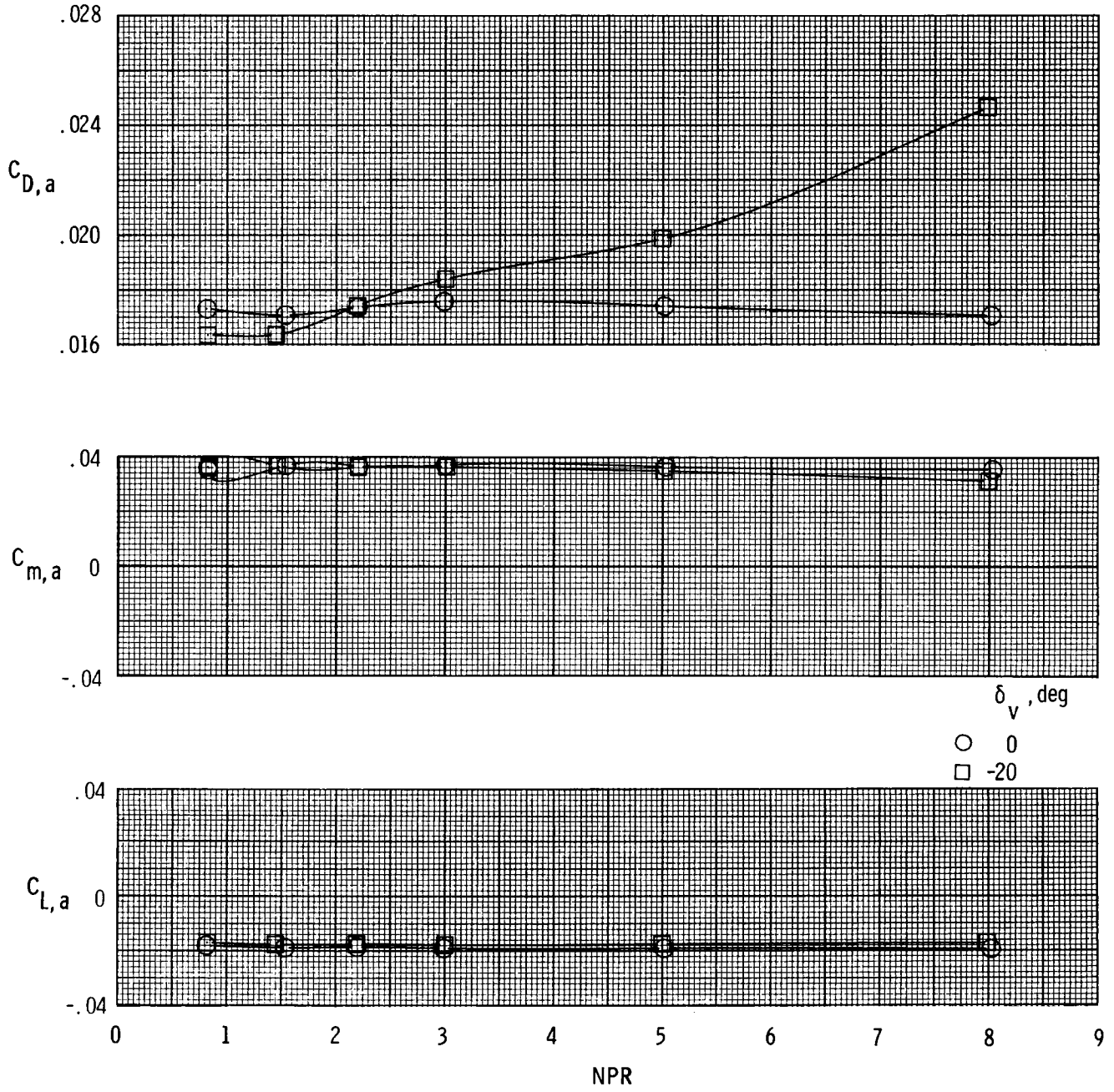

(n) Afterbody characteristics with $M = 1.25$ and $\alpha = 2°$.

Figure 8. Continued.

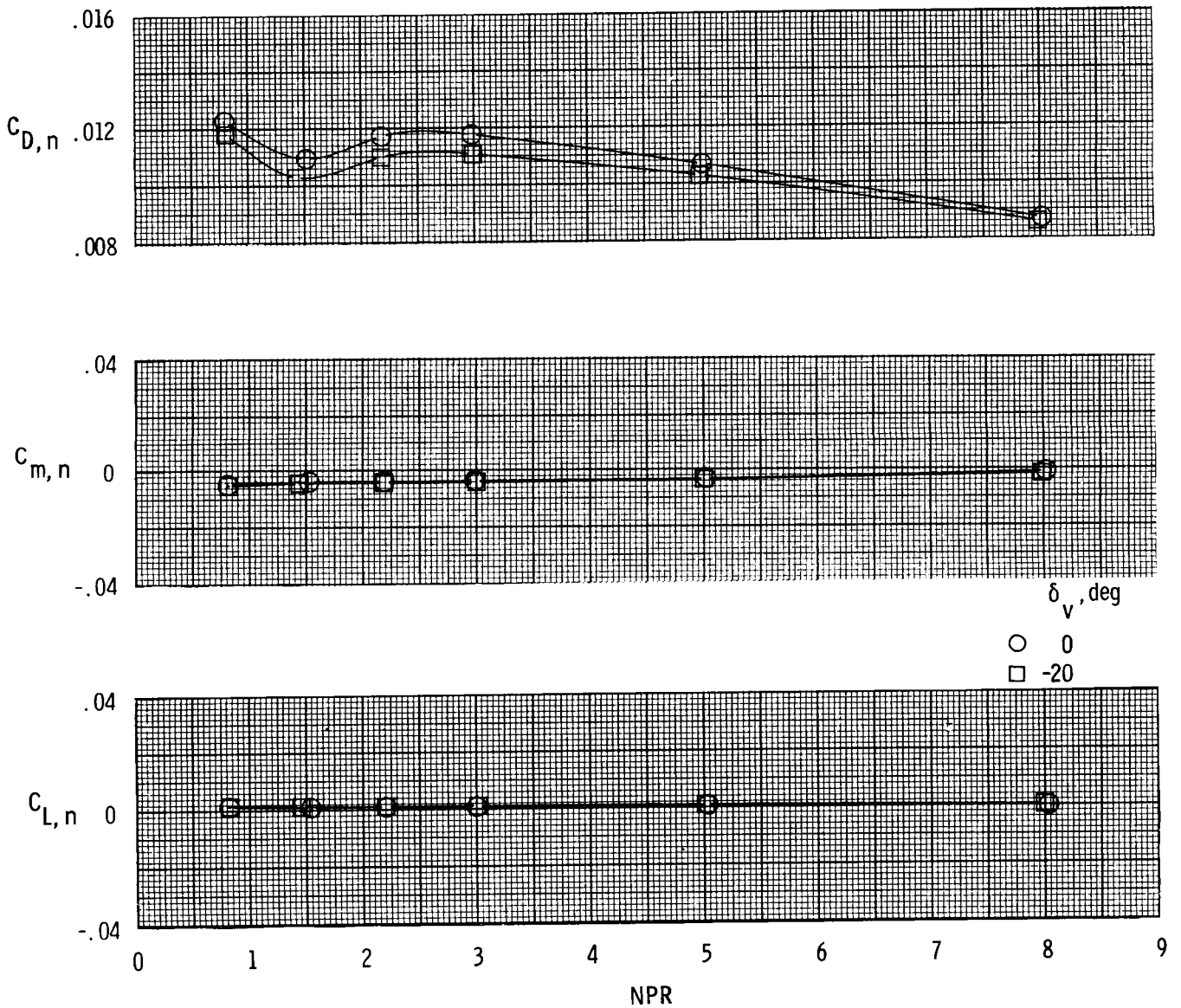

(o) Nozzle characteristics with $M = 1.25$ and $\alpha = 2°$.

Figure 8. Concluded.

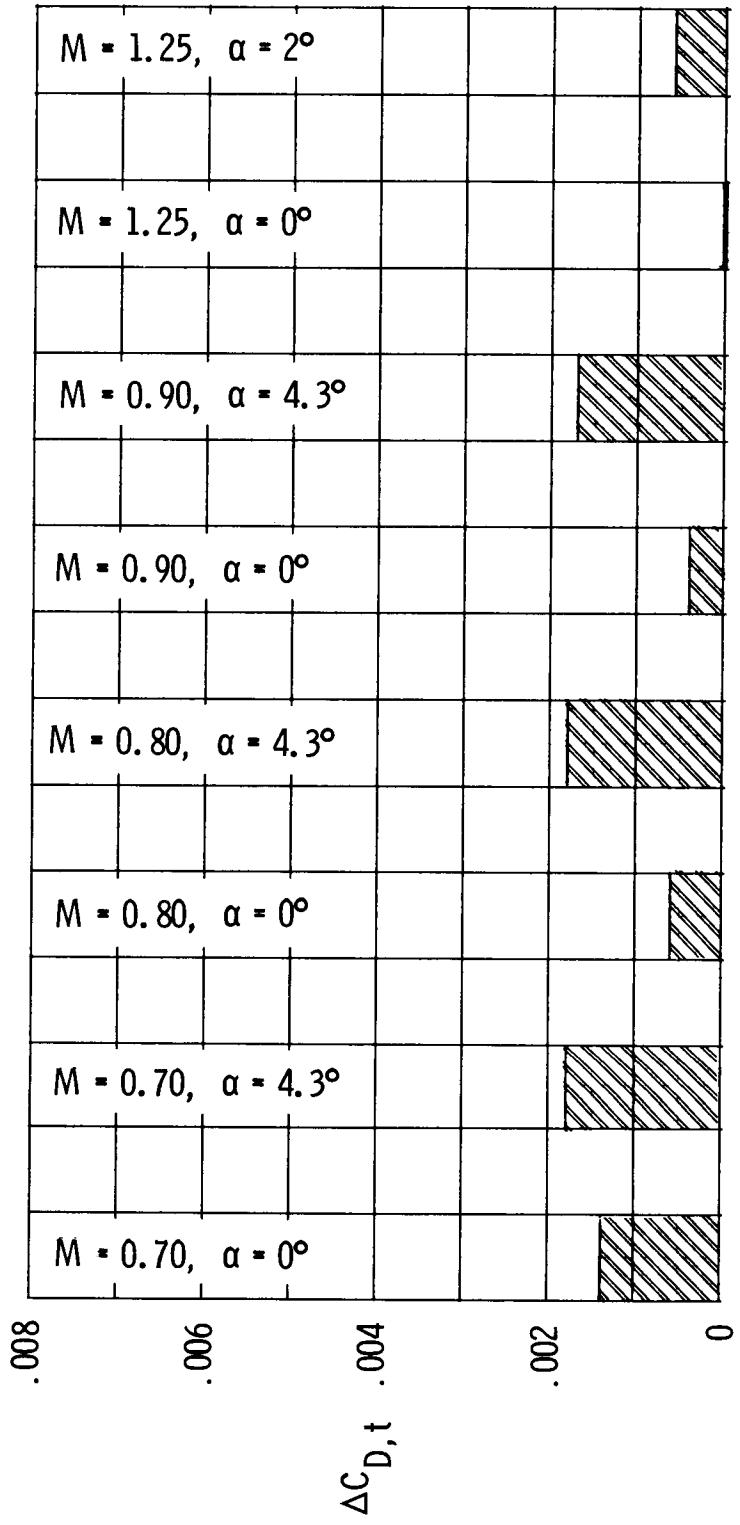

Figure 9. Drag increments for installation on yaw vanes on F-14 with F110 A/B nozzles. NPR = 3; $\Lambda = 68°; \delta_v = 0°; \delta_h = 0°$.

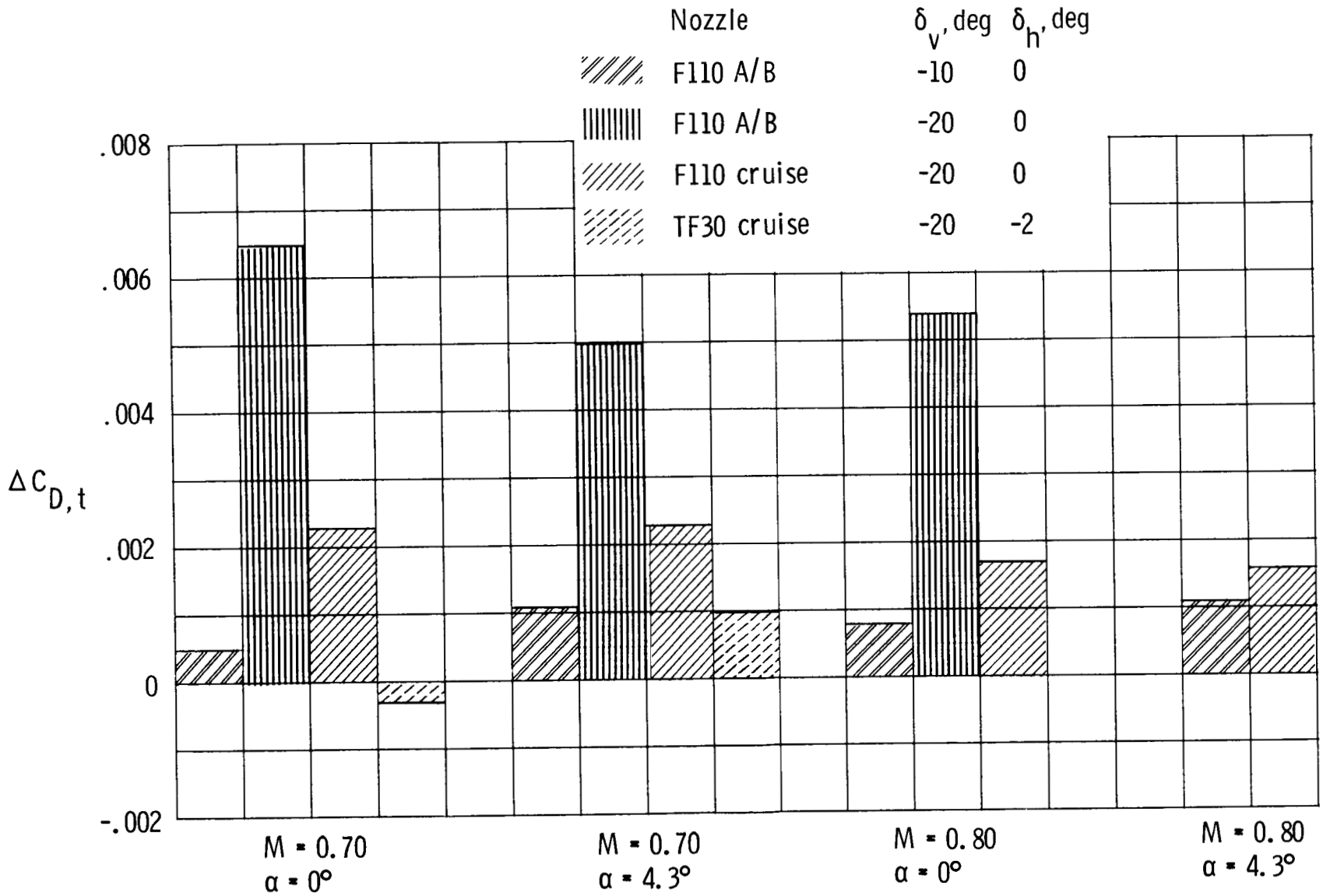

(a) $M = 0.70$ and 0.80.

Figure 10. Drag increments for deflection of yaw vanes from 0°. NPR = 3°; $\Lambda = 68°$.

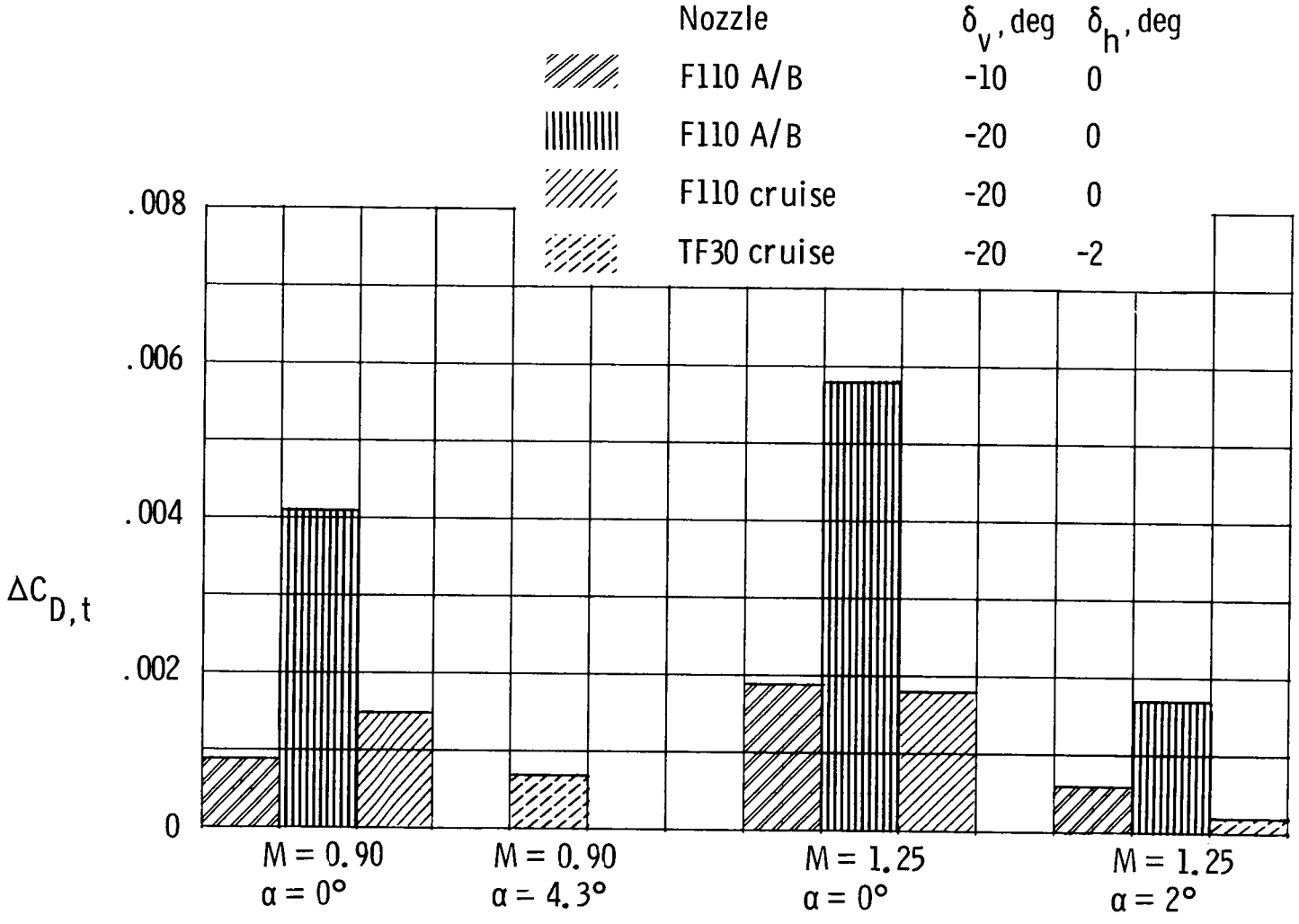

(b) $M = 0.90$ and 1.25.

Figure 10. Concluded.

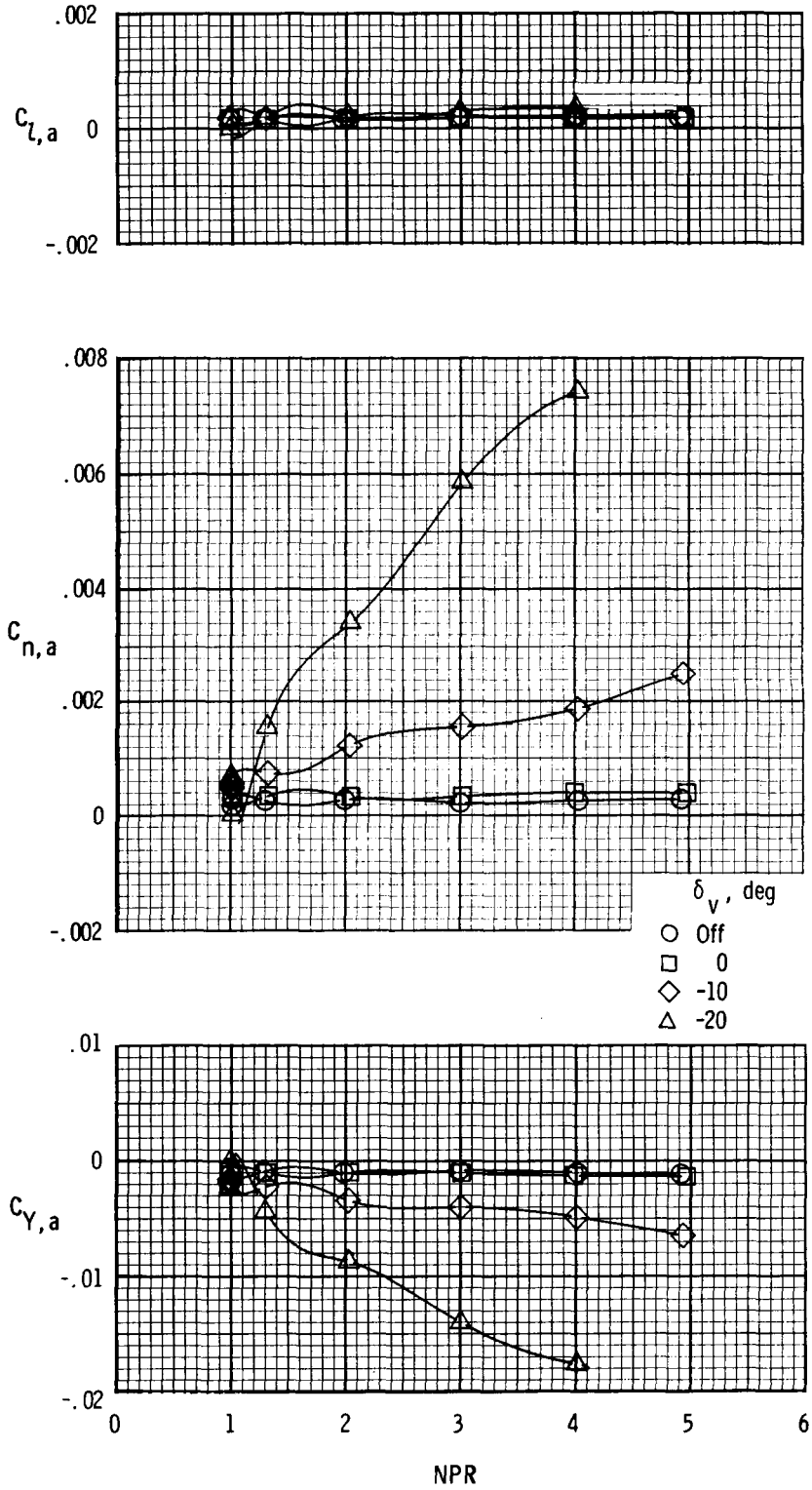

(a) $M = 0.70$ and $\alpha = 0°$.

Figure 11. Afterbody lateral-directional characteristics for model with F110 A/B nozzles and yaw vanes installed. $\Lambda = 68°$; $\delta_h = 0°$.

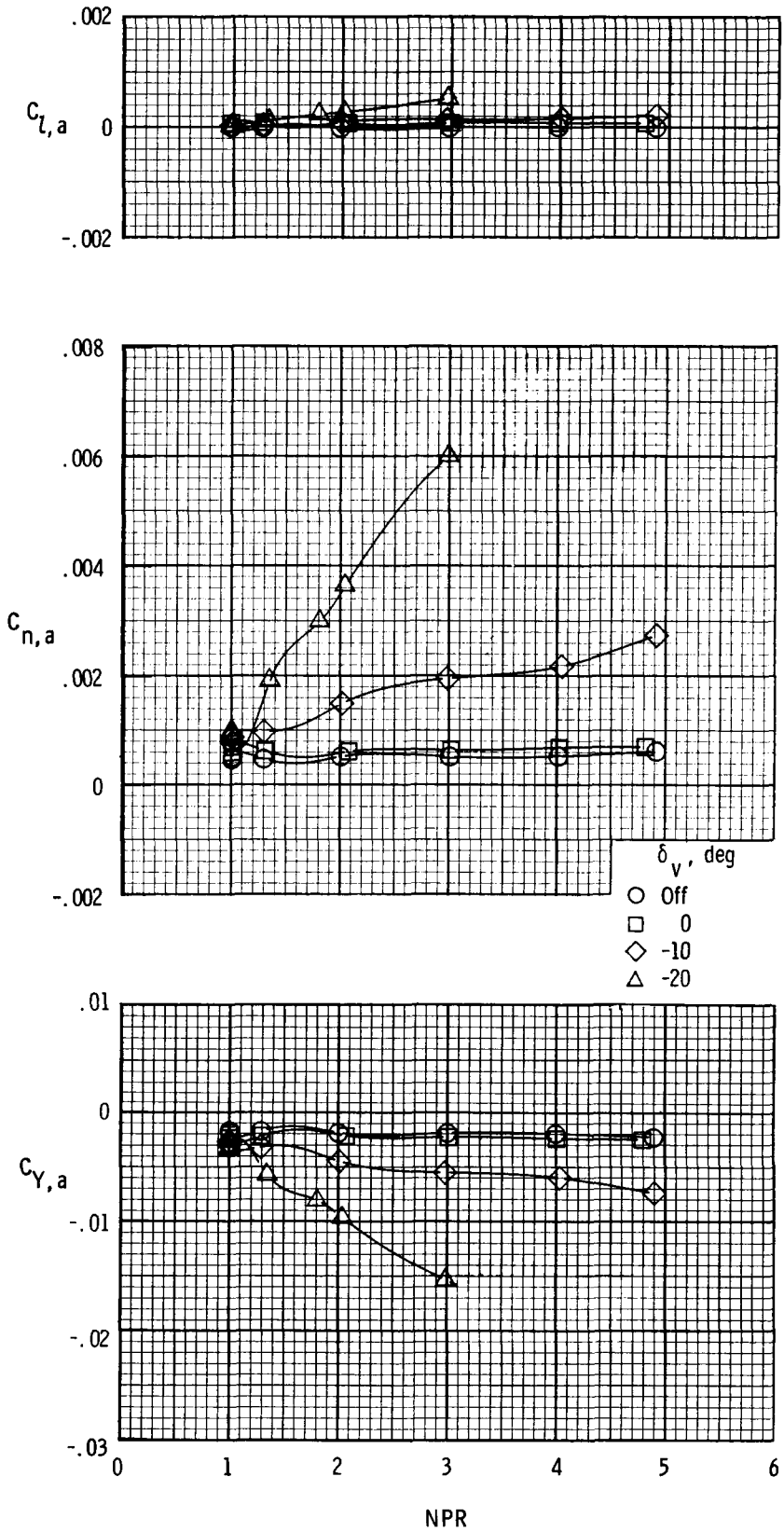

(b) $M = 0.70$ and $\alpha = 4.3°$.

Figure 11. Continued.

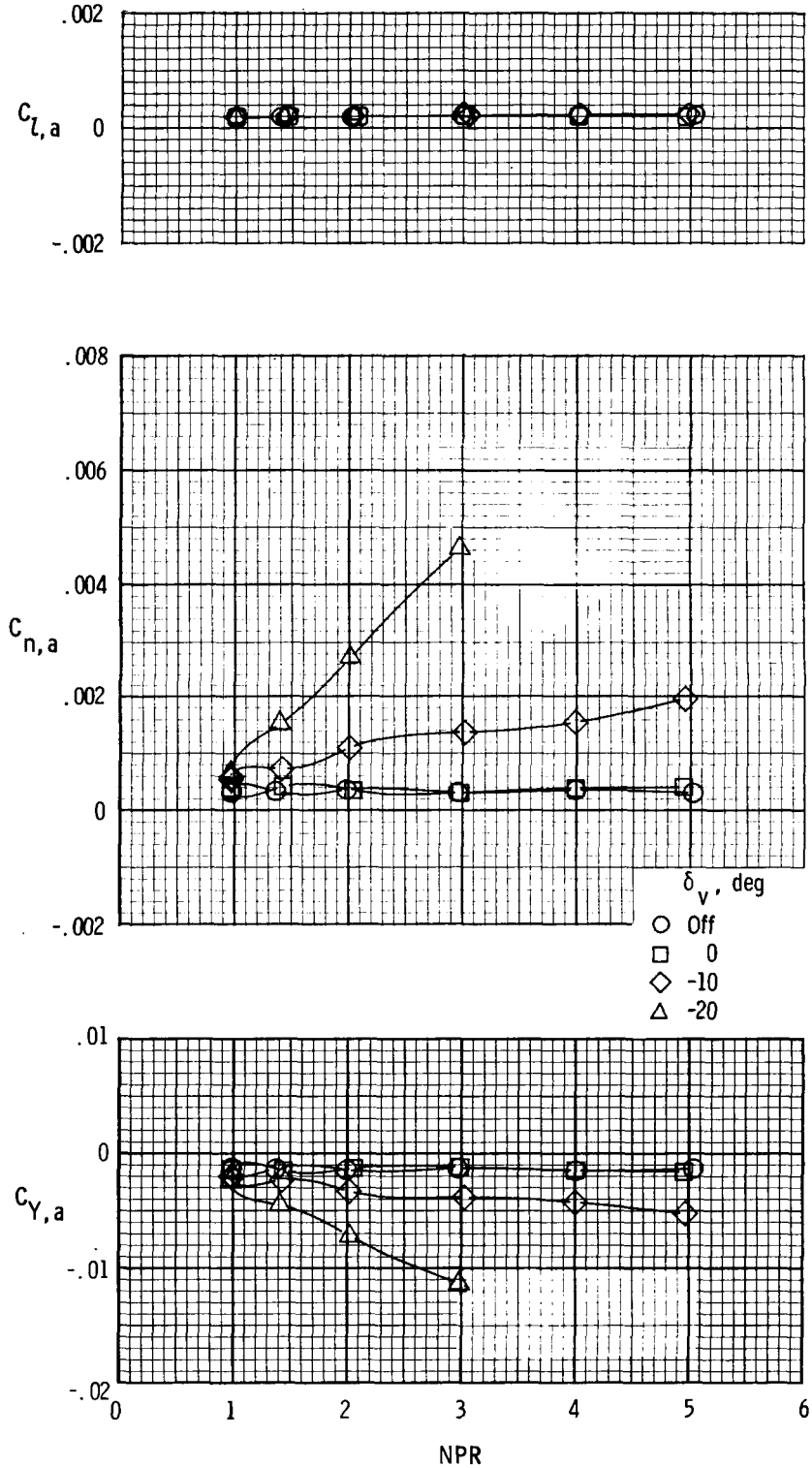

(c) $M = 0.80$ and $\alpha = 0°$.

Figure 11. Continued.

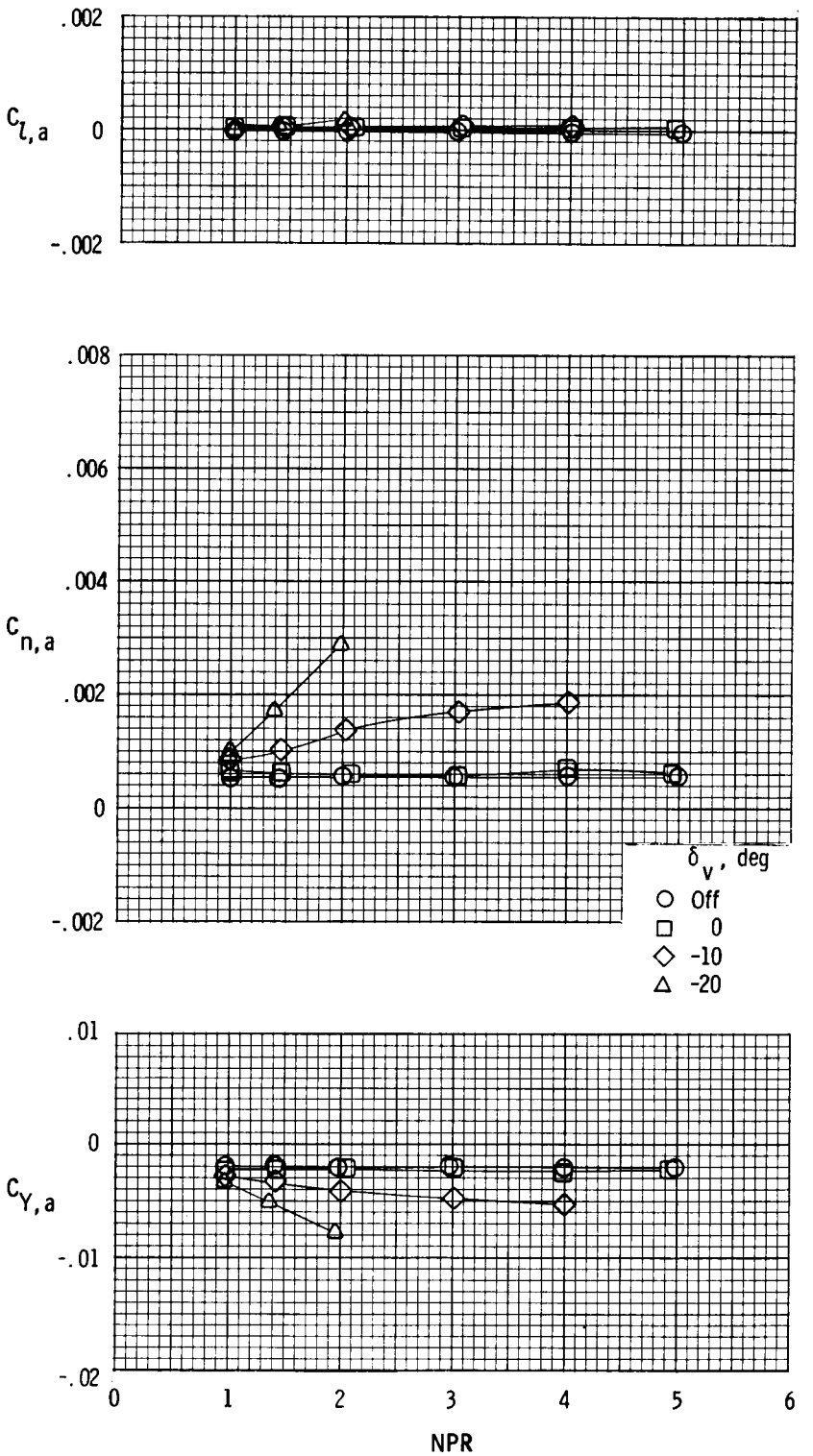

(d) $M = 0.80$ and $\alpha = 4.3°$.

Figure 11. Continued.

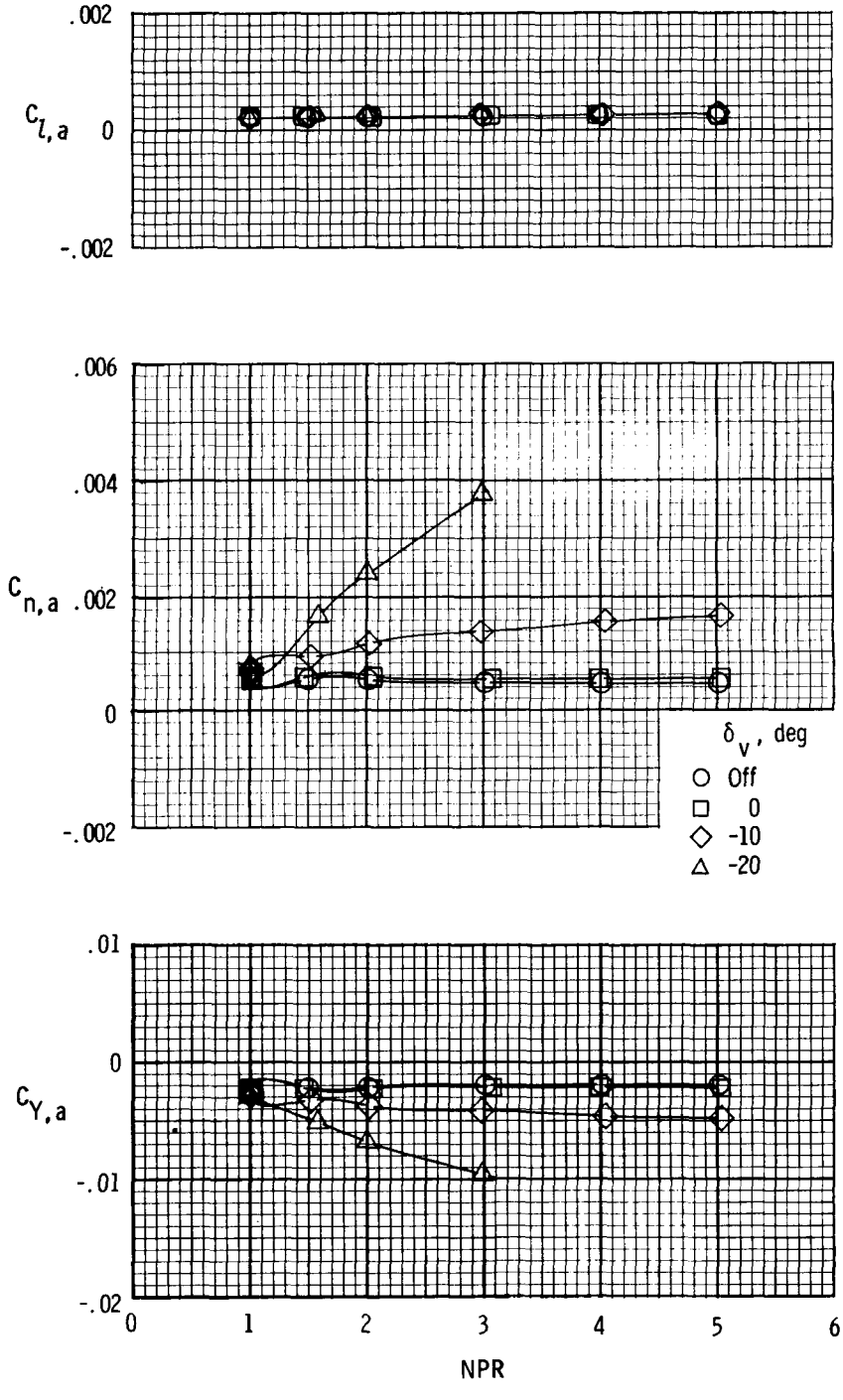

(e) $M = 0.90$ and $\alpha = 0°$.

Figure 11. Continued.

C-2

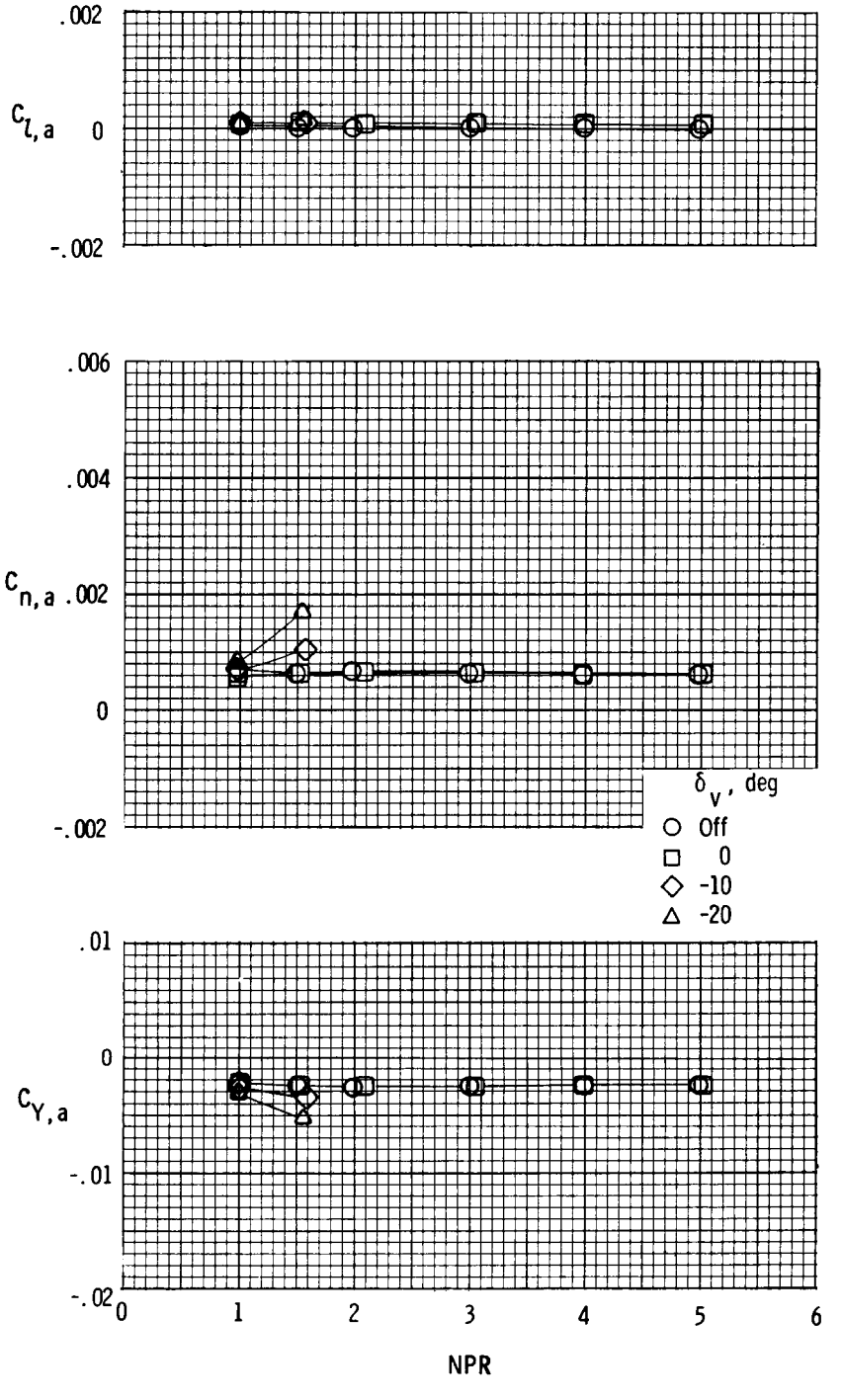

(f) $M = 0.90$ and $\alpha = 4.3°$.

Figure 11. Continued.

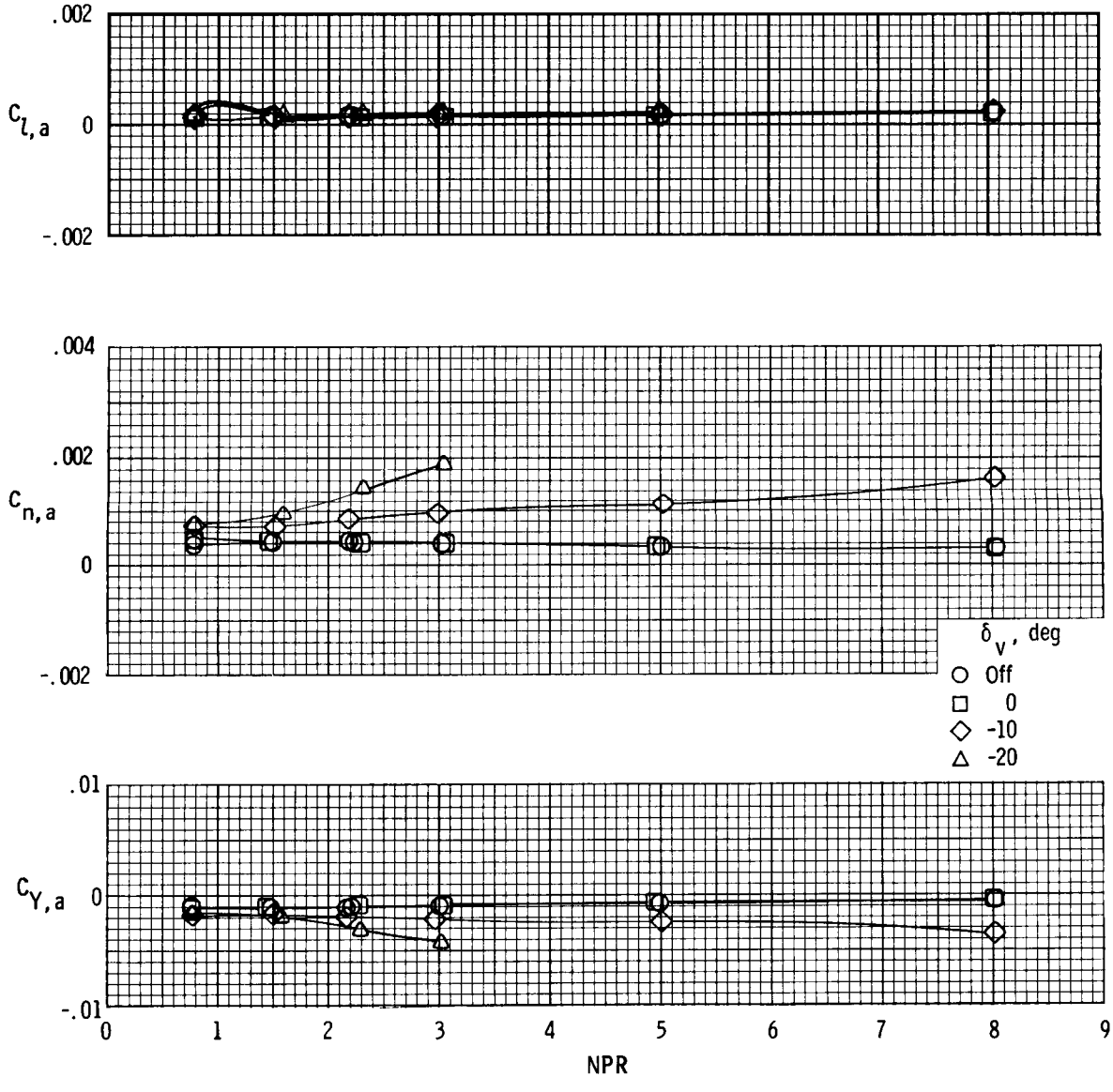

(g) $M = 1.25$ and $\alpha = 0°$.

Figure 11. Continued.

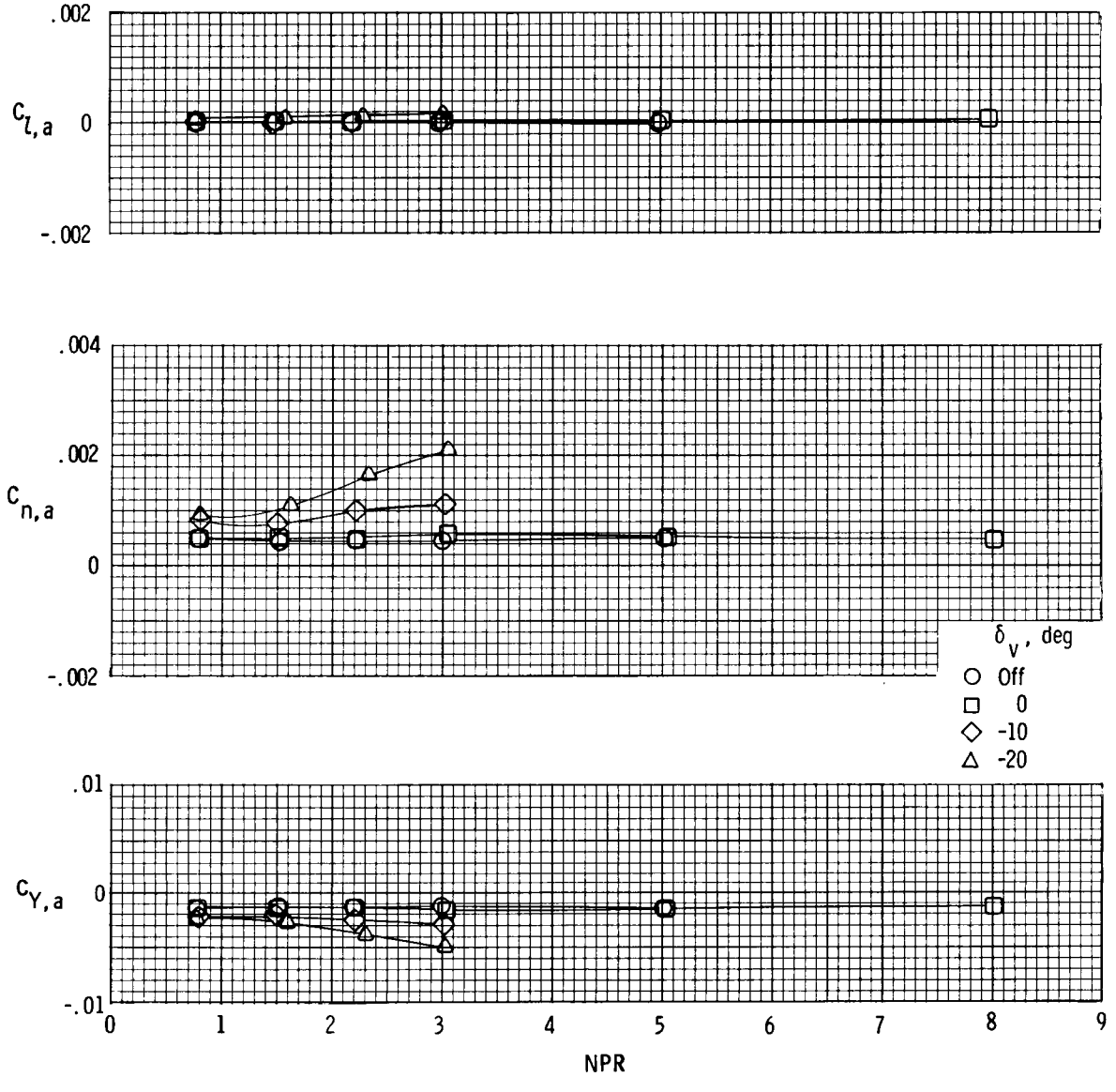

(h) $M = 1.25$ and $\alpha = 2°$.

Figure 11. Concluded.

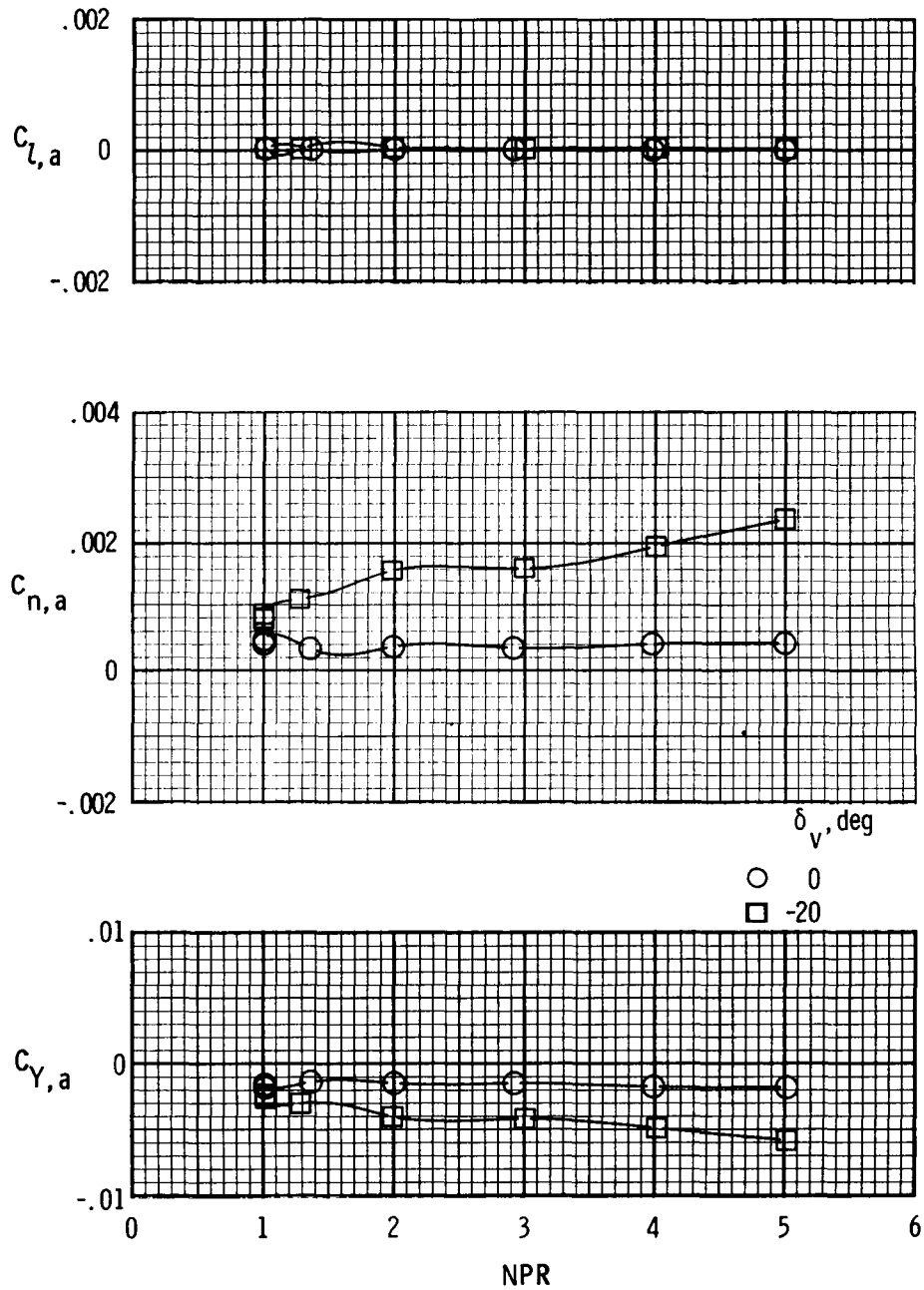

(a) $M = 0.70$ and $\alpha = 0°$.

Figure 12. Afterbody lateral-directional characteristics for model with F110 cruise nozzles and yaw vanes installed. $\Lambda = 68°$; $\delta_h = 0°$.

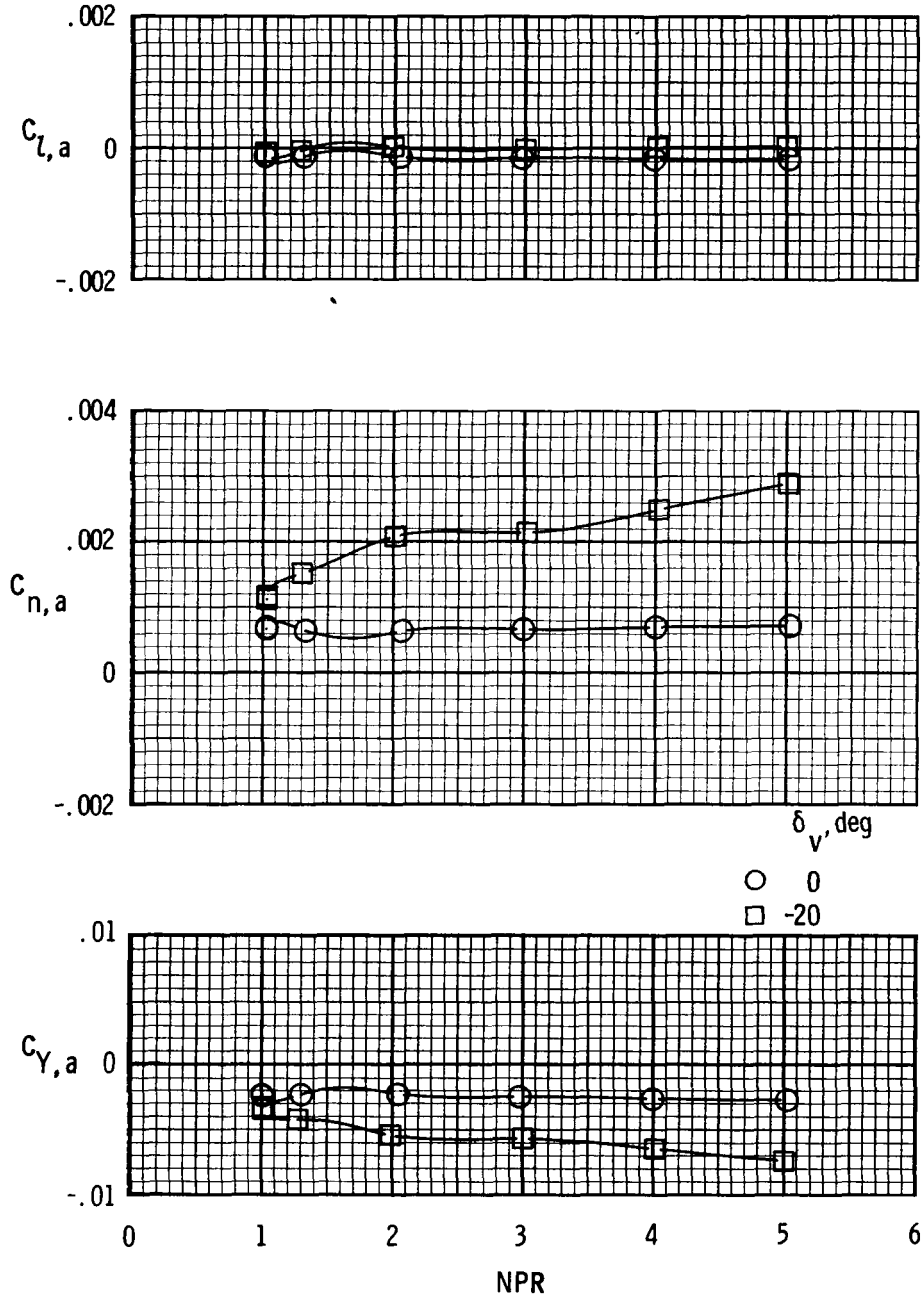

(b) $M = 0.70$ and $\alpha = 4.3°$.

Figure 12. Continued.

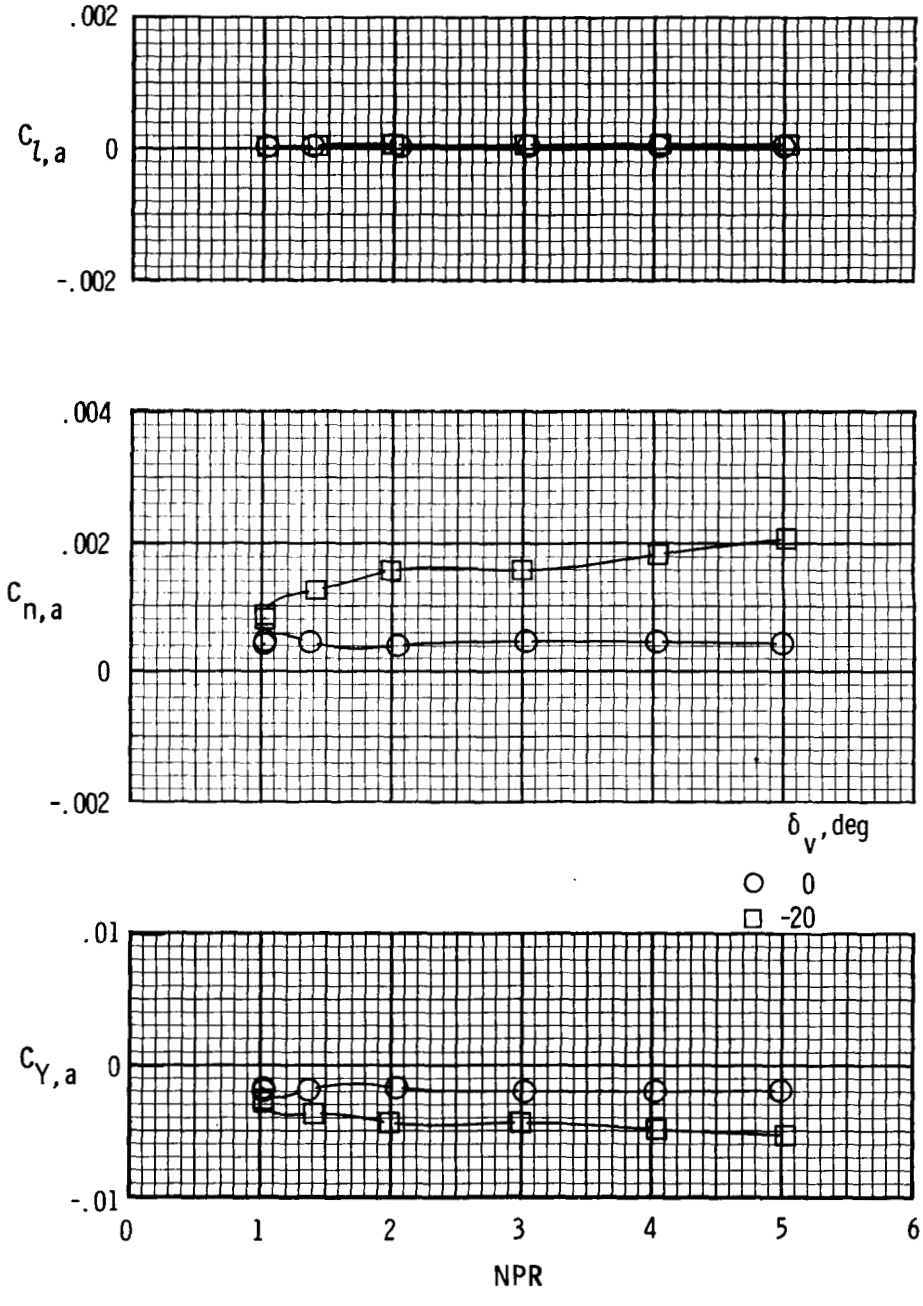

(c) $M = 0.80$ and $\alpha = 0°$.

Figure 12. Continued.

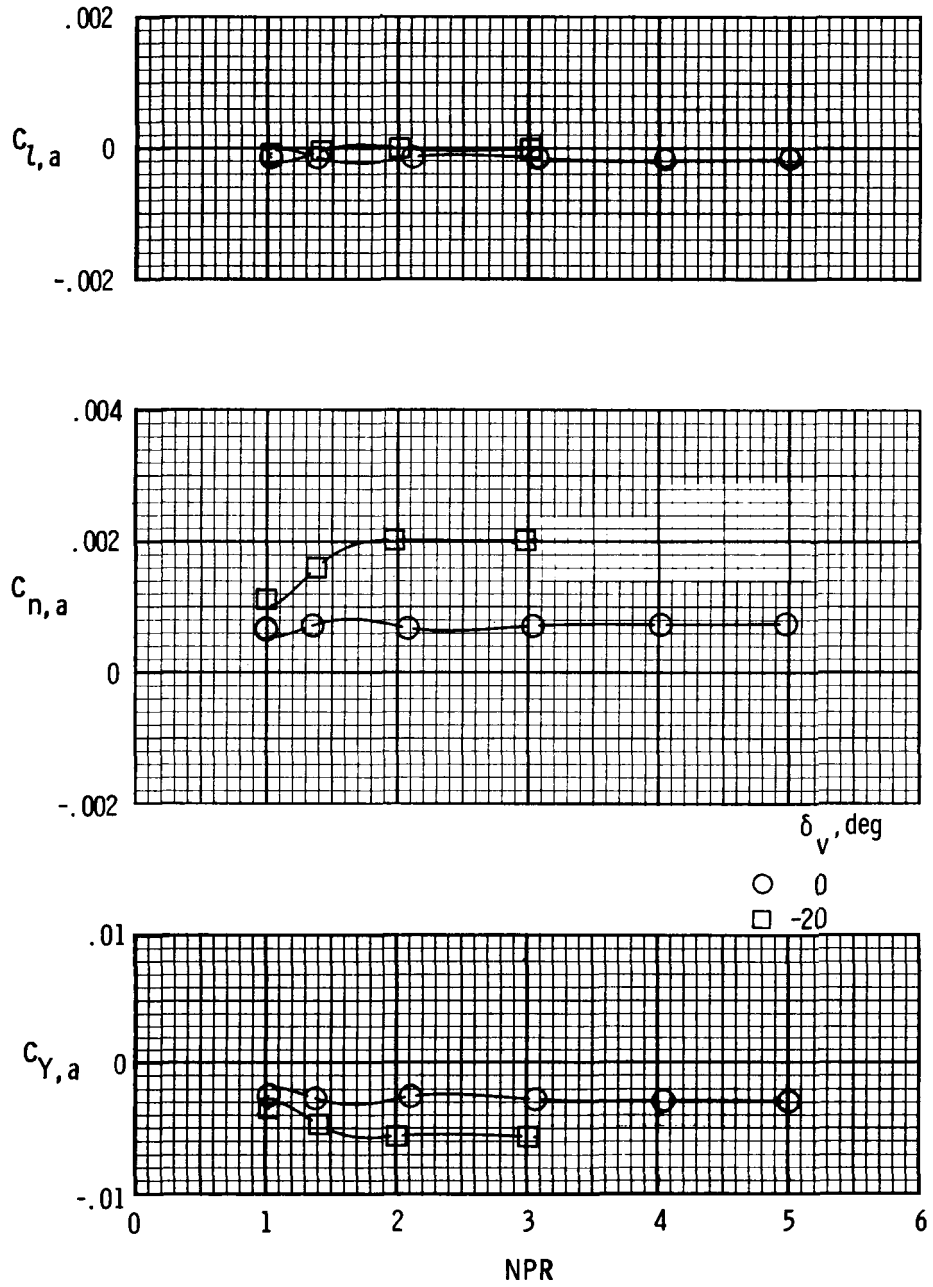

(d) $M = 0.80$ and $\alpha = 4.3°$.

Figure 12. Continued.

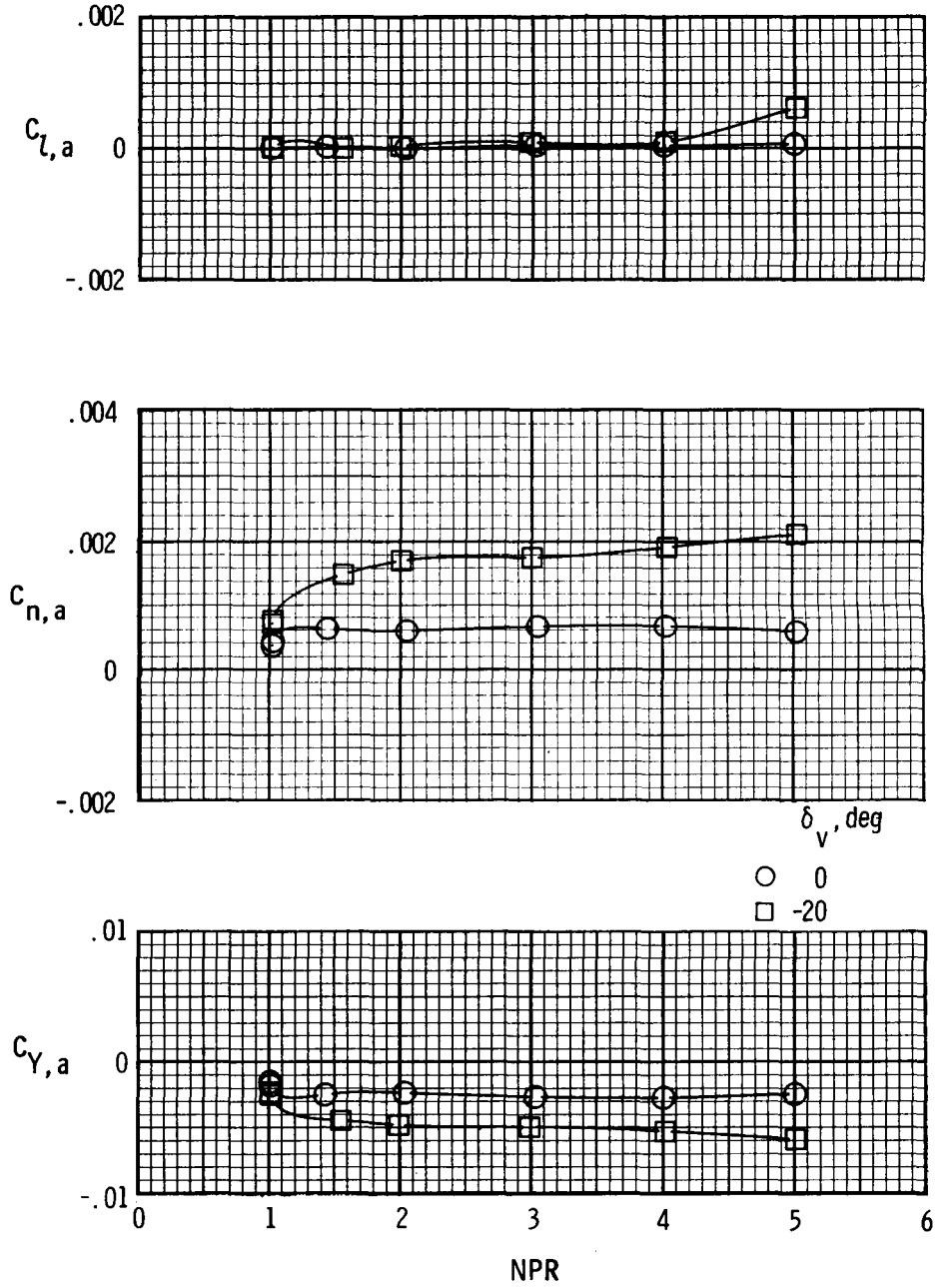

(e) $M = 0.90$ and $\alpha = 0°$.

Figure 12. Continued.

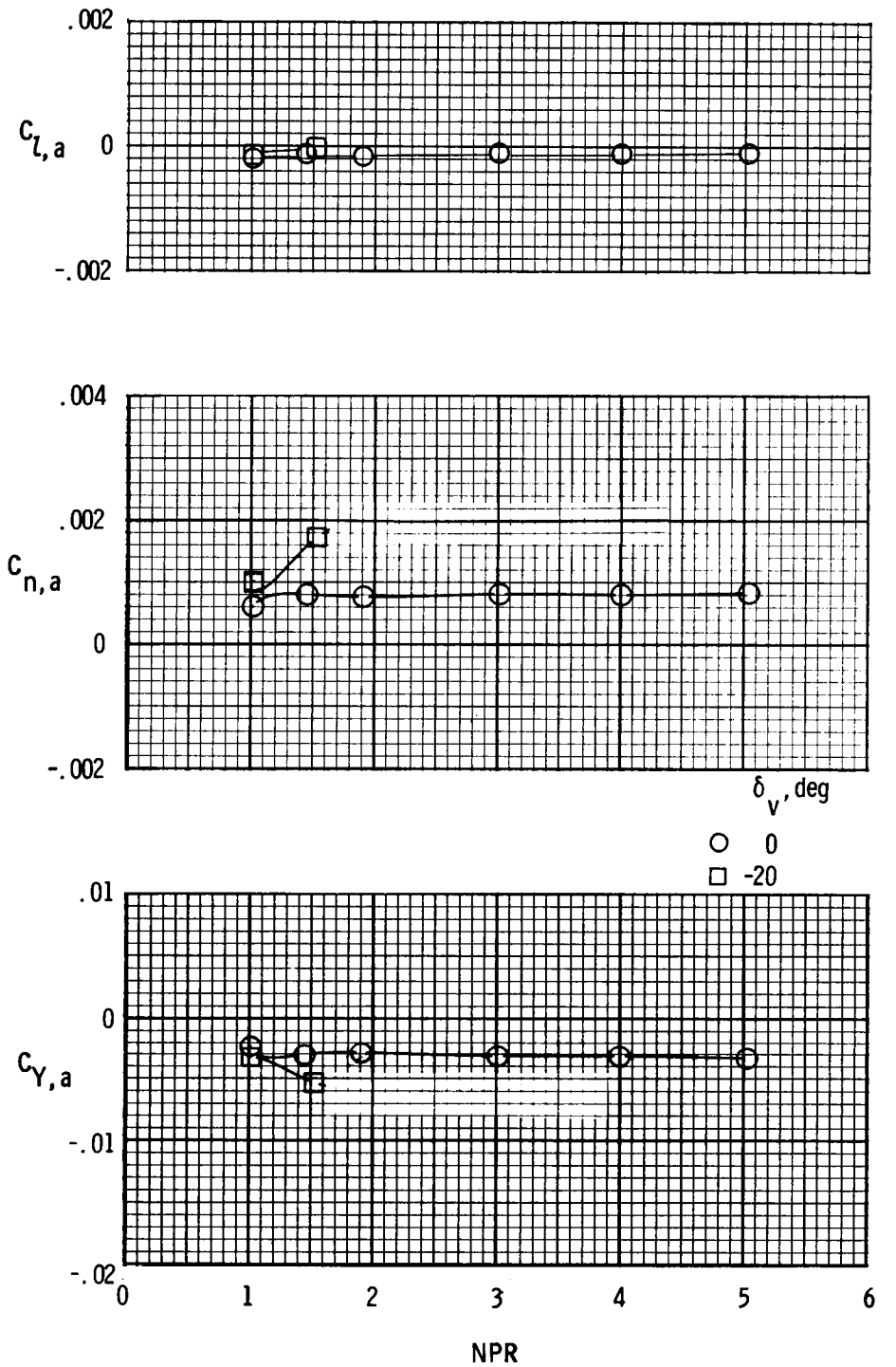

(f) $M = 0.90$ and $\alpha = 4.3°$.

Figure 12. Continued.

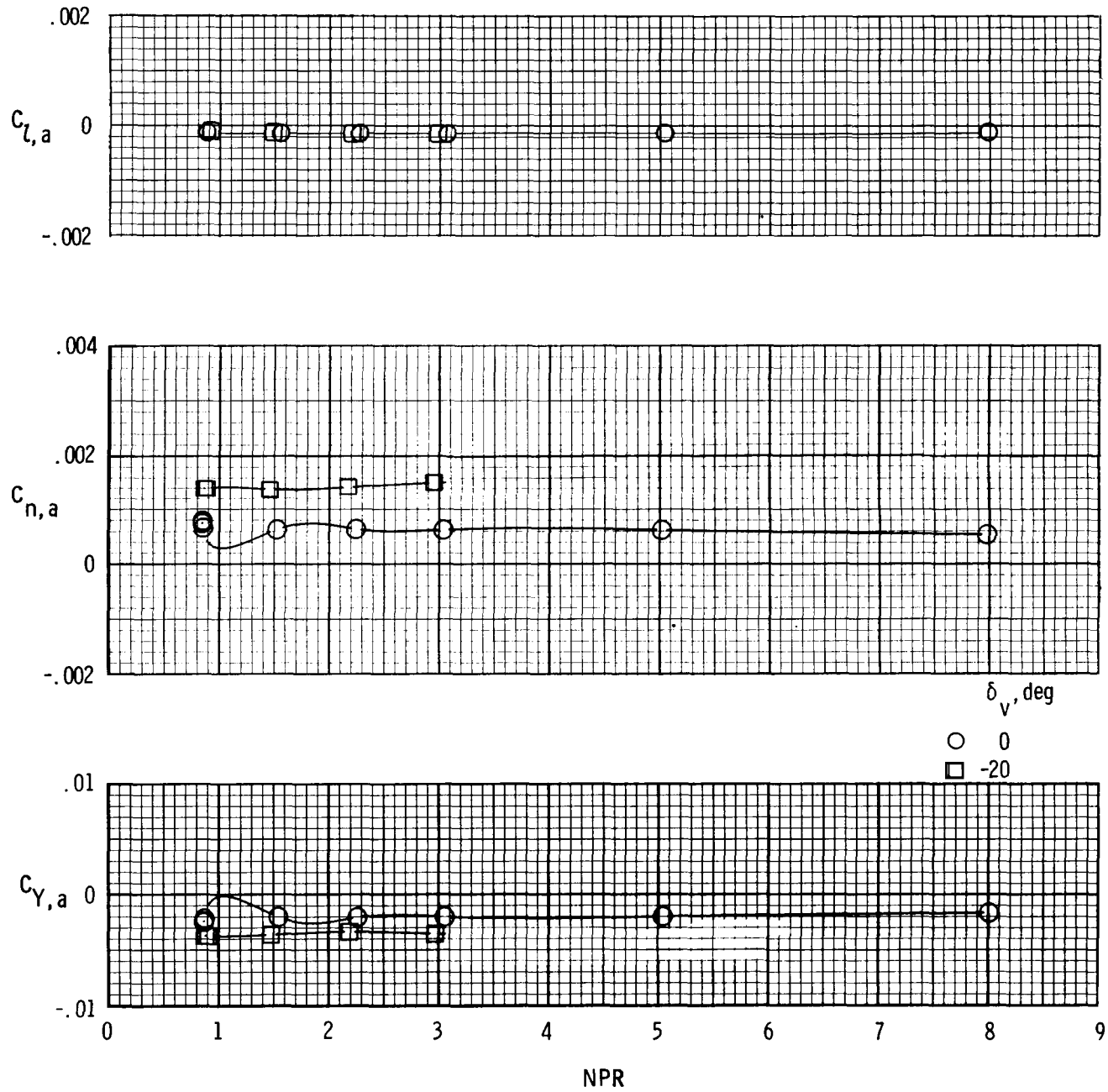

(g) $M = 1.25$ and $\alpha = 0°$.

Figure 12. Continued.

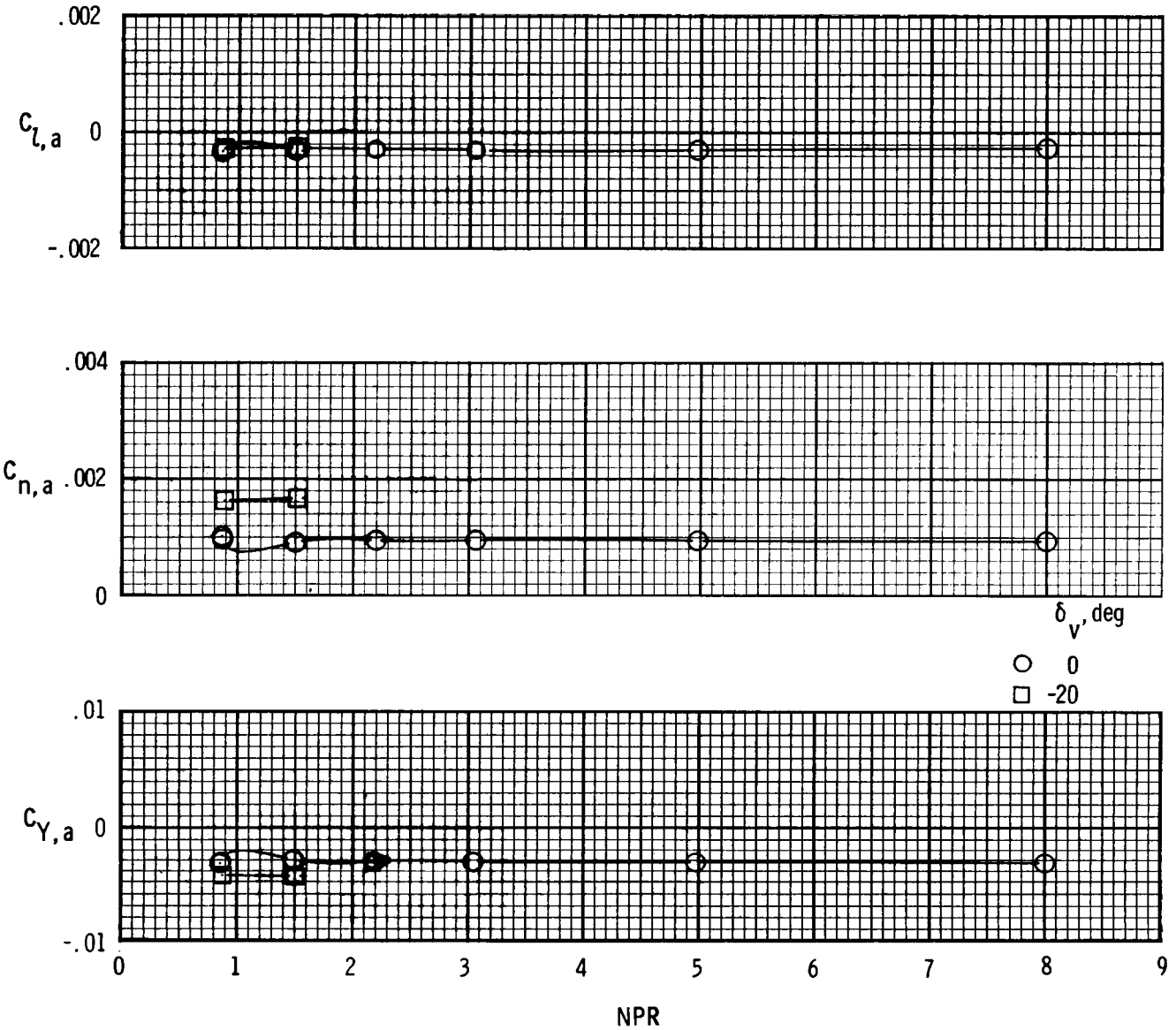

(h) $M = 1.25$ and $\alpha = 2°$.

Figure 12. Concluded.

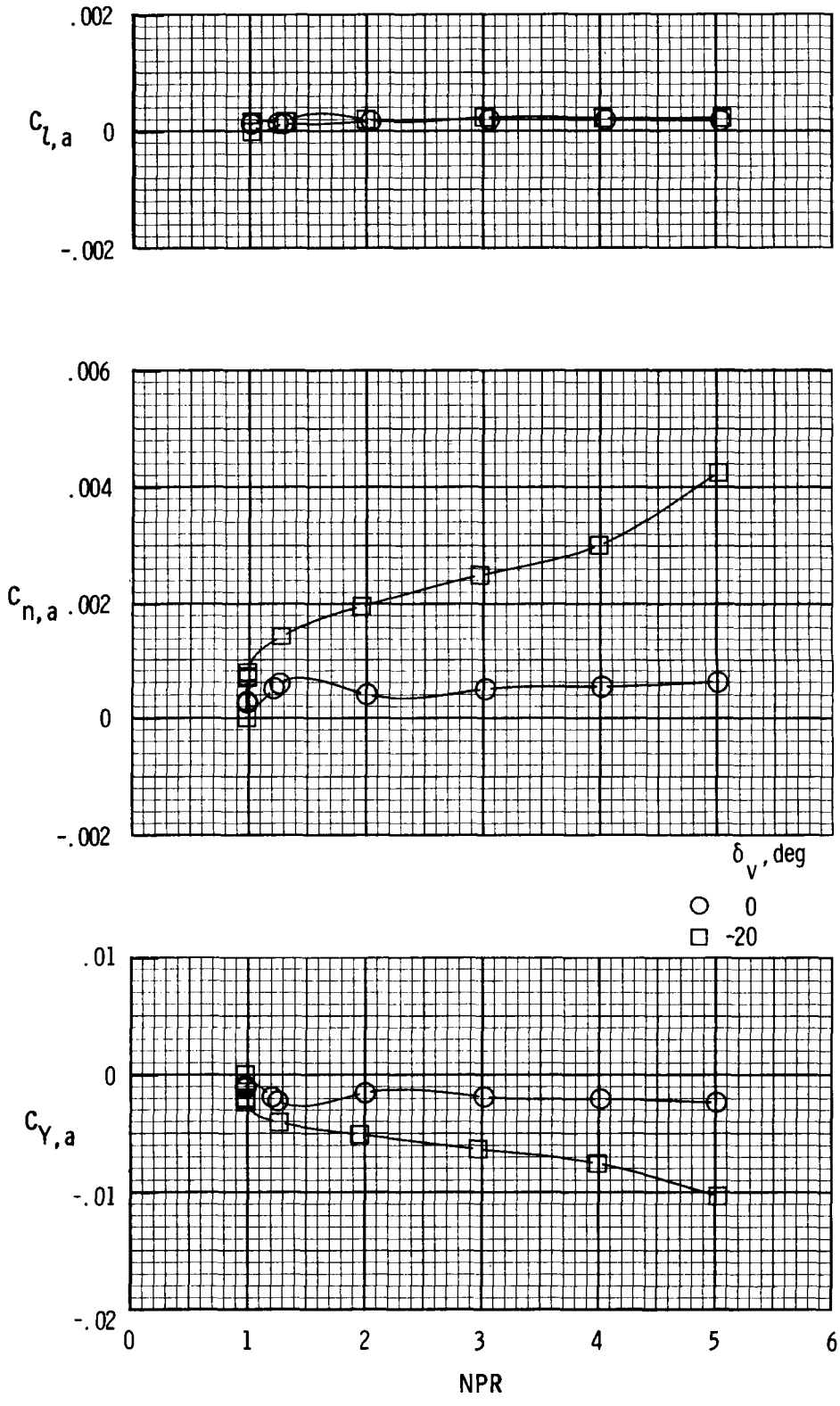

(a) $M = 0.70$ and $\alpha = 0°$.

Figure 13. Afterbody lateral-directional characteristics for model with TF30 cruise nozzles and yaw vanes installed. $\Lambda = 68°$; $\delta_h = -2°$.

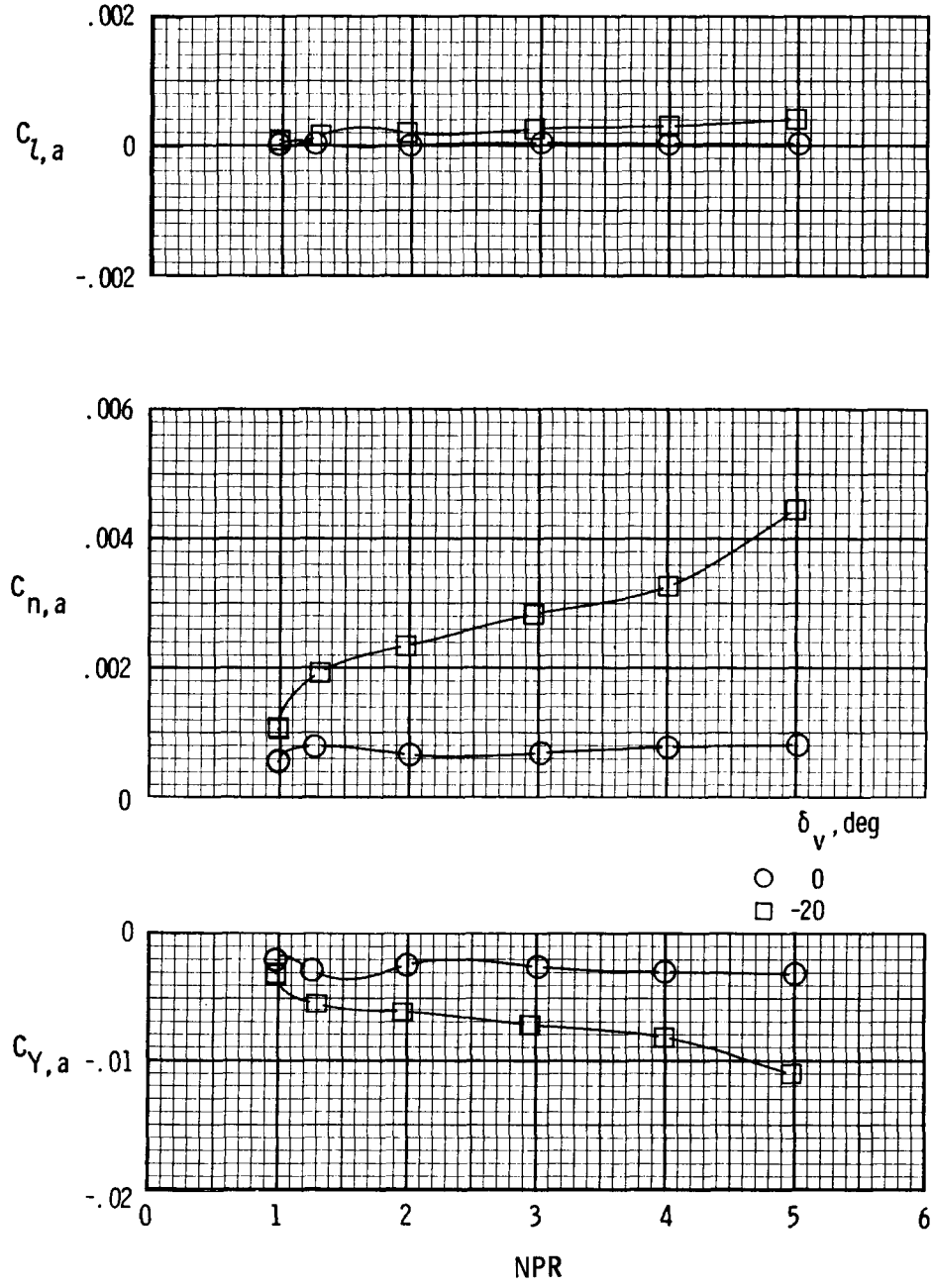

(b) $M = 0.70$ and $\alpha = 4.3°$.

Figure 13. Continued.

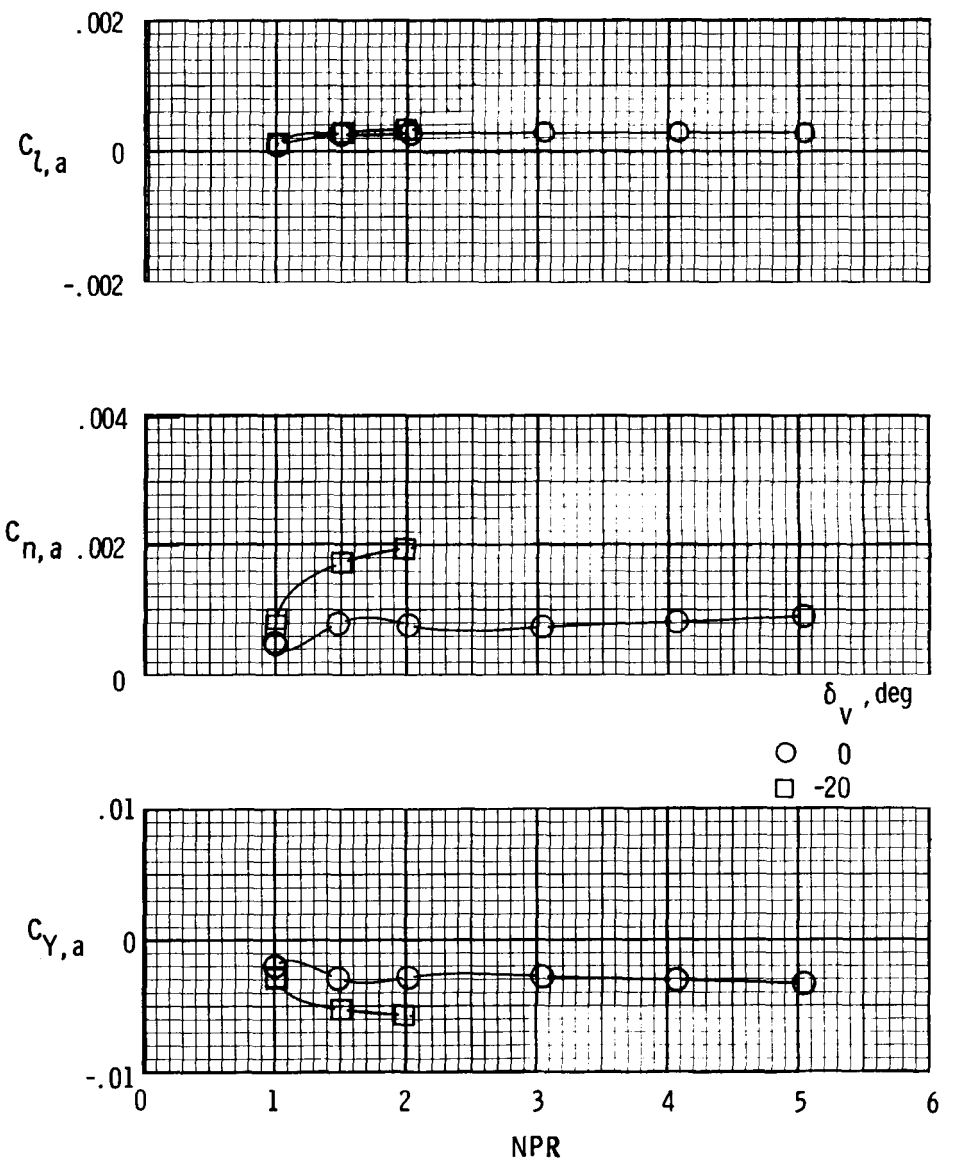

(c) $M = 0.90$ and $\alpha = 0°$.

Figure 13. Continued.

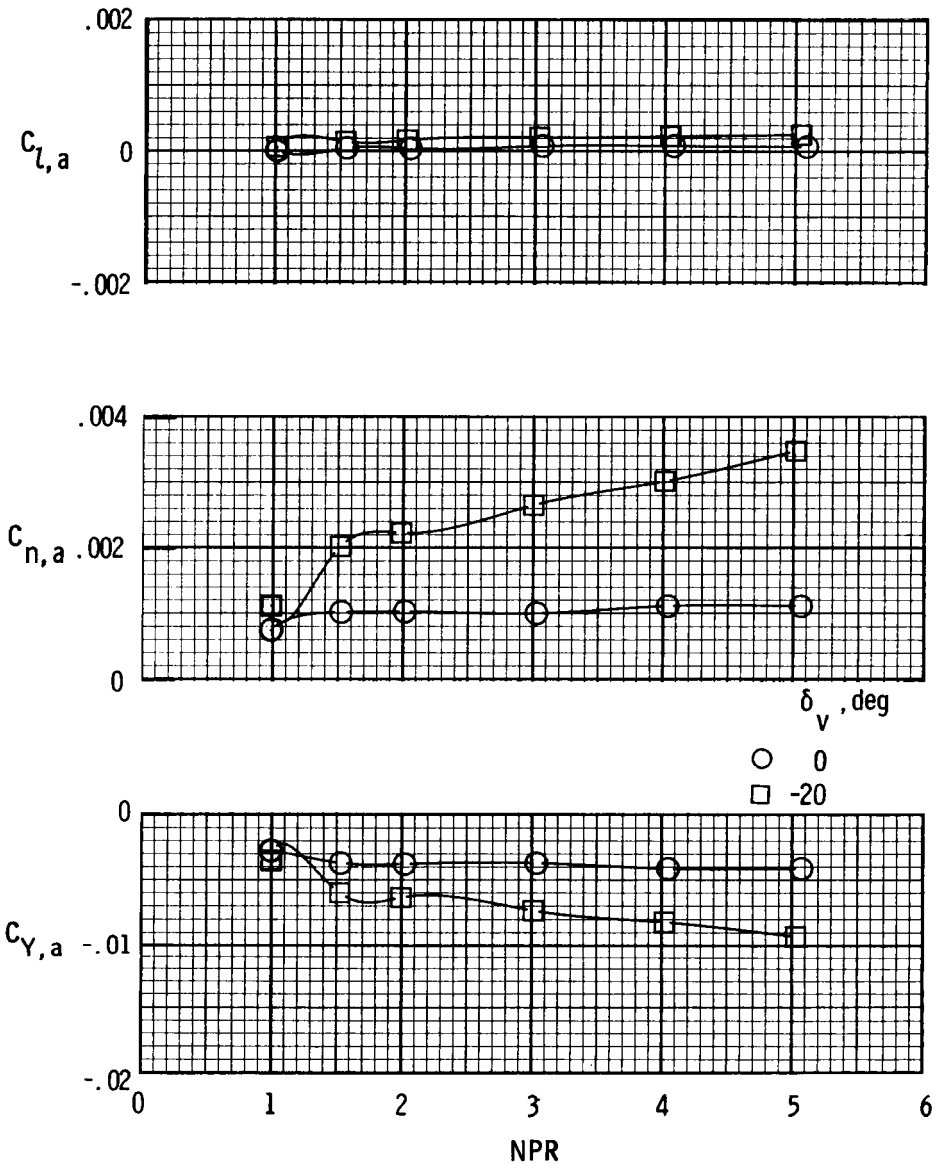

(d) $M = 0.90$ and $\alpha = 4.3°$.

Figure 13. Continued.

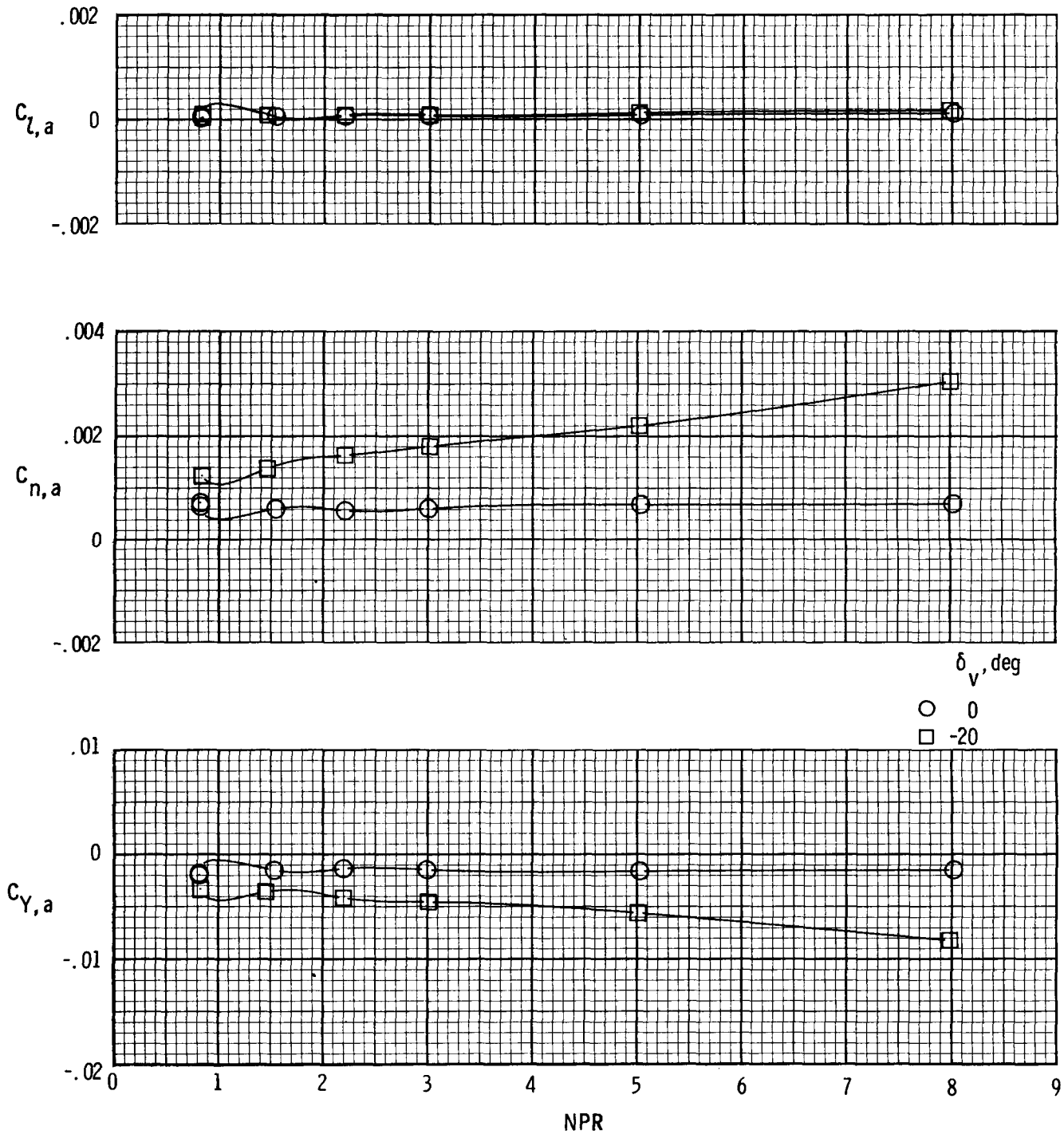

(e) $M = 1.25$ and $\alpha = 2°$.

Figure 13. Concluded.

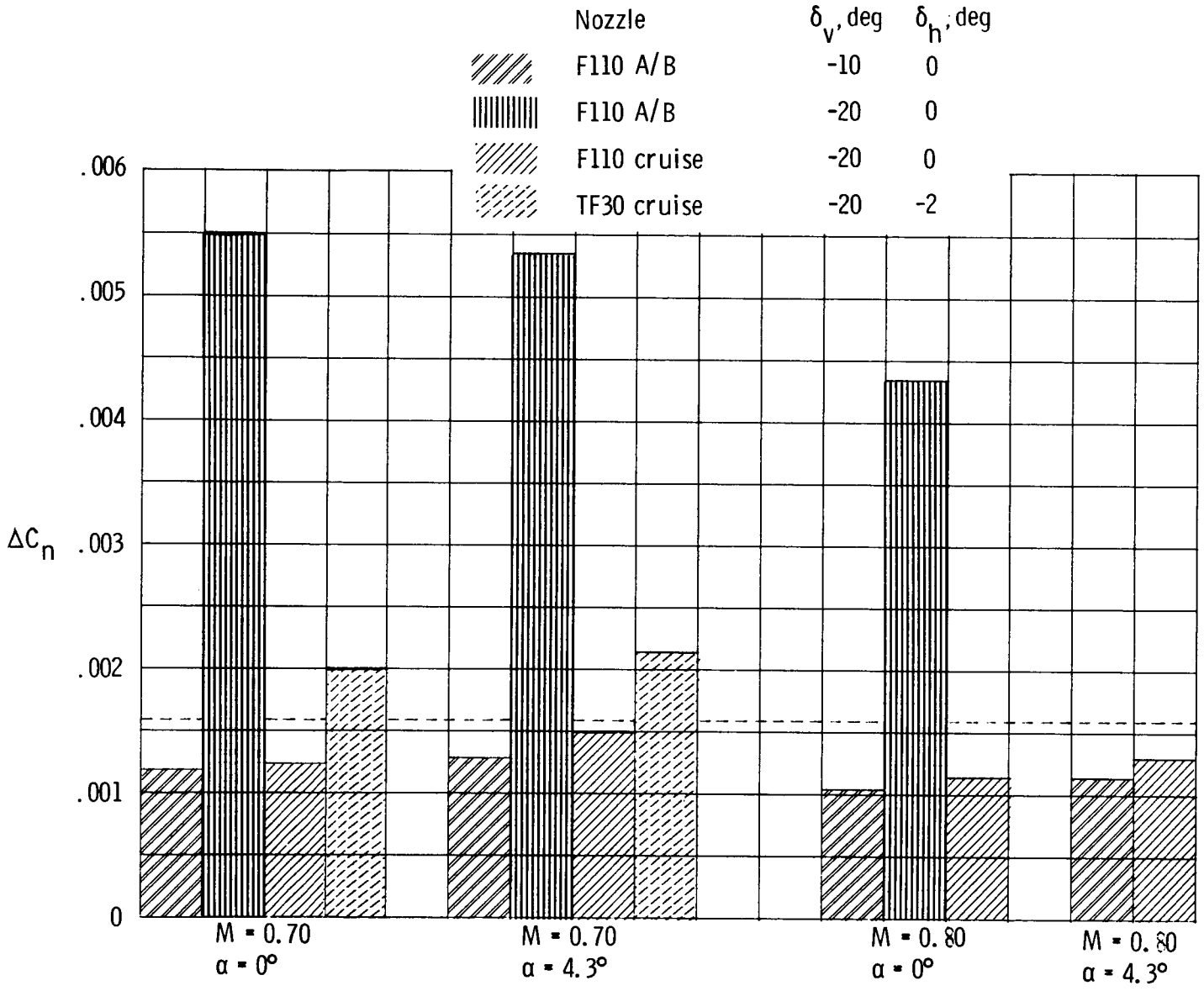

(a) $M = 0.70$ and 0.80.

Figure 14. Yawing-moment increments for deflection of yaw vanes from 0° at NPR = 3. Dashed line indicates yawing moment produced by $\delta_r = -1°$ at $\alpha = 0°$ (ref. 12).

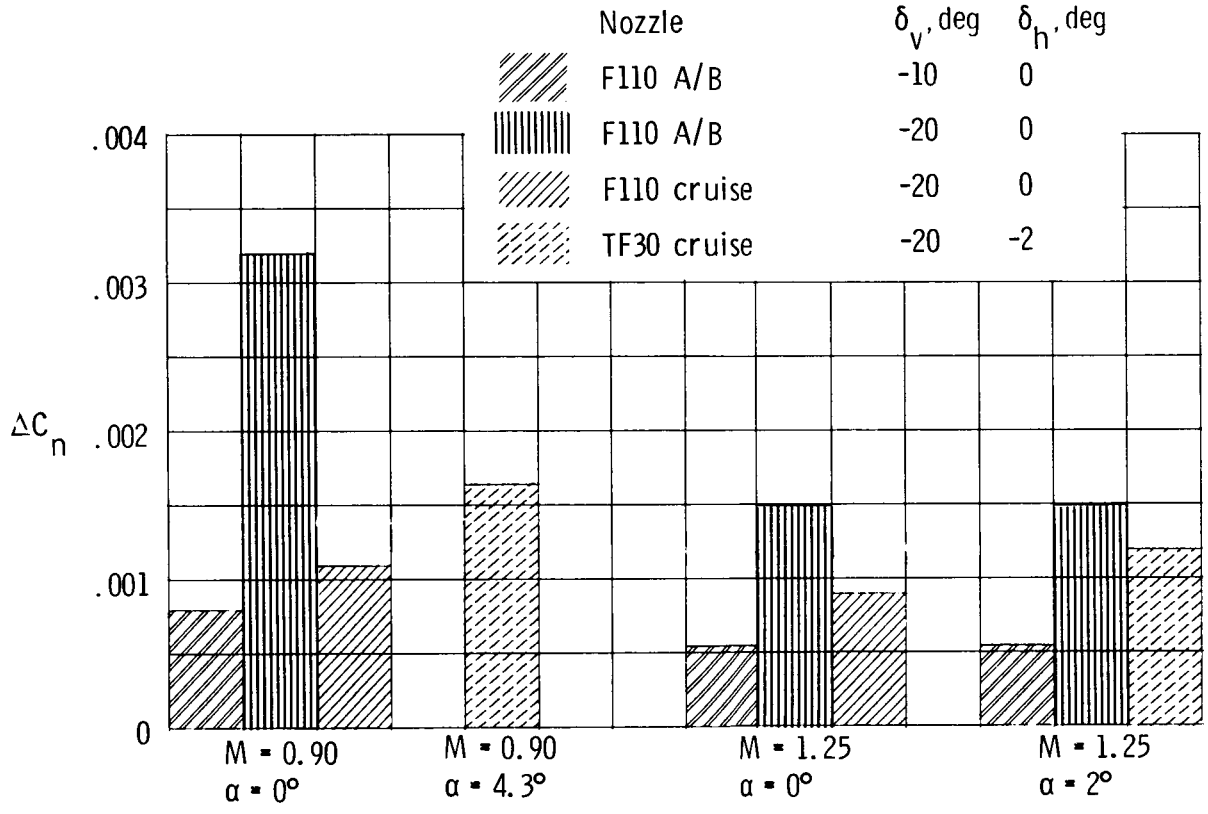

(b) $M = 0.90$ and 1.25.

Figure 14. Concluded.

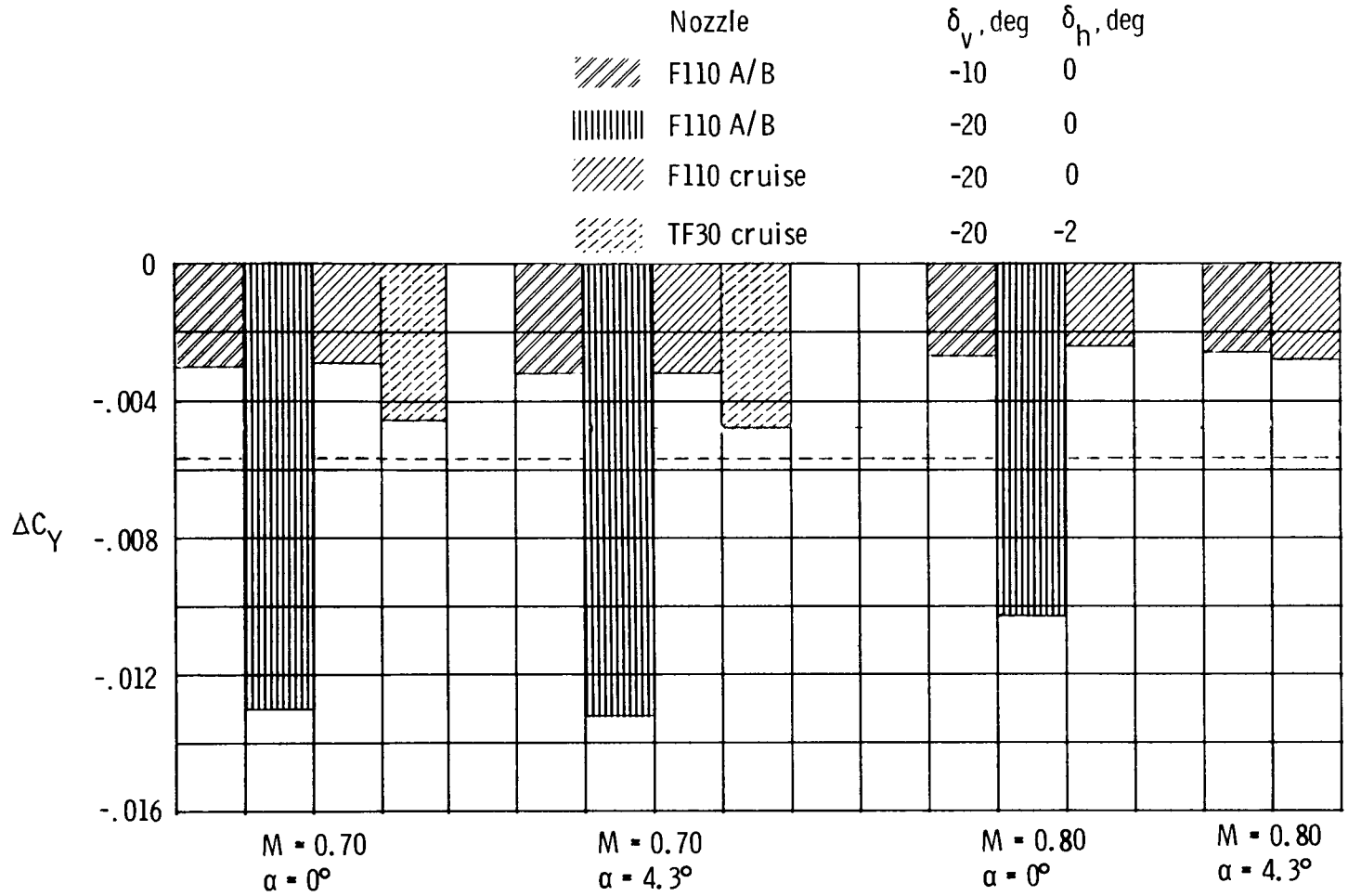

(a) $M = 0.70$ and 0.80.

Figure 15. Side-force increments for deflection of yaw vanes from 0° at NPR = 3. Dashed line indicates side force produced by $\delta_r = -1°$ at $\alpha = 0°$ (ref. 12).

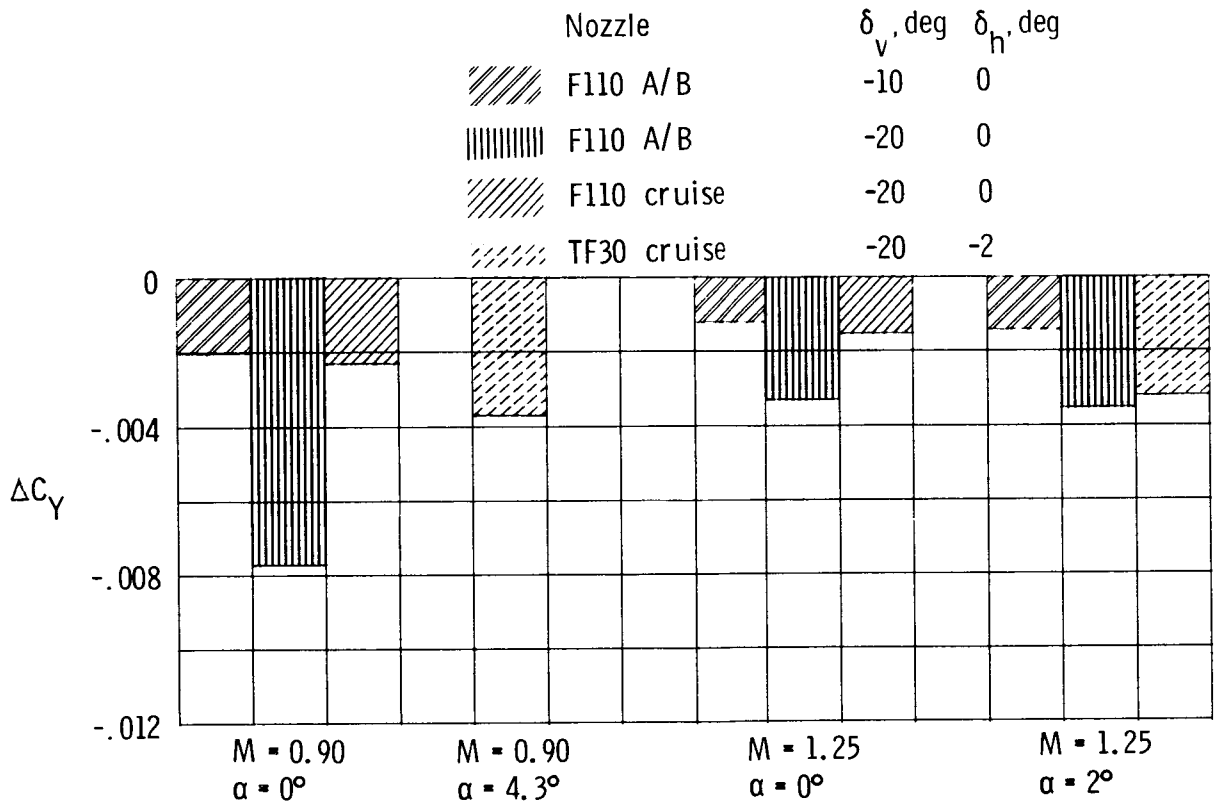

(b) $M = 0.90$ and 1.25.

Figure 15. Concluded.

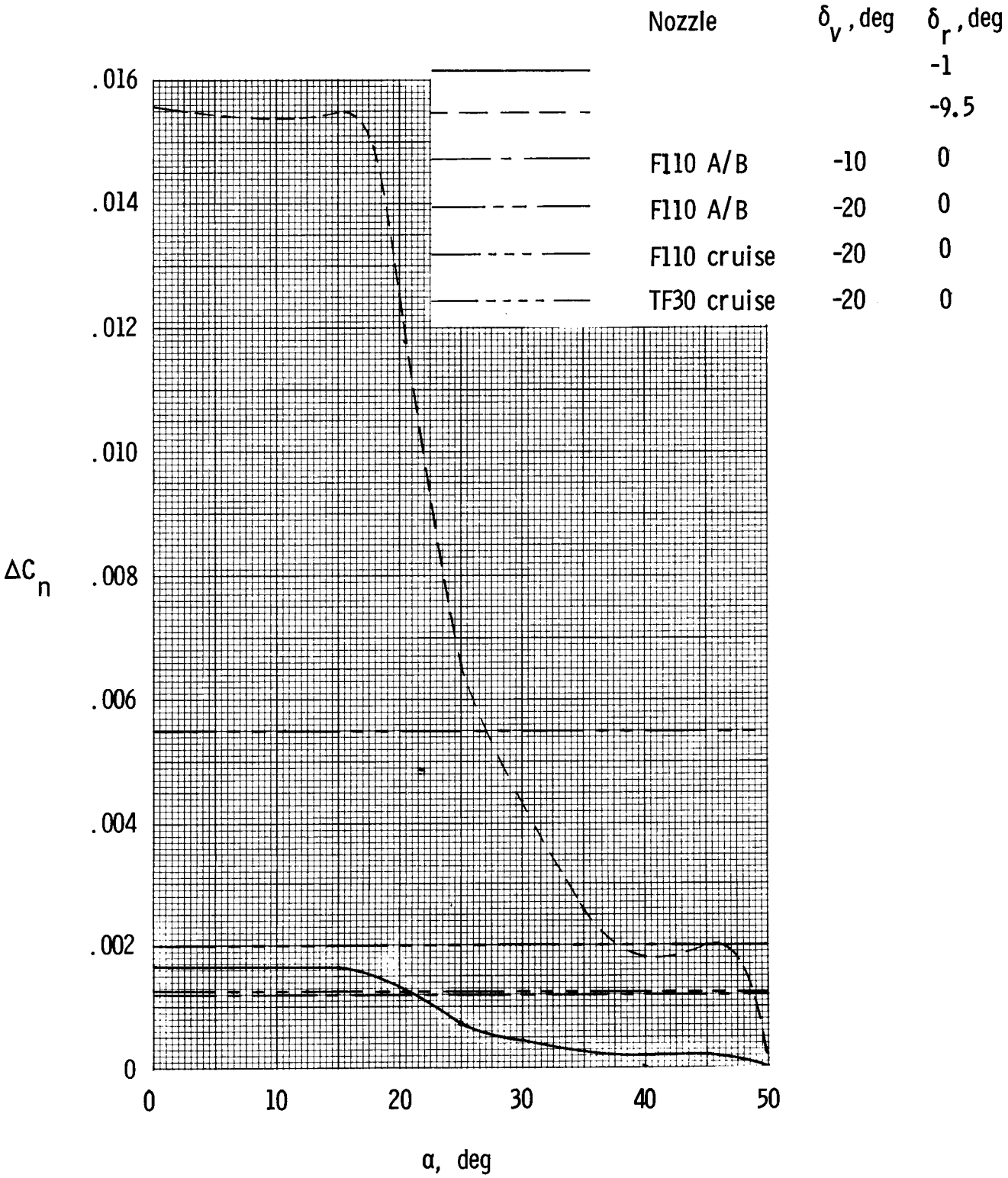

Figure 16. Comparison of yawing-moment coefficients produced by rudders and yaw vanes. $M = 0.70$; NPR = 3.

NASA
National Aeronautics and Space Administration

Report Documentation Page

1. Report No.	2. Government Accession No.	3. Recipient's Catalog No.
NASA TP-2769		

4. Title and Subtitle	5. Report Date
Effects of the Installation and Operation of Jet-Exhaust Yaw Vanes on the Longitudinal and Lateral-Directional Characteristics of the F-14 Airplane	December 1987
	6. Performing Organization Code
7. Author(s)	8. Performing Organization Report No.
David E. Reubush and Bobby L. Berrier	L-16302
9. Performing Organization Name and Address	10. Work Unit No.
NASA Langley Research Center Hampton, VA 23665-5225	505-62-91-01
	11. Contract or Grant No.
12. Sponsoring Agency Name and Address	13. Type of Report and Period Covered
National Aeronautics and Space Administration Washington, DC 20546-0001	Technical Paper
	14. Sponsoring Agency Code

15. Supplementary Notes

16. Abstract

An investigation was conducted in the Langley 16-Foot Transonic Tunnel to determine the effects of the installation and operation of jet-exhaust yaw vanes on the longitudinal and lateral-directional characteristics of the F-14 airplane. The model was tested at Mach numbers from 0.70 to 1.25 at angles of attack from 0° to 4.3°. Compressed air was used to simulate nozzle exhaust flow from jet off up to a nozzle pressure ratio of 8. The results of the investigation show that the yaw vanes can augment the rudders to provide directional control, but further investigation will be necessary to optimize the deflection schedule associated with the various nozzle power settings.

17. Key Words (Suggested by Authors(s))	18. Distribution Statement
Yaw vanes Afterbody drag Thrust vectoring	Unclassified—Unlimited Subject Category 02

19. Security Classif.(of this report)	20. Security Classif.(of this page)	21. No. of Pages	22. Price
Unclassified	Unclassified	118	A06

NASA FORM 1626 OCT 86 NASA-Langley, 1987
For sale by the National Technical Information Service, Springfield, Virginia 22161-2171